Impact of oncogene expression in the respiratory system of *Drosophila melanogaster*

Dissertation

zur Erlangung des Doktorgrades

der Mathematisch-Naturwissenschaftlichen Fakultät der

Christian-Albrechts-Universität zu Kiel

Vorgelegt von

Judith Bossen

aus

Kiel

Kiel, Februar 2018

Prüfer:

Prof. Dr. Thomas Roeder

Prof. Dr. Holger Heine

Termin der Disputation: 28.03.2018

Table of Contents

Zusammenfassung

Krebserkrankungen, insbesondere Brust- und Lungenkrebs, gehören zu den weltweit häufigsten Todesursachen. Diese Erkrankungen werden oft erst in einem späten Stadium dignostiziert und sind aus diesem Grund mit einer schlechten Prognose assoziiert; eine Situation, die neue Therapieansätze und die Entdeckung neuer Medikamente zwingend erforderlich macht. In dieser Arbeit wurde das Tracheensystem der Taufliege *Drosophila melanogaster* genutzt, um ein geeignetes Lungenkrebsmodell zu entwickeln.

Die ektopische Expression unterschiedlichster Onkogene im gesamten Tracheensystem der Taufliege rief strukturelle Veränderungen sowie Meta- und Hyperplasien des Epithels hervor. Die ektopische Expression einer konstitutiv aktiven Isoform des Epidermalen Wachstumsfaktor Rezeptors ($Egfr^{CA}$) führte zu einer extremen Verdickung des Epithels sowie einer massiven Veränderung der zellulären Struktur. Der damit einhergehende Verlust der sauerstoffleitenden Fähigkeit der Tracheen führte zum Tod in einem frühen Larvenstadium. Unter Verwendung der Embryonen dieser Kreuzung wurde ein Testsystem entwickelt, mit dem Substanzen identifiziert werden können, die diesen letalen Phänotyp aufheben. Das Überleben der Larven und die Entwicklung von Puppen und adulten Fliegen dienten als Anzeige für Substanzen, welche die Krebsentstehung effektiv hemmen. Die beiden spezifischen EGFR Inhibitoren, Afatinib und Gefitinib, konnten mit Hilfe dieses Screeningsystems verifiziert und ihre Wirkung anschließend näher charakterisiert werden. Die Behandlung mit beiden Stoffen konnte den Gewebeveränderungen entgegenwirken und das Überleben und die Metamorphose zu adulten Fliegen gewährleisten. Darüber hinaus erwies sich das etablierte Testsystem als vielversprechend, um Substanzkombinationen zu identifizieren, die synergistisch wirken.

Des Weiteren konnte gezeigt werden, dass die Aktivierung von Komponenten des Ras/MAPK Signalwegs in den terminalen Atemwegsepithelzellen zu einer Vergrößerung und einer vermehrten Anzahl von Verzweigungen dieser sauerstoffversorgenden Zellen führt. Dies ging, zum Teil, mit einer erhöhten Hypoxiesensitivität einher. Im Gegensatz dazu führte die Aktivierung des angeborenen Immunsystems, ermöglicht durch ektopische Expression des Rezeptors PGRP-LCx, zu einem Absterben dieser Zellen. Diese sehr fragilen Terminalzellen zeigen normalerweise keine Immunreaktion, was eventuell als Schutz vor einer Schädigung dieser Strukturen durch die eigene Immunabwehr dienen soll.

Abstract

Cancer entities, especially breast and lung cancer, are among the most important causes of death worldwide. These diseases are mostly diagnosed at late stages and are therefore associated with poor prognoses. This situation represents an urgent need for new therapeutic approaches and the discovery of new drugs. In this thesis, the tracheal system of the fruit fly *Drosophila melanogaster* was used to develop tailored lung cancer models.

The ectopic expression of several oncogenes targeted to the tracheal system of the fruit fly induced structural changes comprising meta- and hyperplasia of the epithelium. The ectopic expression of a constitutively active isoform of the epidermal growth factor receptor ($Egfr^{CA}$) led to thickening of the epithelium and obvious changes in the cellular structure. The loss of the oxygen-conducting ability of the trachea led to death in an early larval stage. Using the $Egfr^{CA}$ embryos, a test system with the ability to identify substances that rescue this lethal phenotype was developed. The survival of the larvae and the development into pupae and adult flies served as an indicator of substances that effectively inhibit cancer development. The specific EGFR inhibitors, Afatinib and Gefitinib, were verified with this novel screening system and their effects on disease development were analysed in detail. Treatment with both substances rescued structural changes and ensured survival and metamorphosis into adult flies. In addition, the established approach is promising in identifying combinations of substances with synergistic mode of action.

Moreover, activation of different components of the Ras/ MAPK pathway in a specialized cell type of the tracheal system that is devoted to the direct oxygen supply of the tissue, the so called terminal cells, resulted in enlargement and an increased number of branches of these cells. This was partially associated with increased hypoxia sensitivity. In contrast, activation of the local innate immune system, triggered by overexpression of the immune-activating receptor PGRP-LCx led to death of these cells. Usually, these very fragile terminal cells show no immunoreaction, presumably to avoid damage of their structures caused by activation of the endogenous immune system.

List of abbreviations

AJ	Adherens junctions
ALK	Anaplastic lymphoma kinase
Apc	APC-like
APC	Adenomatous polyposis coli
Arm	Armadillo
ATP	Adenosine triphosphate
Bnl	Branchless
Btk	Brutons tyrosine kinase
Btl	Breathless
CA	Constitutive active
Cdk	Cyclin-dependent kinase
CGARN	Cancer genome atlas research network
CM	Concentrated medium
Cora	Coracle
CSC	Cancer stem cell
Csw	Corkscrew
d	days
DAP	Diaminopimelic acid
DAPI	4`,6-diamino-2-phenylindole
DB	Dorsal branch
Dcp-1	Death caspase-1
DIC	Differential interference contrast
Dlg	Disc large
DN	Dominant negative
DNA	Deoxyribonucleic acid
Dof	Downstream of receptor
Dredd	Death related ced-3/Nedd2-like caspase
Drk	Downstream of receptor
Drs	Drosomycin
DSRF	*Drosophila* serum response factor
Egfr	Epidermal growth factor receptor
$Egfr^{CA}$	Constitutive active isoform of Egfr
EMT	Epithelial-mesenchymal transitiion
ERK	Extracellular signal-regulated kinase
et al.	*et alii*
Fadd	Fas-associated death domain
FDA	Food and drug administration
FGFR	Fibroblast growth factor recpetor
GFP	Green fluorescent protein
GOF	Gain of function
h	hour
HER	Human epidermal growth factor receptor
Hid	Head involution defective
Hif-α	Hypoxia inducing factor-α
Iap-2	Inhibitor of apoptosis-2
IκB	Inhibitor of kappa B
IKK	IκB kinase
IL-1	Interleukin-1
IMD	Immune deficiency
InR	Insulin-like receptor

Ird5	immune response deficient 5
JNK	c-Jun N-terminal kinase
Lgl	Lethal giant larvae
LUAD	Lung adenocarcinoma
LUSC	Lung squamous cell carcinoma
MAPK	Mitogen-activated protein kinase
MARCM	Mosaic analysis with repressible cell marker
Mb	Mega base
MEK	MAPK/ERK kinase
MET	Mesenchymal-epithelial transition
Nf-κB	Nuclear factor- κB
NSCLC NOS	Non-small cell lung cancer not otherwise specified
NSCLC	Non-small cell lung cancer
PDGFR	platelet-derived growth factor receptor/
PGN	Peptidoglycane
PGRP	Peptidoglycane recognition protein
pH3	phospho-Histone 3
PI3K	Phosphatidylinositol-3-kinase
Pnt	Pointed
ppk	pickpocket
PRR	Pattern recognition receptor
PTEN	Phosphatase and tensin homolog
Pvr	PDGFR-/VEGFR related
Raf	Rapidly accelerated fibrosarcoma
Ras	Rat sarcoma
RIP	Receptor interacting protein
Rl	Rolled
Rpr	Reaper
RPTK	Receptor protein tyrosine kinase
RTK	Receptor tyrosine kinase
SC	Stem cell
SCLC	Small cell lung cancer
SD	Standard deviation
SEM	Standard error oft he mean
SJ	Septate junctions
Sos	Son of sevenless
SQCLC	Squamous cell lung cancer
Tak1	Transforming growth factor beta-activated kinase 1
TCT	Tracheal cytotoxin
TGF-α	Transforming growth factor-α
TKI	Tyrosine kinase inhibitor
TM	Transmembrane
TNF	Tumor necrosis factor
TP53	Tumor protein 53
Trh	Trachealess
UAS	Upstream activating factor
UV	Ultraviolet light
VEGFR	Vascular endothelial growth factor receptor
Wt	Wildtype

List of figures

1 Introduction

1.1 Cancer incidence and tumor progression

Cancer is an increasing burden in economically developed but also in developing countries. The reasons for this development comprise growth and aging of the population as well as life style behaviors that are known to increase the cancer risk. These factors include smoking, poor diet, physical inactivity and reproductive changes. In 2012 about 14.1 million new cancer cases and 8.2 million cancer associated deaths occurred worldwide. Among them, lung and breast cancer were the most frequently diagnosed cancer entities in males and females, respectively (Torre *et al.*, 2012).

Physiological processes are strictly regulated and controlled in normal tissues and organs to maintain homeostasis. In tumors severe disbalances in growth regulation, proliferation but also apoptosis dominate. Cancer cells are characterized by genomic instability and mutations that further drive tumor progression. They are able to sustain in a proliferative state, evade growth suppression, resist cell death and enable replicative immortality. Tumors can avoid destruction through the immune system and surprisingly, inflammation can promote their progression. Deregulated cellular energy homeostasis is associated with angiogenesis which in turn promotes tumor invasion and metastasis. All these hallmarks are enabled through the stepwise development from normal cells into malignant tumor cells through occurring mutations and changes of the cellular characteristics (Hanahan and Weinberg, 2011).

Tumor progression can be divided into different steps (Fig. 1). From the normal epithelium, tumor activation starts with proliferation and the formation of a benign adenoma that progresses further into a malignant carcinoma *in situ*. The growing tumor becomes invasive and invades into other closely situated tissues. A metastatic stage is achieved, when the cells start to migrate from the primary tumor and spread to distant body sites. This process is supported by epithelial-mesenchymal transitions (EMT). EMT is the biological process that allows a polarized epithelial cell to accept a mesenchymal phenotype with the ability to initiate metastasis in epithelial cancer (Kalluri and Neilson, 2003). The reversed process likely follows metastasis is mesenchymal-epithelial transition (MET) to colonize distant organs (Kalluri and Weinberg, 2009). Tumor growth is accompanied by neovascularization

to assure the maintenance of the tumor tissue with nutrients and oxygen. Tumor therapy can often lead to the development of resistant cells and subsequent recurrence of the tumor (Fig. 1).

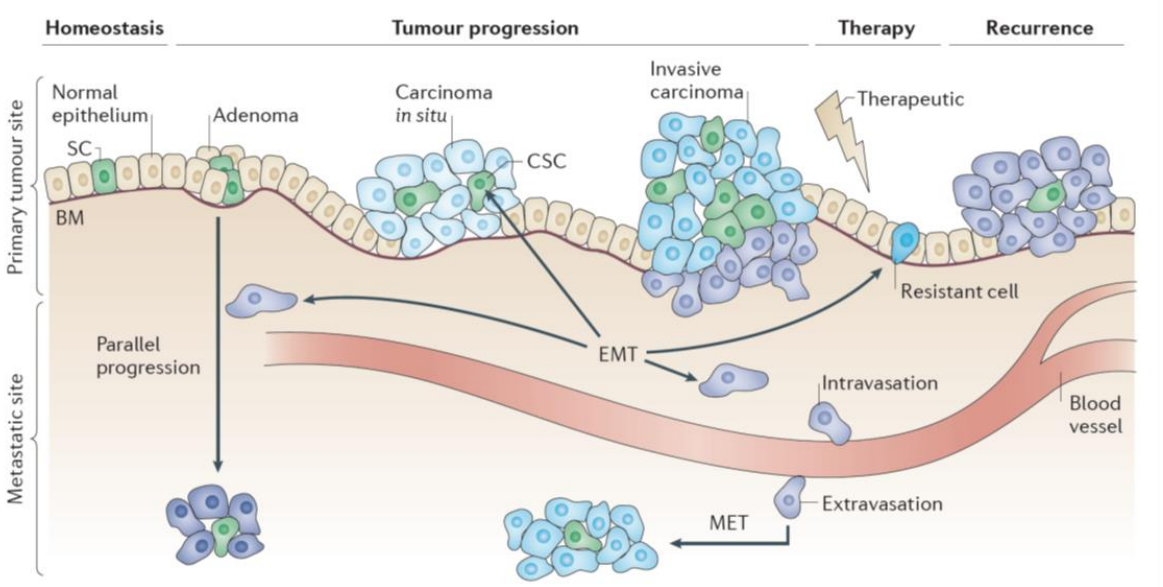

Figure 1: Tumor progression from homeostasis of a normal epithelium to therapy and recurrence of the tumor. The tumor develops out of the normal epithelium on the primary tumor site and spreads to a metastatic site by blood vessel intravasation and extravasation of cancer cells. The cancer cells undergo EMT and leave the primary tumor site. Subsequent MET supports colonization of distant sites. Therapy of the tumor can lead to the development of resistant cells and recurrence of the tumor. SC = stem cell, CSC = cancer stem cell, EMT = epithelial-mesenchymal transition, MET = mesenchymal-epithelial transition (De Craene and Berx, 2013).

Sequentially activating mutations of proto-oncogenes and disabling mutations in tumor suppressor genes are required for cancer development (Greenman *et al.*, 2007; Bozic *et al.*, 2010). The mutations that confer a selective growth advantage to the tumor cell are called driver gene mutations. A mutation that has no direct or indirect effect on the growth advantage of the cell is called a passenger mutation (Vogelstein *et al.*, 2013).

The differentiation between cancer types relies on the tissue site of origin and is classified based on pathological and histological criteria. Large-scale genomics projects have shown that subtypes of these cancer types share similar molecular alterations and specific signatures (Hoadley *et al.*, 2016).

1.2 Lung cancer

Lung cancer was the leading cause of death in man with 1.1 million estimated deaths worldwide in 2012. By differentiation between developed and developing countries, lung cancer was the leading cause of death in males and females in developed countries (Torre *et al.*, 2012). Lung cancer is the second most common diagnosed type of cancer with 25 % of all cancer diagnoses and is still the leading cause of death in males and females in 2017 in the US. The death rates have declined since 1990 due to reductions in smoking behavior. The symptoms do not occur until the cancer is in an advanced state. The high death rates presumably result from this late state detection. The 5-year relative survival rate for lung cancer is 15 % in males and 21 % in females. Only 16 % of the cases are diagnosed at a localized state with a 5-year relative survival rate of 55 %. Cigarette smoking is the most important risk factor for developing lung cancer. The risk increases with quantity and duration of smoking history (Siegel *et al.*, 2017). Lung cancer does also occur in never smokers. There, it is frequently more diagnosed in younger ages and in women (Rudin *et al.*, 2009). Reasons for the development of lung cancer in never smokers can be occupational and environmental exposure to carcinogens (asbestos, radon, environmental tobacco smoke, cooking fumes), genetic susceptibility, hormonal factors, pre-existing lung diseases and viral infections. It is most frequently diagnosed in Asia (Subramanian and Govindan, 2007). The lung cancer types can not only be characterized and classified by histology but also by generating molecular profiles of the tumors regarding mutation profiles, structural rearrangements, copy number alterations, DNA methylation, mRNA, miRNA and protein patterns.

1.2.1 Molecular profiling of different lung cancer types

Lung cancer is traditionally classified into non-small cell lung cancer (NSCLC) and small cell lung cancer (SCLC). NSCLCs can be sub classified in adenocarcinoma (LUAD), squamous cell lung cancer (LUSC), non-small cell lung cancer not otherwise specified (NSCLC NOS) or large cell carcinoma (Travis *et al.*, 2015). 70 % of the NSCLC cases in never smokers are LUADs and only 6 % are LUSCs (Rudin *et al.*, 2009).

Large sequencing projects like *The Cancer Genome Atlas Research Network* (CGARN) of SCLC, LUAD and LUSC revealed distinct differences in lung cancer types on molecular level and highlighted the candidate driver genes and mutations underlying tumor progression (Peifer *et al.* 2012; CGARN, 2012; CGARN, 2014). The average mutation frequency in smokers is 10-fold higher than in never-smokers. Tumors with in a higher stage accumulate more mutations (Ding *et al.*, 2008; Govindan *et al.*, 2012).

LUADs represent 40 % of the lung cancer cases and show high rates of somatic mutations (8.87 mutations/Mb) and genomic rearrangement. They are heterogeneous with diverse combinations of mutations (CGARN, 2014; Imielinski *et al.,* 2012; Govindan *et al.,* 2012; Ding *et al.,* 2008). Activation of RTK/RAS/RAF genes occurred in 76 % (Fig. 2). Second most alterations appeared in the TP53 pathway (65 %). PI3K-mTOR activations were seen in 25 %. Cell cycle regulators were altered in 64 % as well as various chromatin and splicing factors in 49 %. Oxidative stress pathways were altered in 22 % of the cases. The important oncogenes with the highest mutation rates were *KRAS*, *EGFR*, *BRAF*, *CDK4* and *MET*. The important tumor suppressors were *TP53*, *STK11*, *KEAP1*, *NF1* and *RB1* (CGARN, 2014).

LUSCs arise in the main bronchi and represent 25-30 % of the lung cancer cases. Sequencing displayed a high mutation rate with 8.1 mutations/Mb and marked genomic complexity including a very high mutation rate in the tumor suppressor genes *TP53*, *CDKN2* and *RB1*. Mutations and copy number alterations in the oxidative stress response genes *NFE2L2* and *KEAP1* and/or deletion or mutation of *Cul3* were found in 34 % of the tumors. 44 % of the LUSCs showed alterations in the genes with known roles in squamous cell differentiation. Mutated genes belonging to the phosphatidylinositol-3-OH kinase (PI3K) pathway showed a high significance in 47 % of the tumors. A rather low mutation rate was confirmed in *EGFR* and *KRAS* genes, without the typical known mutations (CGARN, 2014).

Sequencing of the different lung cancer types display distinct differences in the molecular profiles and mutations. This makes molecular testing of tumors and the development of new treatment options and so called personalized therapies exceptionally important.

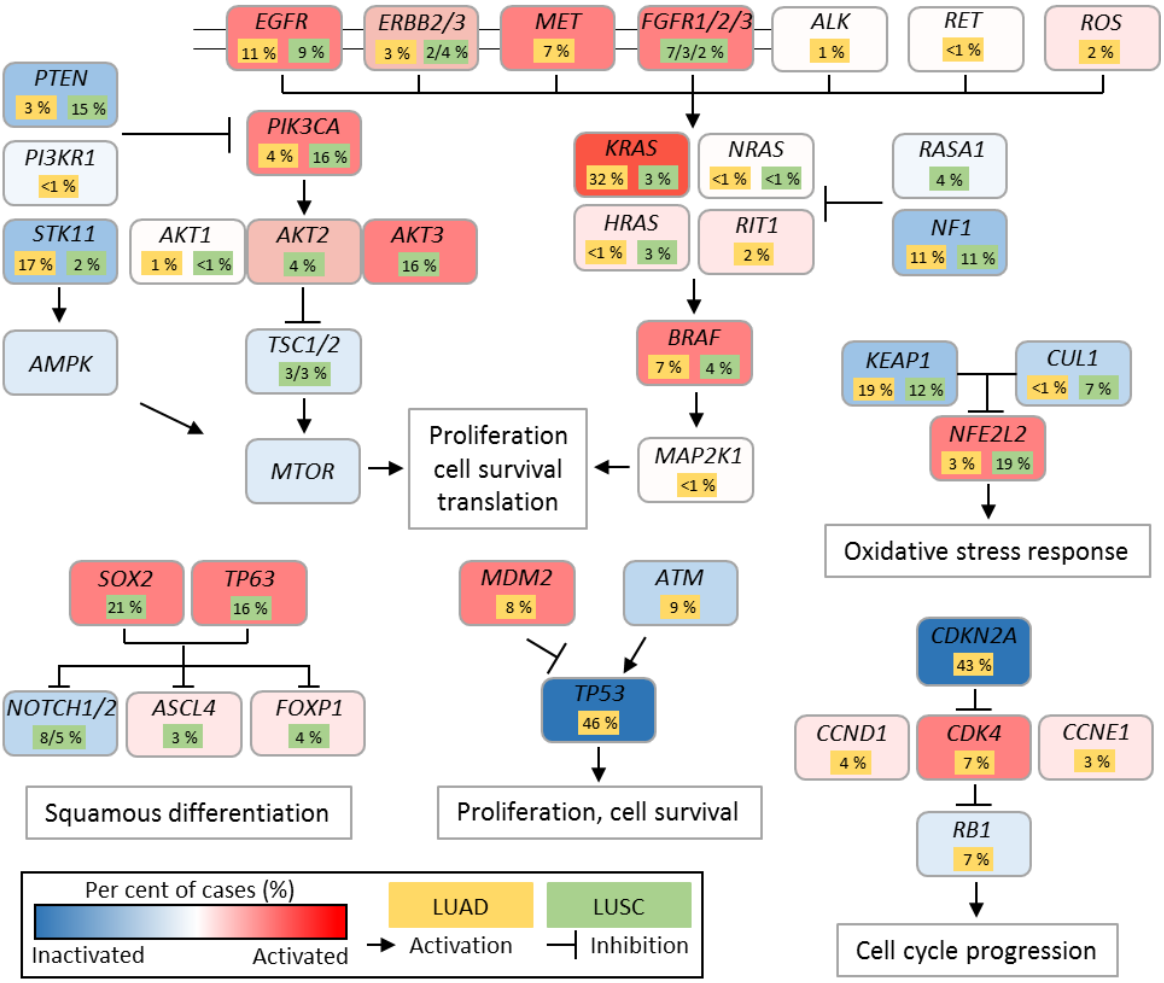

Figure 2: Molecular profiles of the NSCLC subtypes LUAD and LUSC. Proto-oncogenes (red) and tumor suppressor genes (blue) of lung adenocarcinoma (LUAD) and squamous cell carcinoma (LUSC). The molecular profiles are divided in proliferation, cell survival, translation; oxidative stress response; squamous differentiation and cell cycle progression. Color intensities reflect the incidence of occurring mutations, percentages are stated below the genes. Arrows display activation or inhibition of pathways, genes or processes (modified from CGARN, 2012; CGARN, 2014 and Herbst *et al.,* 2018).

1.2.2 Lung cancer therapy and prediction

Based on type, stage and molecular characteristics of lung cancer, treatment options are surgery, radiation therapy, chemotherapy, immunotherapy and targeted therapy.

Surgery is the first option for clinical stage I for early or locally advanced tumors (stage II). Adjuvant platinum-based chemotherapy for stage II NSCLC was shown to be beneficial representing the best option for long-term survival. For patients with unresectable tumors, radiation therapy is recommended. It is one of the most common treatment options for

cancer and can be used alone or in combination with other treatment choices like surgery or chemotherapy (Sangha *et al.*, 2010; Howington *et al.*, 2013).

More than 70 % of NSCLC patients are diagnosed at advanced or even metastatic stage (stage III and IV) (Travis *et al.*, 2013). Stage III NSCLC is heterogeneous and the treatment strategies are determined by tumor location and whether it is resectable or not. The 5-year survival rate is between 10-15 %. Besides surgery and radiotherapy, first line chemotherapy alone or combined with targeted therapy is recommended and often used as palliative treatment (Lemjabbar-alaoui *et al.*, 2016). Chemotherapy works through the whole body by targeting cells with high duplication rates and cannot distinguish between cancer cells and healthy cells. Drugs used in the context of targeted therapies focus on specific differences of the cancer cells that set them apart from healthy cells. The possibility of molecular profiling of the tumor tissue enables a personalized targeted tumor therapy.

Molecular testing is recommended in all patients with advanced LUAD to identify oncogenic driver mutations to predict the response to specific therapies (Villaruz *et al.*, 2013). Non-invasive blood based analysis from somatic mutations and biomarkers provide prognostic values and can help with treatment decisions and tumor monitoring during treatment without invasive procedures (Garcia *et al.*, 2017; Xu-Welliver and Carbone, 2017).

One possibility to directly target the cancer cells are monoclonal antibodies directed to the receptor on the ligand binding site. The other option uses small molecule compounds that interact with different relevant targets. Targeted therapy directly interacts with the modified proteins and usually interrupts the corresponding signaling process. Most small molecule compounds target receptor tyrosine kinases or serine/threonine protein kinases and interact with the kinase domain and the ATP binding pocket of the proteins (Fry, 2003). In the last years first line treatment with chemotherapeutics was partially extended or replaced by targeted therapies.

Activating mutations in EGFR and KRAS occurred more frequently in never smokers than in smokers (Rudin *et al.*, 2009). Somatic mutations in the EGFR occur in 10 % of NSCLC cases in North America and Western Europe. In patients with Asian descent, 30-40 % of the cases have these mutations. In non-smokers with NSCLC the EGFR mutation rate is even greater than 50 % (Sharma *et al.*, 2007). EGFR mutations are associated with prolonged progression free time and showed significantly better clinical outcomes than patients with wildtype EGFR tumors (Eberhard *et al.*, 2005). The modified kinases are 10 to 50-fold more active

than the wildtypes. Some compounds bind with a greater affinity to the mutant, than to the wildtype kinase (Eck and Yun, 2010). Tumors with activating mutations in *EGFR* show striking responses to TKIs like Gefitinib (Lynch *et al.* 2004). 85 % of the mutations in exon 19 and exon 21 in the EGFR gene are associated with sensitivity of treatment with TKIs like Erlotinib and Gefitinib (Fig. 3) (Paez *et al.*, 2004; Pao *et al.*, 2004). However, 50 % of the patients treated with TKIs develop drug resistance by additionally occurring mutations in presence of the drug. The emerging EGFR T790M mutations as well as KRAS mutations are most frequently associated with Erlotinib and Gefitinib treatment and resistance (Pao *et al.* 2005a; Pao *et al.* 2005b). It is assumed that the T790M mutation alone may mediate alterations in EGFR signaling, too. A germline mutation in this amino acid is associated with familiar NSCLC (Bell *et al.*, 2005).

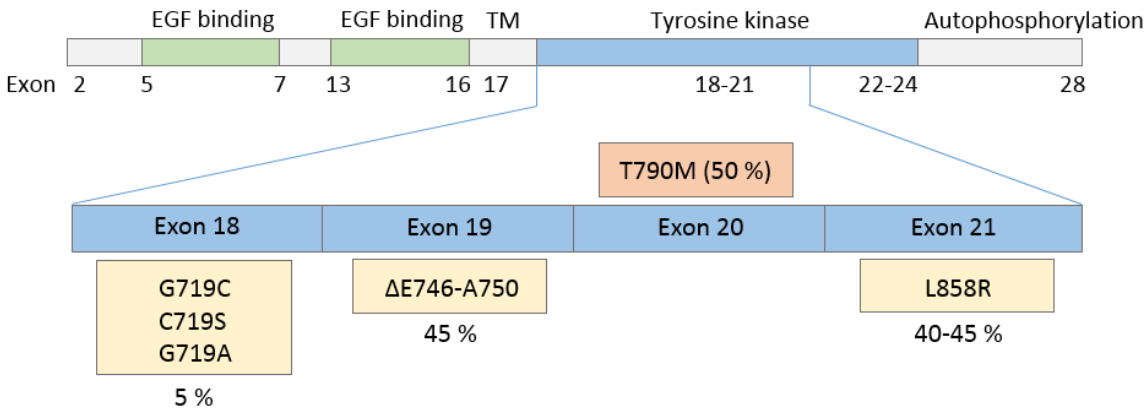

Figure 3: Most frequently activating mutations in the tyrosine kinase domain of the EGFR. The gene sequence of the EGFR gene is depicted, showing the corresponding domains of the protein above. The epidermal growth factor (EGF) binding sites of the extracellular domain, transmembrane domain (TM) and the intracellular domain with the tyrosine kinase domain and the autophosphorylation site is represented. Exon 18-21 of the tyrosine kinase domain is expanded. Recurrent mutations and deletions are represented in yellow boxes (percentages of the cases are shown). The arising mutation after treatment with specific TKIs (Gefitinib and Erlotinib) is represented in the orange box (according to Sharma *et al.,* 2007).

1.3 *Drosophila melanogaster* in cancer research

The fruit fly *Drosophila* is a favored model organism with the advantages of a rapid life cycle, low chromosome number and genome size and easy genetic manipulation. The complete life cycle from the fertilization to the emergence of the adult fly is completed in ten days at 25 °C (Fig. 4 A). From fertilization to the hatching of the embryo into the first

larval instar it takes one day. The larvae molt after 24 h (second instar) and 48 h (third instar) while feeding and growing. The third instar larvae crawl out of the medium, pupate and undergo metamorphosis by dramatic reorganization of all larval tissues. Most adult structures are generated from imaginal discs that are already set in the early embryo. After pupation the adult flies eclose from the pupae after four to five days.

There are diverse possibilities to genetically modify the fly. The Gal4 system, known from yeast, was introduced in 1993 and became an essential part in the *Drosophila* research field. The bipartite Gal4/UAS expression system enables the targeted expression of genes in a temporal and spatial manner (Fig. 4 B). The transcriptional activator Gal4 is coupled to a tissue-specific promotor/enhancer region and binds to the upstream activating sequence (UAS) fused to a target gene. By crossing of a Gal4 expressing fly (driver) with a UAS carrying fly (responder), the activation of the gene of interest in a tissue-specific pattern dependent on the Gal4 expression can be achieved. This expression system can simply be regulated, by altering the temperature for maximal Gal4 activity (Brand and Perrimon, 1993).

Since the invention of this bipartite system, many improvements were generated. This includes the possibility of site-specific integrations into the genome to provide more reproducibility and more control over the level of construct expression (Groth *et al.*, 2004). Continuing modification guided into a number of improved and refined extensions of the system. In combination with the ubiquitous expression of the heat sensitive Gal4 inhibitor Gal80, temporal control of gene expression can be achieved. The TARGET (temporal and regional gene expression targeting) system is an extension of the Gal4/UAS system and utilizes the temperature sensitive Gal4 repressor Gal80. With a shift to higher temperatures, Gal80 loses the ability to block Gal4 resulting in recovered transcriptional activity of Gal4 (McGuire *et al.*, 2003).

Another advanced approach is to label single cell lineages by generating marked clones of cells. The FLP/FRT-Gal4 system combined with the ability of Gal80 to inhibit Gal4 activity is used in the Mosaic Analysis with a Repressible Cell Marker (MARCM). The FLP recombinase catalyses site-specific recombination between the FRT sites resulting in either wildtype cells carrying the Gal4 repressing Gal80 or mutant cells without Gal80 (Lee and Luo, 1999).

In addition, it is possible to reduce or remove gene expression by RNAi or CRISPR/Cas 9 technologies in combination with the Gal4/UAS system (Dietzl *et al.*, 2007; Gratz *et al.*, 2013).

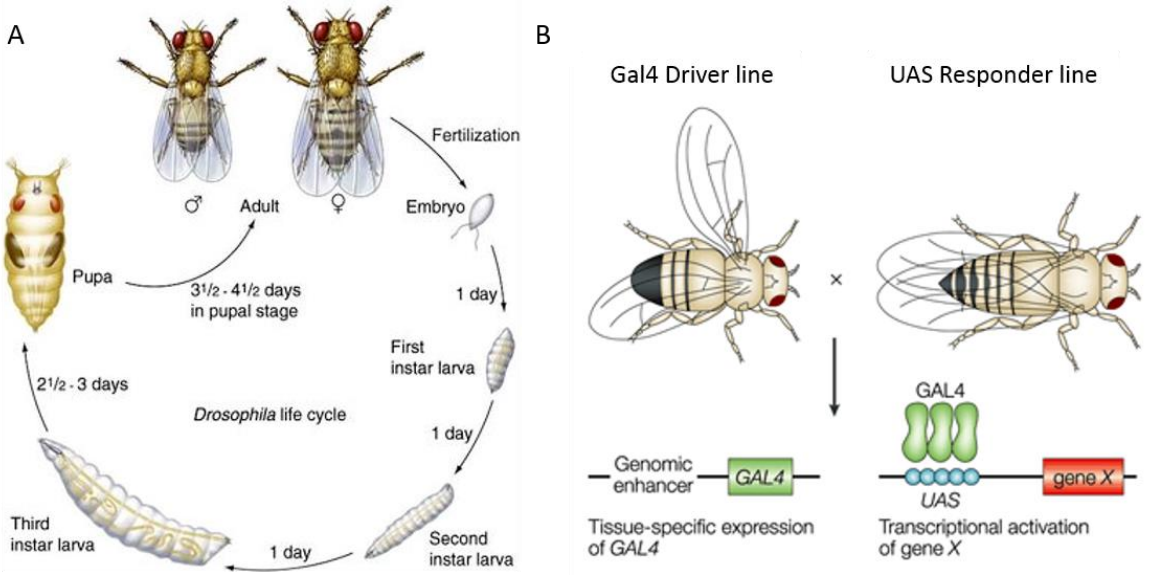

Figure 4: Life cycle and bipartite Gal4/UAS expression system of the model organism *Drosophila melanogaster*. A Life cycle of the fruit fly from the embryo via three larval stages, the pupal stage into the adult fly takes about 10 days at 25 °C (from https://www.creative-diagnostics.com/Drosophila.htm.htm). **B** The driver line comprise the tissue specific enhancer/promotor fused to the transcriptional activator Gal4. The responder line comprises the upstream activating sequence (UAS) fused to the gene of interest. By crossing of both lines, a tissue specific gene expression in a spatial and temporal manner dependent on Gal4 expression is achieved (according to St Johnston, 2002).

1.3.1 Modelling cancer in *Drosophila*

The whole genome of the fruit fly was sequenced in 2000. The genome is 180 Mb in size and contains approximately 13,600 genes distributed on four chromosomes (Adams *et al.*, 2000). Roughly, 60 % of human disease genes appear to have an ortholog in *Drosophila*. From the examined cancer genes, there are even 68 % with a counterpart in the fly (Rubin *et al.*, 2000).

Based on this information, it is possible to study important factors in order to understand not only the function of single oncogenes and tumor suppressor genes, but also complex tumor promoting mechanisms like cell polarity, cell-cell competition, EMT, relevance of the tumor microenvironment, apoptosis and metastasis (Papagiannouli and Mechler, 2013).

Four of the hallmarks of cancer can be adopted in *Drosophila*: self-sufficiency in growth/proliferation signals, insensitivity to anti-proliferative signals, evading apoptosis and invasion/metastasis. The simplicity of the model has the consequence that fewer

mutations are needed for the development of tumors. This makes the study of specific gene functions and processes much easier (Brumby and Richardson, 2005).

Lethal giant larvae (*Lgl*) was the first discovered tumor suppressor gene in *Drosophila*. Lack of Lgl function leads to tumor phenotypes in the imaginal disc and the adult brain of *Drosophila* (Gateff and Schneiderman, 1974). Mutations in the *Disc large* (*Dlg*) gene, a protein of the septate junctions and a *Scribble* mutant caused very similar phenotypes (Stewart *et al.*, 1972; Bilder *et al.,* 2000). Not only tumor suppressor genes were discovered in *Drosophila*. The presence of proto-oncogenes like *Egfr*, *Ras* and *Raf* as well as the high sequence similarities to their vertebrate counterparts is not only well-known, it was also pioneered in *Drosophila* (Shilo, 1987).

There are many studies where alteration of a single gene leads to hyperplasia and changes in a variety of tissues, but only additionally occurring alterations of a second gene can result in overgrowth and invasive neoplastic tumors. Constitutive activation of Egfr in the wing imaginal discs leads to overgrowth. In combination with the tumor suppressor gene *Socs36E* neoplastic transformation with loss of apical-basal polarity can be observed (Herranz *et al.*, 2012).

Nevertheless one-hit gene models with altered tumor suppressor genes or proto-oncogenes are suitable to analyze loss of tissue architecture, overproliferation, differentiation defects and increased invasion (Brumby and Richardson, 2005). *Drosophila* can serve as an alternative to vertebrates and is successfully used in cancer research and also in drug screenings. Actually, there is already a clinical application of a compound investigated in *Drosophila* as a lead hit with effect on a Ret-based tumor model (Vidal *et al.*, 2005; Das and Cagan, 2013).

1.3.2 Epidermal growth factor receptor (Egfr) pathway

EGFR belongs to the human epidermal growth factor receptor (HER/*erb*B) protein family of receptor tyrosine kinases (RTKs) in mammals. This family includes HER1 (EGFR/*erb*B1), HER2 (*erb*B2), HER3 (*erb*B3) and HER4 (*erb*B4) (Yarden and Sliwkowski, 2001). The receptors show a similar structure with extracellular cysteine-rich ligand binding domains, an alpha-helical transmembrane domain, cytoplasmic tyrosine kinase domain and a carboxy-terminal signaling domain with five autophosphorylation motifs and at least three

internalization motifs (Wells, 1999). There are seven known ligands for the EGFR receptor in humans. All of them are membrane bound and undergo cleavage for activation. The cysteine rich EGF motif is crucial for receptor binding (Harris *et al.*, 2003). Ligand binding induces homodimerization or heterodimerization with a second HER/*erbB* receptor. This is followed by ATP-dependent autophosphorylation of the kinase domain in the cytoplasm (Yarden and Schlessinger, 1987). The targeted signaling pathway depends on the cellular context, the ErbB dimer and on the binding ligand. Ligand dependent activation of the pathway activates several downstream pathways, including Ras/MAPK pathway, PI3K/AKT and phospholipase C (PLC)/ protein kinase (PKC) signaling cascade, involved in cell division and migration, adhesion, differentiation and apoptosis (Yarden and Sliwkowski, 2001).

In the fly´s genome there is only one member of the EGFR/*erb*B family present. The *Drosophila* epidermal growth factor receptor (Egfr) is similar to the mammalian counterparts in structure and in the addressed signaling pathways (Livneh *et al.*, 1985; Shilo, 2003). There are four activating and one inhibitory ligand present in *Drosophila*. The three TGF-α homologues Spitz, Keren and Gurken are produced as transmembrane precursors and bind to Egfr in the processed form (Rutledge *et al.*, 1992; Reich and Shilo, 2002; Shmueli *et al.*, 2002) (Fig. 5). Vein is a secreted ligand with tissue specific low activation level and similarities to vertebrate neuregulins (Schnepp *et al.*, 1996). Argos, the last secreted ligand inhibits Egfr signaling by competing with the other activating ligands on receptor binding (Jin *et al.*, 2000). The transmembrane protein Kekkon is the second part of the negative feedback regulation of receptor signaling, by interacting directly with the receptor (Ghiglione *et al.*, 1999). The third component is the intracellular protein Sprouty, whitch interacts with downstream signaling elements that are shared with other signaling pathways (Casci *et al.* 1999).

After ligand binding, Egfr forms a dimer, which is followed by autophosphorylation of the kinase domain. Downstream of receptor kinase (Drk, homolog of mammalian Grb2) binds to the phosphorylated tyrosine kinase domain of the receptor (Fig. 5). Drk interacts with Son of sevenless (Sos) which activates Ras by promoting GTP binding. Ras activates the serin-threonine protein kinase Raf. This is followed by direct phosphorylation and thereby activation of Mitogen activated protein kinase (MAPK)/Extracellular signal-regulated kinase (ERK) kinase (MEK). MEK activates Rolled, the *Drosophila* MAP kinase Extracellular Signal-Regulated Kinase (ERK). Activated Rolled phosphorylates the transcription factors Pointed

and Yan (Lusk *et al.,* 2017). Yan acts as repressor of the Egf pathway, whereas activation of Pointed leads to target gene transcription (Gabay *et al.*, 1996).

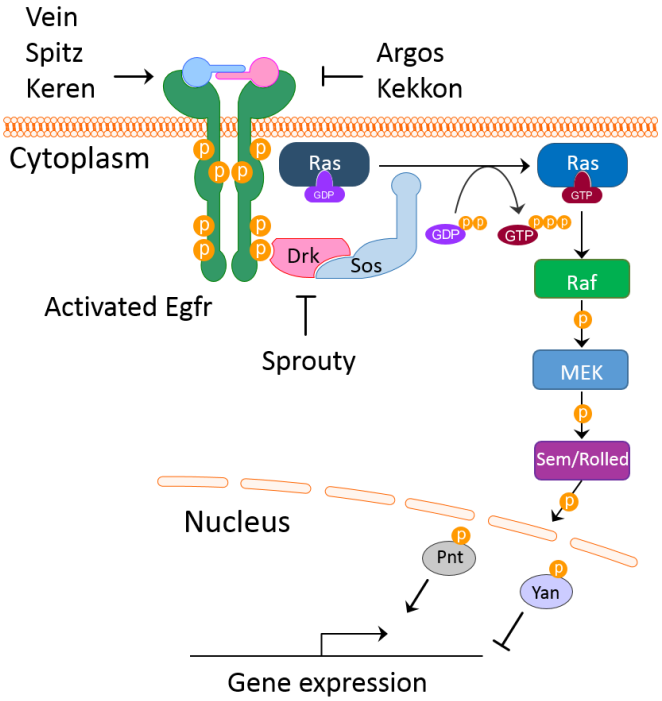

Figure 5: Epidermal growth factor receptor (Egfr) pathway in *Drosophila*. Egfr signaling is activated by the three ligands Vein, Spitz and Keren. The fourth ligand, Argos, inhibits signaling, as well as the membrane protein Kekkon does. Ligand binding leads to receptor dimerization and phosphorylation. Signal transduction occurs via Drk, Sos, Ras, Raf, MEK and Rolled to the activation of the transcription factors Pnt and Yan. Yan acts as repressor, whereas activation of Pointed leads to target gene transcription. Drk = Downstream of receptor, Sos = Son of sevenless, Ras = Rat sarcoma, Raf = Rapidly accelerated fibrosarcoma, MEK = Mitogen Activated Protein Kinase (MAPK)/ Extracellular Signal-regulated Kinase (ERK) kinase, Pnt = Pointed (according to Lusk *et al.,* 2017).

The EGFR is one of the most frequently mutated genes in lung cancer. Overexpression and somatic mutations of the EGFR have been described as well as ligand overexpression and amplification. Somatic mutations comprise in-frame deletions in exon 19 or amino acid substitutions in exon 21 around the ATP-binding pocket of the tyrosine kinase domain. These mutations are the most common mutations in EGFR positive tumors (Lynch *et al.*, 2004).

1.3.3 NF-κB signaling

The immune deficiency (IMD) signaling in *Drosophila* is part of the humoral immune response and regulates the activity of Relish, one of three *Drosophila* Nuclear factor κB (NF-κB) proteins representatives (Fig. 6). Microbial recognition occurs by the pattern recognition receptors (PRRs) called peptidoglycan recognition proteins (PGRPs) (Dushay *et al.*, 1996; Hedengren *et al.*, 1999). Insect PGRPs are classified as long (L) or short (S) and can be intracellular, extracellular or transmembrane proteins with different functions (Werner *et al.*, 2000, 2003). Transmembraneous PGRP-LC is the main activator of IMD signaling that recognizes diaminopimelic acid (DAP) type peptidoglycane (PGN) or tracheal cytotoxin (TCT), a monomeric fragment of gram-negative PGN (Kaneko *et al.*, 2004; Chang *et al.*, 2006). PGRP-LE can be secreted extracellularly into the hemolymph and support PGRP-LC mediated signaling, or being present in the cytoplasm and acting as an intracellular receptor (Kaneko *et al.*, 2006).

Binding of PGN to the receptor leads to dimerization and to activation of the downstream signaling cascade with the activation of Immune deficiency (IMD), the homolog to the human Receptor Interacting Protein (RIP), that acts upstream of the Inhibitor of κB (IκB) complex and the caspase Dredd (Death related ced-3/Nedd-like caspase) in NF-κB signaling (Georgel *et al.*, 2001; Choe *et al.*, 2005). Dredd, the *Drosophila* homolog to mammalian Caspase-8, is thought to be the endoprotease for the transcription factor Relish (Stoven *et al.*, 2003). It interacts and is proteolytically processed by Fadd (Fas-associated death domain) (Hu and Yang, 2000). Dredd is induced by ubiquitylation by Inhibitor of apoptosis-2 (Iap-2) and is also required for IMD processing (Meinander *et al.*, 2012). The *Drosophila* IκB kinase complex with the proteins Kenny and Ird5 is homologous to mammalian IKKγ and IKKβ and induce proteolytic cleavage of Relish by phosphorylation (Silverman *et al.*, 2000). The N-terminal part of Relish then translocates to the nucleus and activates transcription of immune relevant genes.

The Transforming growth factor-activating kinase-1 (Tak1) is homologous to the mammalian MAPK kinase kinase and activates both Relish and JNK pathway, by phosphorylating the IκB complex and by activation of Hemipterous (Hep) the *Drosophila* JNK kinase activating-kinase (Silverman *et al.*, 2003). Furthermore, there is a regulated cross-talk between both pathways via TAK1 degradation (Park *et al.*, 2004). The *Drosophila*

IMD pathway is homologous to mammalian TNF/ NF-κB signaling. The NF-κB pathway is a common pathway for the adaption of cells to stressors such as infections and hypoxia. It mediates a number of genes that are also involved in tumorigenesis (Garg and Aggarwal, 2002). NF-κB is upregulated in lung cancer and was detected in LUAD with oncogenic KRAS or with EGFR mutations representing a possible target in lung cancer treatment (Tang *et al.*, 2006; Chen *et al.*, 2011). In mutant EGFR tumors treated with Erlotinib, an increased NF-κB expression was detected. Combined NF-κB and EGFR inhibition in mutant EGFR tumors could display a promising treatment approach (Bivona *et al.* 2011). In tumors a dual role of NF-κB was observed. On one side NFκB is seen as an anti-apoptotic factor with tumor promoting properties. Activated Ras or oncogenic kinases as well as the Akt pathway can activate NF-κB. On the other side NF-κB can function as a proapoptotic factor in certain circumstances (Radhakrishnan and Kamalakaran, 2006).

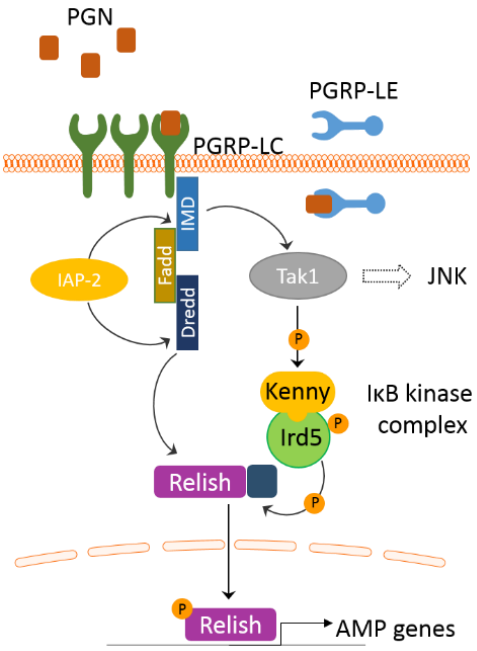

Figure 6: Immune deficiency (IMD) pathway in *Drosophila*. PGN from gram-negative bacteria is recognized by PGRP receptors. Downstream IMD is processed by Iap-2, which is also responsible for Dredd activation via Fadd activity. IMD activates Tak1 which in turn activates the IκB complex by phosphorylation. Subsequent phoyphorylation of Relish with accompanied cleavage by Dredd leads to translocation of the N-terminal part of Relish to the nucleus and activation of AMP genes. Tak1 activates both, NF-κB and JNK signaling. PGN= peptidoglycane, PGRP = peptidoglycane recognition protein, Iap-2 = inhibitor of apoptosis, IMD = immune deficiency, Fadd = Fas-associated death domain, Dredd = death related ced-3/Nedd-like caspase, Tak1 = transforming growth factor-activating kinase1, Ird5 = immune response deficient 5, IκB = inhibitor of kappa B, AMP = antimicrobial peptides, JNK = c-Jun N-terminal kinases (according to Falschlehner and Boutros, 2012).

1.3.4 The tracheal system of *Drosophila* larvae

The respiratory system of the larvae consists of an interconnected tubular network of branched trachea that is made of a simple epidermal monolayer (Fig. 7 A). The air enters through the spiracular openings into the main dorsal trunks and it diffuses further into the primary and secondary branches up to the fine blindly ending branches of the terminal cells. These cells are connected to all organs of the larvae to supply oxygen directly to the target tissues (Ghabrial *et al.*, 2003). The whole tracheal system is covered by a stabilizing and protective chitinous lining (Uv *et al.*, 2003).

The network is bilaterally symmetrically constructed with repeated segmental organization. It origins from ten clusters (Tr1-Tr10) of around 80 precursor cells on each side of the embryo, which occur already five hours after egg laying. The total number of cells does not increase after stage 11 of the embryonic development (Fig. 7 B). Hence, the growth of the tracheal system occurs by migration, rearrangement of tracheal cells and cell elongation (Samakovlis *et al.* 1996a). The key regulator of tracheal fate determination of the precursor cells is the pHLH-PAS transcription factor trachealess (trh) (Wilk, Weizman and Shilo, 1996). The placodes of the precursor cells invaginate from the ectoderm and form the epidermal tracheal sacs, whereof a migration of six primary tracheal branches occurs. Several hours later, the secondary branches are formed and sprout into numerous terminal branches (tracheoles) in each thoracic and abdominal hemisegment (T2 to A8) (Samakovlis *et al.* 1996a). The branching pattern of the primary and secondary branches in the individual hemisegments differ, but the overall organization is still stereotypical. Each secondary branch is formed by a single tracheal cell. The terminal cells originate out of a subset of secondary branch cells. The sprouting of these cells starts in late embryogenesis and continues throughout the larval period. The cells of the dorsal trunks are connected through intercellular junctions (Fig. 7 C). The secondary branches build autocelluar junctions with the same cell. The terminal cells form the lumen in the cytoplasm to build seamless tubes without junctions, the terminal branches. The apical side of all tracheal cells is orientated to the lumen of the tube (Samakovlis *et al.* 1996a). The dorsal trunks, primary and secondary branches of the adjacent hemisegments fuse symmetrically to the interconnected network of the completed embryonic tracheal system to build a continuous and closed tubular network (Samakovlis *et al.* 1996b).

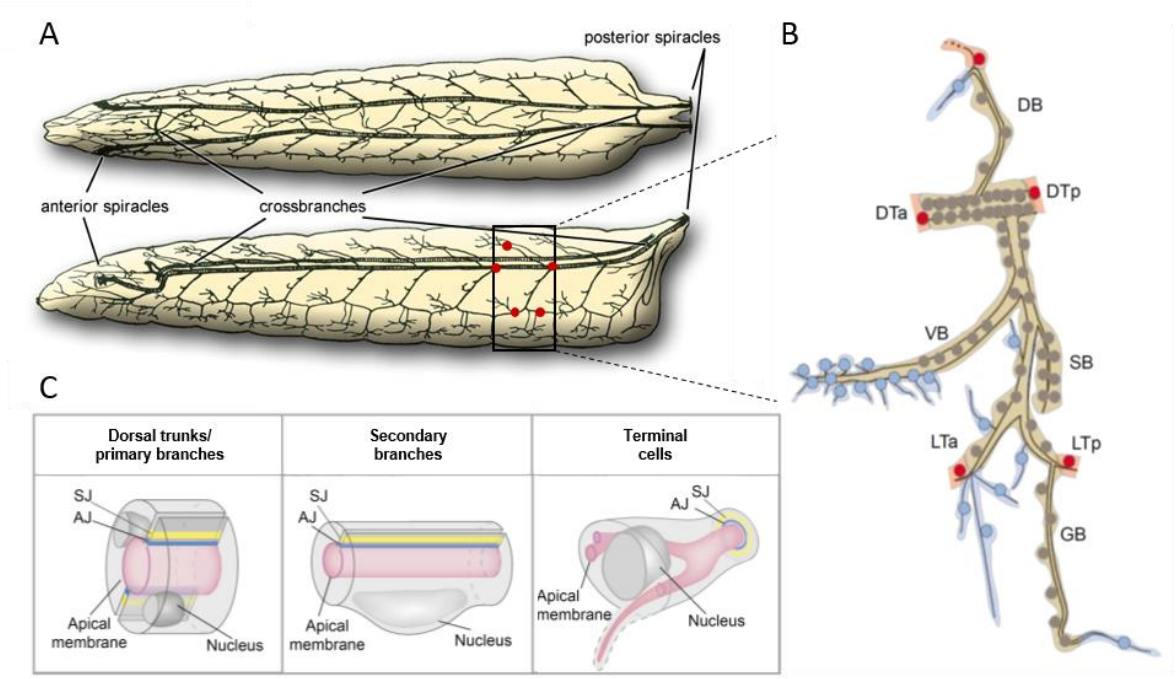

Figure 7: Organization of the tracheal system in *Drosophila* larvae. A The tracheal system throughout the whole larval body from dorsal (top) and lateral side (below) (FlyMove). **B** Single tracheal metamere with dorsal trunks, branched into primary, secondary and terminal branches. Single cell types are displayed as circles in brown (stalk cells of the branches), red (fusion cells between the metameres) and blue (terminal cells). DTa = Dorsal trunk anterior, DTp = Dorsal trunk posterior, DB = Dorsal branch, VB = Visceral branch, SB = Spiracular branch, LT = Lateral trunk (anterior/posterior), GB = Ganglionic branch. **C** Cellular structure in dorsal trunks and primary branches with intracellular junctions, Secondary branches with autocellular junctions and seamless terminal cells. SJ = Septate junction, AJ = Adherens junction (modified according to Uv *et al.,* 2003).

The fibroblast growth factor receptor (FGFR) signaling is required for tracheal cell migration and branching events during embryonic development, in the terminal cells while the larval stages as response to hypoxia and in the remodeling from larval to adult tracheal system (Klämbt *et al.* 1992; Lee *et al.* 1996; Jarecki *et al.* 1999; Sato and Kornberg 2002). The Breathless (Btl) pathway in *Drosophila* is homologous to the FGFR pathway in mammals and is involved in comparable processes (Peters *et al.*, 1994; Sekine *et al.*, 1999). The Btl ligand branchless (Bnl) is homologous to the mammalian FGF (Sutherland *et al.*, 1996). Localized expression of Bnl in the surrounding tissue acts as a chemoattractant and activates the receptor tyrosine kinase Btl through binding and thereby induces directed tracheal branching and outgrowth, similarly as FGF-10 does in mammals (Glazer and Shilo, 1991; Bellusci *et al.*, 1997; Park *et al.*, 1998). The triggered signaling cascade proceed via Ras/MAPK in the transcription of target genes in cell division and survival (Cabernard and Affolter, 2005). Transmission of the signal to Ras occurs through the adaptor protein

Downstream of FGFR (Dof). Dof is only expressed in FGFR expressing cells and functions exclusively for FGFR-mediated signal transduction. By interaction with the receptor, Dof becomes phosphorylated and recruits the phosphatase Corkscrew (Csw) which guides to activation of cell migration and the Ras/MAPK pathway (Vincent *et al.*, 1998). Sprouty acts as an FGF antagonist and inhibits tracheal branch formation, as well as lung growth and morphogenesis in the mouse (Hacohen *et al.*, 1998; Mailleux *et al.*, 2001).

Terminal cell branching in the embryo requires the transcription factor *Drosophila* Serum Response Factor (DSRF) (Guillemin *et al.*, 1996). Terminal cell branching and cytoplasmic outgrowth arise towards oxygen starved tissues during the larval stages. Oxygen undersupply of the tissue or the whole larvae can induce branching (Jarecki *et al.*, 1999). This process is stimulated by the expression of Bnl. Hypoxia leads to the accumulation of Sima in non-tracheal cells through the oxygen sensor Fatiga. Sima represents the *Drosophila* homolog of the mammalian Hypoxia-Inducing Factor (HIF)-α. Simultaneous expression of the Bnl receptor Btl in the tracheal cells leads to a sensitized cell for Bnl recognition and induction of branching (Centanin *et al.*, 2008). The development and plasticity of the tracheal system provides similarities to the tubulogenesis of tubular organs like the vascular system or the lung. This includes not only the mechanisms of epithelial cell cohesion, cell rearrangement and regulated growth of subcellular domains but also the underlying effector molecules (Uv *et al.*, 2003; Affolter and Caussinus, 2008).

1.4 Aim of the study

Cancer and in particular lung cancer is a consistent burden characterized by numerous new cases and death cases each year and an exceptionally low survival rate. The severe clinical outcome underlines the necessity of new treatment options and new therapeutics could contribute to prevent recurrence and resistance of tumors to enable a better outcome even at late state detection. The generation of molecular profiles of tumors provides us with the information about the mutations that underlie tumor progression, which is a prerequisite to utilize targeted treatments. Small compounds with inhibiting effects on tumor driver gene products improved the clinical outcome in the last decades substantially. Traditionally, small molecule drug screening approaches are based on *in vitro* cell culture systems, biochemical assays or receptor binding assays with limited predictive values for a

future clinical outcome. Many of the identified small molecule hits did not pass the requirements or turned out toxic *in vivo*, making a subsequently following chemical optimization necessary (Pandey and Nichols, 2011). Whole animal screening models provide many advantages over *in vitro* testings but require large numbers of animals to ensure the desired outcome. The discovery of new drugs requires experimental testings and finally have to be verified using vertebrate models as well as in other pre-clinical and clinical studies. Invertebrates like the fruit fly *Drosophila melanogster* are suitable models to confine the use of vertebrates like mice or even pigs substantially (Segatto *et al.*, 2017). *Drosophila* models are a good alternative to other experimental models by providing a whole animal background in contrast to cell culture systems, while being less complex than vertebrate systems such as mice. It is a well-established model organism in several research fields including the modelling of human disease. Orthologues of most cancer genes can be found in the *Drosophila* genome and take part in similar pathways and similar physiological processes.

The major aim of this study was, to investigate the impact of different LUAD and LUSC related oncogenes on the tracheal system of *Drosophila melanogaster*. It should be elucidated if tailored *Drososphila* models where these oncogenes are specifically targeted to the airway epithelium of the fly can induce tumor like structures in the organ. Moreover, suitable transgenic systems should be developed that allow for informative high-throughput screening approaches in a whole animal setting.

In a second part of the thesis, the effects of targeted manipulation of a subtype of airway epithelial cells, namely the tracheal terminal cells should be elucidated.

2 Material and Methods

2.1 Devices

Analytical balance (ABS)	Kern & Sohn GmbH(Balingen, Germany)
AxioImager	Zeiss (Oberkochen, Germany)
Balance (MXX-412)	Denver Instrument GmbH (New York, USA)
Bead ruptor 24	Omni International (Kennesaw, USA)
Centrifuge (5415 D)	Eppendorf (Hamburg, Germany)
Centrifuge (5417 R)	Eppendorf (Hamburg, Germany)
Electrophoresis chambers	Biometra GmbH (Göttingen, Germany)
Geldocumentation (Transilluminator)	Heinrich Eimecke GmbH (Kiel, Germany)
Incubator (TH30)	Edmund Bühler GmbH (Tübingen, Germany)
Incubators (WB250K)	Heinrich Eimecke GmbH (Kiel, Germany)
LabGard (IBS)	INTEGRA biosciences GmbH (Biebertal, Germany)
Light source (U-RFL-T)	Olympus (Hamburg, Germany)
Magnetic stirrer (RET)	IKA®(Staufen, Germany)
Magnetic stirrer (MR3001)	Heidolph (Schwabach, Germany)
Multipette (Xstream)	Eppendorf (Hamburg, Germany)
O_2 electrode (GOX 100)	Greisinger (Regenstauf, Germany)
pH 340/ION	WTW (Weilheim, Germany)
Power supply (EV245)	Consort^{NT} (Nürnberg, Germany)
Stereo microscope (MZ10F)	Leica Microsystems (Wetzlar, Germany)
Stereo microscope (S6E)	Leica (Wetzlar, Germany)
Stereo microscope (Stemi 506)	Zeiss (Oberkochen, Germany)
Stereo microscope, fluorescence (SZX12)	Olympus (Hamburg, Germany)
Spectrophotometer (DS-11)	DeNovix® (Wilmington, USA)
Thermocycler (Labcycler)	SensoQuest GmbH (Göttingen, Germany)
Thermomixer comfort	Eppendorf (Hamburg, Germany)
Water bath	Memmert (Schwabach, Germany)

2.2 General materials

Air-permeable membrane	nerbe plus GmbH (Winsen, Germany)
Ceapren stopper (Ø 50 mm)	Greiner Bio-One (Kremsmünster, Austria)
Cellulose stopper (Ø 29 mm)	nerbe plus GmbH (Winsen, Germany)
Cell spreader	nerbe plus GmbH (Winsen, Germany)
Combitips (advanced, 10 ml)	Eppendorf (Hamburg, Germany)
Cover slips (24 x 50 mm)	Carl Roth (Karlsruhe, Germany)
Deep well plates, 96-well	nerbe plus GmbH (Winsen, Germany)
Drosophila food vial (50 ml)	nerbe plus GmbH (Winsen, Germany)
Drosophila food vial (16 ml, 175 ml)	Greiner Bio-One (Kremsmünster, Austria)
Embryo collection container	Kisker Biotech GmbH (Steinfurt, Germany)
Falcon tubes (15 ml, 50 ml)	nerbe plus GmbH (Winsen, Germany)
Filtropour BT50	Sarstedt (Nümbrecht, Germany)
Forceps	neoLab® (Heidelberg, Germany)
Gossamer, 150 µm	Eydam (Kiel, Germany)

Petri dishes, plastic	nerbe plus GmbH (Winsen, Germany)
Reaction tubes, low binding (0.2, 0.5, 1.5, 2 ml)	nerbe plus GmbH (Winsen, Germany)
Reaction tube, screw, 2 ml	Sarstedt (Nümbrecht, Germany)
Serological pipettes (5 ml, 10 ml, 25 ml)	nerbe plus GmbH (Winsen, Germany)
Slides	Carl Roth (Karlsruhe, Germany)
Tips, low-binding (10, 100, 1000 µl)	nerbe plus GmbH (Winsen, Germany)

2.3 General chemicals

Agarose	Biolab products (Bebensee, Germany)
Agarose (low-melt)	Biolab products (Bebensee, Germany)
Afatinib	Enzo Life Sciences (Lörrach, Germany)
Alectinib	Selleck Chemicals (Munich, Germany)
Ampicillin	Sigma Aldrich (Munich, Germany)
Apple juice	Stute (Paderborn, Germany)
brewer`s yeast	Leiber (Bramsche, Germany)
Ceritinib	Selleck Chemicals (Munich, Germany)
Cornmeal	Mühle Schlingemann (Waltrop, Germany)
Crizotinib	Enzo Life Sciences (Lörrach, Germany)
dNTPs	Promega (Madison, USA)
Docetaxel	Selleck Chemicals (Munich, Germany)
Erlotinib	Selleck Chemicals (Munich, Germany)
Fluvastatin	Enzo life Sciences (Lörrach, Germany)
Gefitinib	Selleck Chemicals (Munich, Germany)
Kanamycin	Sigma Aldrich (Munich, Germany)
Mops	Sigma Aldrich (Munich, Germany)
Molasses	Biohof Heidelicht (Gerdau, Germany)
Methyl 4-Hydroxybenzoate reagentplus® (nipagin)	Sigma Aldrich (Munich, Germany)
Midori green	Nippon Genetics Europe (Düren, Germany)
Normal goat serum	Sigma-Aldrich (Munich, Germany)
Paclitaxel	Selleck Chemicals (Munich, Germany)
PFA	Polysciences Inc. (Warrington, USA)
Sugar beet syrup	Kanne Brottrunk (Selm-Bork, Germany)
Trametinib	Selleck Chemicals (Munich, Germany)
Tryptone	BD (Franklin Lakes, USA)
Xylene cyanol FF	AppliChem (Darmstadt, Germany)
Yeast extract	BD (Franklin Lakes, USA)

Unless not otherwise stated, all other chemicals were purchased from Carl Roth (Karlsruhe, Germany).

2.4 Drug libraries

FDA-approved drug library-978	Selleck Chemicals (Munich, Germany)

2.5 Oligonucleotides

Table 1: Primer and primer sequences for cloning of *ppk11*-Gal4

Primer	**5´ → 3` Sequence**
PPK11-Prom-BamHI-F2	GAGAGGATCCGGCAACCTTGGTTTTGAAACG
PPK11-Prom-R-XhoI	GAGACTCGAGACTACTTGGAAAGTAATCAATG
Ppk11-Prom113-F3	GTAACGGAGGGAGGCTTATC
Ppk11-Prom2222-R2	GAGCTTGCAGGAATCCAAGG
pENTR-454seq_F	GGCTTCGAAGGAGATAGAAC
pENTR-2101seq_R	GCAGCTGGATGGCAAATAATG
pBPGUw41-seq-F	GGCGTATCACGAGGCCC
pBPGUw1814-seq-R	CCGCTGCGCTCGATCCC

2.6 Enzymes and Kits

*Bam*HI	Thermo Scientific (Waltham, USA)
GeneRuler 1 kb DNA Ladder	Thermo Scientific (Waltham, USA)
FastAP Thermosensitive Alkaline Phosphatase	Thermo Scientific (Waltham, USA)
Gateway™ LR Clonase™ Enzyme mix	Thermo Scientific (Waltham, USA)
JETSTAR Plasmid Purifikation Kit	Genprice (San Jose, USA)
T4 DNA Ligase	Thermo Scientific (Waltham, USA)
NucleoSpin Gel and PCR Clean-Up	Macherey-Nagel (Düren, Germany)
Pwo DNA POlymerase	Roche (Basel, Switzerland)
SureClean	Bioline (London, UK)
Taq DNA Polymerase	Thermo Scientific (Waltham, USA)
*Xho*I	Thermo Scientific (Waltham, USA)

2.7 Vectors

pBPGUw	Addgene (# 17575) (Gerald Rubin)
pENTR11	Thermo Scientific (Waltham, USA)

2.8 Bacteria

DH5α:

Transformation buffer I (TfBI):

30	mM	kaliumacteat
50	mM	$MnCl_2*4H_2O$
100	mM	KCl
10	mM	$CaCl_2$
15	%	glycerol

ad with H_2O, filter sterilize, storage at 4 °C

Transformation buffer II (TfBII):

10	mM	Mops
75	mM	$CaCl_2$
10	mM	KCl
15	%	glycerol

ad with H_2O, adjust to pH7.0 with NaOH, filter sterilize, storage at 4 °C up to two month

- dilute 1 ml over night culture 1:100 in LB (2.17.4)
- incubate at 37 °C until OD_{600}=0.48-0.5
- centrifugation for 5 min at 3000 rpm in 50 ml tubes
- resolve the pellets in 15 ml ice cold TfBI/50 ml culture
- incubate 15 min on ice
- centrifugation for 5 min at 3000 rpm in 50 ml tubes
- resolve in 4 ml ice cold TfBII
- incubate 15 min on ice
- store 200 µl aliquots at -80 °C

One shot™ *ccdb* Survival™ 2T1^R Invitrogen

2.9 Fly husbandry

Normal medium (NM), 500 ml:

31.25	g	brewer`s yeast
31.25	g	cornmeal
5	g	agar-agar
10	g	glucose monohydrate
15	g	molasses
15	g	sugar beet syrup

add 500 ml H_2O

cooking for 10-15 min in the water bath, autoclaving 15-20 min, cool down to 60 °C

add:

5	ml	10 % (v/v) propionic acid
15	ml	10 % (w/v) nipagin (in 70% Ethanol)

fill directly into appropriate fly vials, storage at 4 °C after cooling

Fly stocks were kept in *Drosophila* food vials with NM at 18 °C at a 12 h light/dark cycle. The flies for the experiments were taken from the stocks and kept at RT. The flies were transferred to new medium every two to three weeks. The handling of the flies was performed on ice, after anesthetization with nitrogen.

2.10 *Drosophila* fly lines and crossings

Concentrated medium (CM):

25	g	yeast extract
43	g	cornmeal
25	g	sucrose
5	g	agar-agar

ad 500 ml H_2O
cooking for 10-15 min in the water bath, autoclaving 15-20 min, cool down to 60 °C
add:

5	ml	10 % (v/v) propionic acid
15	ml	10 % (w/v) nipagin (in 70% Ethanol)

fill directly into appropriate fly vials, storage at 4 °C after cooling

Crossings were performed by using the Gal4/UAS system to get the desired genotypes. The virgin females were collected and mated with the corresponding males in a 1:3 ratio. All experiments were additionally performed with the Gal4/UAS lines crossed to w^{1118} as control. The crossings were kept at 25 °C. The parental flies were put on a new food vial at least every four days. All experiments were performed with the L3 larvae of the F1 generation. The fly lines either were from the Bloomington stock center, gifts from other research groups or generated in the same laboratory. The name of the donors and Bloomington stock numbers are given in Tab. 2. All crossings for the experiments with Afatinib and Gefitinib were kept on CM.

Table 2: *Drosophila* fly lines

Name	Genotype	Vendor
DSRF-GFP-Gal4	*DSRF-Gal4;UAS-GFP*	(Gervais and Casanova, 2011)
ppk4-Gal4	*yw67c23;pkk4-gal4;+/+*	Generated from Christina Wagner
UAS-GFP	*y1 w*; wgSp-1/CyO, P{Wee-P.ph0}BaccWee-P20; P{20XUAS-6XGFP}attP2*	Bloomington (52262)
btl-Gal4	*w-; btl-GAL4, UAS-GFP/Sp; TM2/TM6b*	Leptin Group Heidelberg
UAS-Egfr^{CA}	*w[*]; P{w[+mC]=Egfr.2.A887T.UAS}8-2*	Bloomington (9533)
UAS-hEGFR-Pvr	*w[1118]; M{w[+mC]=UAS-hE-Pvr-GFP}ZH-58A*	Bloomington (58432)
UAS-hEGFR-dEgfr	*w[1118]; M{w[+mC]=UAS-hE-Egfr-GFP}ZH-58A/CyO*	Bloomington (58415)
UAS-Btl	*w[*]; P{w[+mC]=UAS-btl.lambda}2*	Bloomington (29045)
UAS-Pvr	*w[1118]; P{w[+mC]=UAS-Pvr.lambda}mP1v*	Bloomington (58428)
UAS-InR	*y[1] w[1118]; P{w[+mC]=UAS-InR.R418P}2*	Bloomington (8250)
UAS-RPTK:Alk	*UAS-RPTK:Alk HA tagged #3 on 2nd*	Ruth Palmer Lab, Gothenburg
UAS-Ras^{V12}	*w;sp/CyO;UAS-Ras[V12]/TM6B*	China
UAS-Raf^{GOF}	*y,w,p{UAS-RAFgof,w+)/y,w,p{UAS-RAFgof,w+); +/+ ; +/+*	Markstein *et al.,* 2014
UAS-sem	*w;;UAS-sem8.7*	China
UAS-Rl.K	*w[1118]; P{w[+mC]=UAS-rl.K}2A*	Bloomington (36270)
UAS-PI3K92E	*P{w[+mC]=UAS-Pi3K92E.CAAX}1, y[1] w[1118]*	Bloomington (8294)
UAS-Akt1.Exel	*P{UAS-Akt1.Exel}1, y1 w1118*	Bloomington (8192)
UAS-Arm.S10	*P{w[+mC]=UAS-arm.S10}C, y[1] w[1118] (activated)*	Bloomington (4782)
UAS-Cdk4	*w[*]; P{w[+mC]=UAS-Cdk4-myc}II.1*	Bloomington (6631)
UAS-p53	*P{w[+mC]=UAS-p53.H159N.Ex}1, y[1] w[1118]*	Bloomington (8422)
UAS-Apc-RNAi	*y[1] sc[*] v[1]; P{y[+t7.7]v[+t1.8]=TRiP.HMS00188} attP2*	Bloomington (34869)
UAS-PGRP-LCx	*Yw; UAS-PGRP-LCx*	Kathryn Anderson, Developmental Biology Program, Sloan-Keltering Institute, New York
UAS-PGRP-LE	*DDI (Drs-GFP; Dipt.-lacZ):UAS-Flag-PGRP-LE (II)/CyO*	Kurata; Ihoichiro Kurata,
UAS-hid;rpr	*UAS-hid; rpr; +; +*	Martin Schwärzte, FU Berlin
w^{1118}	*w[1118]*	Bloomington (5905)

2.11 Microscopy

Microscopic analysis was performed for different approaches with dissected tracheae or the whole larvae. For analysis of the epithelial structure and evidence of distinct proteins,

immunohistochemistry with diverse antibodies was performed with the dissected tracheae (2.11.2). The epithelial thickness, the nuclei number and the nuclei size of the dissected tracheal trunks were analyzed using microscopic pictures (2.11.3). The pictures were quantified using the microscope AxioVision software (AxioVison SE64 Rel. 4.9). In another approach, the branching pattern of the tracheal terminal cells could be observed in the whole larvae or on the dissected intestine either in the GFP or in the DIC channel (2.11.4). To examine the activity pattern of *promotor-Gal4* lines in the whole larvae and in the tissue, these lines were crossed to a *UAS-GFP* line. The originated GFP expression reflects the activity pattern of the promotor and could be observed under the fluorescence microscope (2.17).

2.11.1 Dissection of trachea, intestine and filet preparation from L3 larvae

Phosphate buffered saline (PBS):

136	mM	NaCl
2.7	mM	KCl
1.5	mM	KH_2PO_4
7	mM	Na_2HPO_4

ad with H_2O, adjust to pH 7.3 with HCl, autoclave

Hemolymph-like solution (HL3):

70	mM	NaCl
5	mM	KCl
1.5	mM	CaCl x $2H_2O$
20	mM	$MgCl_2$ x $6H_2O$
10	mM	$NaHCO_3$
5	mM	trehalose
115	mM	saccharose
5	mM	HEPES

ad with H_2O, adjust to pH 7.1 with NaOH, filter sterilize, storage at 4 °C

For the immunohistochemistry and quantification of epithelial thickness and nuclei, the required tissue has to be dissected. For all experimental set-ups, L3 larvae were used. The larvae were washed in PBS to get rid of remaining medium. For intestine dissection the larvae were first fed with 10 % glucose for at least 1 h, to eliminate fluorescent food from the intestinal tract.

For trachea dissection, the head region with the dark mouth hooks was removed at first. The larvae were held near the posterior spiracles with the first forceps. The cuticle was grabbed with the second forceps near the first one and pulled over the larval body until total removal. The dorsal trunks and the branches of the trachea stayed at the posterior part on the spiracles. Remaining parts of the other organs were removed carefully around the trachea.

For dissection of the intestine, the anterior part with the head and posterior end of the larvae was removed. The intestine reclusive came out of the larval body. Remaining parts of other tissues were removed carefully, except the tracheal trunks.

Filet preparation was performed in order to investigate the tracheal terminal cells connected to the cuticle. The larvae were fixed on the ventral side with two needles in the anterior head and the posterior region. The larval body was opened along the full length, with two sharp forceps. The intestine as well as the main part of the fat body was removed from the body cavity. The cuticle on the right and left side was stretched outwards and fixed with further needles. Remaining parts of the fat body and the muscle layer on the inside of the cuticle were removed carefully.

2.11.2 Immunohistochemistry

Fixation solution:

4 % (w/v) paraformaldehyde (PFA)
ad with PBS, heat to 50-60 °C until complete dissolution, storage at -20 °C

Washing buffer (PBST):

0.1 % (w/v) triton X-100
ad with PBS

Blocking buffer:

10 % (v/v) normal goat serum
ad with PBST

The tissue from 5-10 larvae was dissected in cold HL3 buffer in a dissection dish (2.11.1). The tissue was put into a lid of a 1.5 ml low-binding reaction-tube. The HL3 buffer was removed and the tissue fixed with 50 µl fixation solution for 30 min. The fixation was

followed by three washing steps with 100 µl washing buffer, 10 min each. Afterwards a blocking step with 100 µl blocking buffer was carried out for 1 h. Incubation of the first antibody (Tab. 3) occurred over night at 4 °C. On the next day, three additional washing steps with 100 µl washing buffer for 10 min were carried out, before incubation of the second antibody (Tab. 3). The second antibody was incubated at least 3 h at RT or over night at 4 °C in the darkness. After the incubation with the second antibody three washing steps with 100 µl washing buffer were performed, 20 min each. The tissue was arranged on a slide with a drop of Roti®-Mount, before microscopy. The preparation was covered by a cover slip and held in darkness until analysis to prevent photo bleaching.

The fixation step with the filet preparation was performed in the dissection dish with a drop of fixation buffer on the tissue. All other steps were carried out in the lid of a 1.5 ml reaction tube.

Table 3: Antibodies and dilutions.

Primary antibodies:	**Dilution**	**Vendor**
α-Coracle, mouse (C615.16)	1:500	DSHB (Iowa City, USA)
α-phospho-Histone H3 (Ser10) AF 488 Conjugate, rabbit	1:100	Cell Signaling Technology (Danvers, USA)
α-Dcp1, rabbit	1:100	Cell Signaling Technology (Danvers, USA)
α-GFP, mouse (12A6-b)	1:100	DSHB (Iowa City, USA)
α-Armadillo, mouse	1:100	DSHB (Iowa City, USA)
α-Disc-large, mouse	1:200	DSHB (Iowa City, USA)
Secondary antibodies:		
α-mouse-AlexaFluor 488, goat	1:300	Jackson ImmunoResearch Laboratories (West Grove, USA)
α-rabbit-AlexaFluor 488, goat	1:500	Life Technologies (Carlsbad, USA)
α-mouse-AlexaFluor 555, goat	1:500	Cell Signaling Technology (Danvers, USA)
α-rabbit-Cy3	1:300	Jackson ImmunoResearch Laboratories (West Grove, USA)
Fluorescent dyes/ conjugated proteins		
Roti®-Mount FluorCare DAPI (4,6-diamidino-2-phenylindole)	-	Carl Roth (Karlsruhe, Germany)
505 Star-conjugated chitin binding probe	1:200	New England Biolabs (Ipswich, USA)

All antibodies as well as the chitin binding probe were stored at -20 °C in 50 % glycerol. The antibodies were diluted in blocking buffer before use, as indicated.

2.11.3 Quantification of epithelial thickness and nucleus number and size

The dissected tracheae were arranged on a slide in a drop of Roti®-Mount (Tab. 3). During dissection it was important to get the posterior part of the trachea, at least the fusion part between the two dorsal trunks. Thus, it is possible to count the segments from the posterior end onwards, to ensure the use of the same segment for every measurement. The second segment from the posterior end was chosen for quantification (8th segment, Tr8). The pictures were taken in both, DIC and DAPI channel. The pictures were taken either in 10x or in 20x, the magnification depends on the size of the larvae and tracheae. Five slices from the top to the middle of the tracheal tube were made using the Z-stack unity. Adjustment was done in the DAPI channel. The measurement of the epithelial thickness, nucleus number and size were performed in AxioVision.

2.11.4 Branching of the terminal cells

At first a heat block with a metal insert was started and set to 70 °C. The L3 larvae were washed in PBS to remove remaining medium and dried on a paper towel. The larvae were deposited in a drop of glycerol. The slides were placed on the heat block for 20-30 s until the onset of death of all larvae. The dead larvae were all arranged in the same direction with the dorsal side on the top. A cover slip was put on the larvae, before microscopy. The pictures of the terminal cells were taken in the GFP channel (10x or 20x) or DIC channel (20x). To capture all branches of the terminal cell, the Z-stack unity was used. The right terminal cell from the second dorsal segment was chosen for analysis.

The quantification of the terminal cell branches in DIC pictures occurred by counting of the branches in AxioVision.

The measurement of the GFP pictures occurred in the ImageJ plugin NeuronJ (Meijering *et al.*, 2004). Therefore, the pictures were saved in sectional view with scale, as 8 bit, .tiff files, without any compression in AxioVision. The contrast was adjusted for all pictures in the same way. The scale was set in ImageJ (ImageJ 1.8.9) before the measurement (100 µm = 155 pixels = 1.550 pixels/ µm). Afterwards the branches were analyzed using the ImageJ plugin NeuronJ, as described before (Jones and Metzstein, 2011).

2.12 Embryo collection

Apple juice agar plates:

10 % (v/v) apple juice
3 % (w/v) agar-agar
ad with H_2O, boil until it is clear, pour into petri dishes, storage at 4 °C after cooling

For all experiments with compound treatment, the F1 embryos from the crossings were used for the experiments. The flies from the parental crossings were placed into an embryo collection container. The container was closed with an apple juice petri dish. The petri dish was prepared with a small amount of yeast paste out of fresh yeast and water. The container was incubated at 25 °C over night. The embryo collection started at late afternoon and terminated in the morning of the next day.

After the flies were taken off, the embryos were washed off the plates with water, over a piece of gossamer. The embryos were washed several times on the gossamer to remove the remaining yeast. Afterwards the embryos were taken from the gossamer with a wet cotton swap and eluted in 1 ml PBS in a reaction tube. The embryos sank to the bottom of the reaction tube in a few minutes. Afterwards the PBS was removed. For further application of the embryos they were taken with a pipette, directly from the bottom of the pellet. The pipette tip was prepared by cutting off at the 2 µl mark, to ensure a larger opening. The pipette was set at 1.5 µl. By this, it was possible to get amounts of 5-30 embryos per pipetting step.

2.13 Compound preparation

The compounds of the FDA-approved drug library (2.4) were provided in 10 mM stocks, solved in DMSO. For the drug screening, the single compounds were diluted 50:50 with 100 % Ethanol. The compounds were applied on the medium in a 1:100 dilution, to achieve a final concentration of 50 µM in 0.5 % DMSO and 0.5 % Ethanol.

The compounds for the initial screening and for the other experiments were stored as 100 mM stocks in DMSO. The compounds were diluted 1:10 with 100 % Ethanol. The compounds were applied on the medium in a 1:100 dilution, to achieve a final concentration of 100 µM in 0.1 % DMSO and 0.9 % Ethanol.

2.14 Compound application in a 96-well format

Low-melt concentrated medium (low-melt CM):

10	g	yeast extract
17.2	g	cornmeal
10	g	sucrose
1	g	low-melt agarose

ad 200 ml with H_2O
cook for 10-15 min in the water bath, cool down to 60 °C
add:

2	ml	10 % (v/v) propionic acid
6	ml	10 % (w/v) nipagin (in 70% Ethanol)

fill directly into appropriate fly vials/ 96-well plates, storage at 4 °C after cooling

Deep 96-well plates were used for all experiments in this format. The plates were prepared with 300 µl low-melt-CM in each well. The compounds were prepared as described in 2.13. The compounds were applied directly on the medium, incubated for 30 min at RT and stored a 4 °C over night. The solvent served as control on each plate. The compounds were tested in triplicates. At least five embryos (2.12) were deposited in each well and counted immediately. A mean of 10-20 embryos was used. The plates were sealed with an air-permeable membrane and incubated at 25 °C. The pupae were counted on day seven. The pupation rate (% pupae/ embryos) was calculated.

2.15 Development of pupae and larvae

To determine differences in pupae and adult formation, the development was monitored over two weeks from the embryo to the adult fly. Newly formed pupae and adults were counted every day. The experiment was performed with 1.5 ml low-melt CM in small vials. For treatment with compounds, the medium was prepared on the day before (2.13). A total amount of 15 µl was directly pipetted on the medium, to achieve a 1:100 dilution in the medium. The prepared medium was stored at 4 °C over night. The embryos (2.12) were deposited on the medium and counted immediately.

2.16 Hypoxia sensitivity assay

The assay was performed with L3 larvae. The larvae were washed out of the medium in a petri dish with PBS, dried on a paper towel and put into a new vial. 20 larvae were used per replicate. The medium of the new vial was loosened by scratching with a spoon. The vials were incubated for at least 10 min, until all larvae burrowed in the medium and deposited in a desiccator. The desiccator was sealed. Nitrogen gas was passed in until an O_2 rate of 2-3 %. Hence the appropriate O_2 content was achieved, the larvae were treated over a period of 25 min. The number of larvae, outside of the medium, was counted every 5 min. The percentage of the escaped larvae was calculated.

2.17 Generation of *promotor*-Gal4 lines by the Gateway technology

The Gateway technology from Invitrogen was used for the cloning of new Gal4 vectors after manufacturer's instructions. A region of approximately 1 kb length upstream of the gene was chosen for cloning (flybase.org, Annotation Symbol: CG34058, FlyBase ID: FBgn0065109). Specific primers for this genomic region were used for the amplification via PCR (2.17.2). A second set of primers comprised cleavage sites for the two restriction enzymes *Bam*HI and *Xho*I and were added to the promotor sequence via PCR amplification. Genomic DNA from wildtype larvae (w^{1118}) served as target for the PCR reaction (2.17.1). The promotor region was cloned into two different vectors by two steps to produce the entry clone and finally the expression clone by using the Gateway cloning system (2.17).
In the first step the entry vector pENTR11 was used for cloning of the promotor region into the vector, by using restriction enzymes. The vector and the PCR products were digested with the same restriction enzymes (2.17.9). The PCR product was purified from the PCR and restriction reagents before further application (2.17.8). The digested vector was loaded on a gel and purified to get rid of the resected part (2.17.10). Subsequent dephosphorylation of the vector (2.17.11) prevents recircularization during the ligation reaction with the purified PCR product of the promotor region (2.17.12). The ligation reaction was transformed into DH5α bacteria (2.17.6) and plated on LB agar plates by selection with kanamycin (50 µg/ml) (2.17.4). Positive clones were identified by colony check PCR (2.17.7), purified (2.17.5) and sent for sequencing (2.17.14), to ensure the correct insertion of the

promotor region. The confirmed entry clone was used in the LR recombination reaction with the destination vector pBPGUw (Pfeiffer *et al.*, 2008). The LR recombination reaction was directly transformed into DH5α (2.17.6) and cultured on LB agar plates by selection with ampicillin (100 µg/ml). After confirmation by colony check PCR (2.17.7) and sequencing (2.17.14), the finished and purified (2.17.5) expression clone was sent to BestGene Inc. for the injection into *Drosophila* embryos (2.17.13) to generate transgenic flies carrying the *promotor*-Gal4 construct.

2.17.1 Isolation of genomic DNA

Isolation of genomic DNA was performed with the MasterPure DNA purification kit (epicenter) after manufacturer's instructions with the DNA purification protocol for tissue samples. Five larvae from the wildtype *Drosophila* strain (w^{1118}) were used for the isolation.

2.17.2 Polymerase chain reaction (PCR)

For the amplification of specific DNA segments, a polymerase chain reaction (PCR) was performed. The selected designed primers determine the region and size of the PCR product. The *Taq* DNA polymerase from Invitrogen was used after manufacturer's instructions in a 25 µl reaction volume:

2.5	µl	10 x *Taq* Puffer, -$MgCl_2$
1	µl	25 mM $MgCl_2$
1	µl	10 pmol Primer (*forward*)
1	µl	10 pmol Primer (*reverse*)
0.5	µl	10 mM dNTPs
0.2	µl	*Taq* DNA Polymerase

20-100 ng gDNA or plasmid DNA
ad with H_2O

For PCR products with high importance of a sequence without any failures during PCR amplification the *Pwo* DNA Polymerase (Roche) with a 3`-5`exonuclease activity (proofreading activity) was mixed 1:1 with the Taq DNA polymerase.

2.17.3 Gel electrophoresis

Tris-borate-EDTA (TBE) buffer:

89	mM	Tris-HCl
89	mM	boric acid
2	mM	EDTA

ad with H_2O, adjust to pH 8.0 with HCl, autoclave

Agarose gel for gel electrophoresis:

1.5	%	(w/v) agarose

ad 100 ml with TBE, boil until it is clear, storage in a 60 °C water bath until use, add:

4	µl	(v/v) 1 % ethidium bromide

DNA gel loading dye (10x):

500	µl	glycerol
500	µl	H_2O
150	µl	1 % (w/v) bromphenol blue
150	µl	1 % (w/v) xylene cyanol FF

To prove the presence, quality, amount and the size of a PCR product an agarose gel electrophoresis was performed. For this, the warm agarose ethidium bromide solution was poured into a gel chamber. The gel slots were created by a ridge, stack into the gel. After cooling, the ridge was removed. The chamber was filled with TBE buffer until the gel and the slots were coated. The samples were supplemented with DNA loading dye, before loaded into the slots of the gel. To determine the size of the separated nucleic acids, a DNA ladder was added on each gel. The electrophoresis was performed with 100 V for 30-45 min. Ethidium bromide intercalates into the DNA and is visible under UV light. The DNA bands were documented under UV light. All steps with ethidium bromide were performed with nitrile gloves.

2.17.4 Culturing of bacteria

Lysogeny broth (LB) medium:

10	g	NaCl
10	g	tryptone
5	g	yeast extract

ad 1 L with H_2O, autoclave

Lysogeny broth (LB) agar plates:

15 g agar-agar
ad 1 L with LB medium, autoclave, add appropriate antibiotics at ~ 60 °C,
pour into petri dishes, storage at 4 °C after cooling

Culturing and handling of bacteria was carried out under sterile conditions under laminar airflow. Bacterial culturing was mainly used to propagate plasmid DNA. The bacteria grew either in a shaking culture in LB medium at 200 rpm or on LB agar plates. The medium was supplemented with the appropriate antibiotics. Liquid culture served as starting material for plasmid purification from bacteria. The cultures were inoculated from single colonies from a LB agar plate or from a frozen glycerol stock. The cultures were incubated over night at 37 °C. The bacteria were harvested by centrifugation in 50 ml tubes at 3000 rpm for 15 min.

2.17.5 Plasmid purification from bacteria

Tris-EDTA (TE) buffer:

10 ml 1 M Tris-Cl, adjust pH to 7.5 with HCl
2 ml 500 mM EDTA, adjust pH to 8.0 with NaOH
ad 100 ml with H_2O

Plasmid isolation from bacterial cultures was performed with the JETSTAR Plasmid Purification Kit (genprice) after manufacturer's instructions. The DNA was eluted in TE buffer.

2.17.6 DNA transformation into bacteria

Super optimal broth (SOB) with glucose (SOC) medium:

0.5 % (w/v) yeast extract
2 % tryptone
10 mM NaCl
2.5 mM KCl
ad with H_2O, autoclave, add:
10 mM $MgCl_2$
10 mM $MgSO_4$
20 mM glucose
filter sterilize, storage at -20 °C

100 µl of competent DH5α bacteria (2.8) were incubated with the DNA on ice. In the next step the bacteria were heat shocked at 42 °C for 1 min. 900 µl SOC medium were added and incubated for 40-60 min at 37 °C at 800 rpm. The transformed bacteria were plated on LB agar plates (50 µl and 100 µl). The plates were incubated at 37 °C over night. With the grown colonies a colony check PCR was performed.

2.17.7 Colony check PCR

The colony check PCR was performed after transformation of the plasmid DNA into competent bacteria, to check if the insert was integrated into the vector. Therefore, the colonies were picked from the LB plates with a pipette tip and delivered directly into a 25 µl PCR reaction. The PCR ran as described in (2.17.2). The pipette tip was additionally scratched out on a LB agar plate to safe the possibly positive clones.

2.17.8 PCR clean up with SureClean

PCR products were purified after the PCR reaction from all PCR reagents before further use. The purification was performed with SureClean from Bioline after manufacturer instructions. The DNA was eluted in 25 µl TE buffer.

2.17.9 DNA cleavage by restriction enzymes

The digestion with the restriction enzymes was performed with both, the cloning vector and the purified PCR product. The PCR product was provided with the restriction sites by the PCR primers. The reaction was performed with the two restriction enzymes BamHI and XhoI from Thermo Scientific after manufacturer instructions in a 100 µl volume. The buffer R was used for one reaction with both reaction enzymes. The reaction was incubated for 2-3 h at 37 °C.

2.17.10 DNA extraction from agarose gels

The DNA extraction from agarose gels was performed with the entry vector after the digestion with the restriction enzymes to get rid of the remaining cut part. The complete

reaction volume was loaded on an agarose gel (2.17.3). The extraction from the gel was performed after manufacturer's instructions with the NucleoSpin Gel and PCR Clean-Up kit from Macherey-Nagel.

2.17.11 Dephosphorylation of the cloning vector

To prevent recircularization of vector DNA during ligation, a dephosphorylation of the cloning vector was performed. The FastAP Thermosensitive Alkaline Phosphatase from Thermo Scientific was used after manufacturer instructions directly after digestion with the restriction enzymes in the same buffer.

2.17.12 Ligation

The digested PCR product and the digested and dephosphorylated vector backbone were used for ligation. The T4 DNA ligase from Invitrogen was used after manufacturer's instructions for cohesive ends in an insert:vector ratio of 3:1. The amount of the DNA was estimated on a DNA agarose gel. The ligation reaction was incubated over night at 4 °C. For the transformation into 50 µl competent DH5α bacteria, 2 µl of the reaction were used.

2.17.13 *Drosophila* embryo injection

The injection of the *promotor-Gal4*-containing vectors was performed from the BestGene Inc. *Drosophila* embryo injection service. 50 µl of the plasmid with a concentration of 1 µg/µl was sent for the injection. The integration into the genome followed the PhiC31 integrase-mediated transgenesis system. The pBPGUw destination vector carries the mini white marker gene (mini *w+*). This gene is able to convert the white eyes of the used flies for the injection into a red eye color, as proof for the integration into the genome. The red eyed flies were provided by the company after injection.

2.17.14 Sanger sequencing

Sanger sequencing of plasmid DNA for confirmation of the correct insertion into the vector was performed at the Institute of Clinical Molecular Biology (IMKB) in Kiel. Sample

preparation was performed how defined in the specifications. The results were received via email as chromatogram.

2.18 Statistics

Prism Graph Pad 7 was used for statistical analysis. Normal distribution of the data sets was tested with Shapiro-Wilk test. In case of normal distributed data an unpaired t-test was performed. If this was not the case, Mann-Whitney test was used to test for statistical significance.

3 Results

3.1 Ectopic expression of different oncogenes in the tracheal system

In order to reveal oncogenes that can provoke changes, especially in the tracheal system, a screening with focus on cancer-like phenotypes comprising meta- and hyperplasia of the tracheal tissue was performed. Therefore, two different driver lines for the larval trachea were crossed to various oncogene containing UAS responder lines. A *ppk4*-Gal4 driver line achieved relatively weak expression of the genes of interest in the tracheal tissue. The ectopic expression of the genes is constant throughout all larval stages. The second driver line, *btl*-Gal4, activates the expression in early embryonic tracheal development, throughout all larval stages and even in the adult tracheal system. To achieve a stronger phenotype, the *btl*-Gal4 crossings were incubated at higher temperatures (30 °C). The different oncogene containing UAS responder lines consist mostly of activated genes, inactivated genes by RNAi technique or simply provide overexpression of a gene of interest. A selection of different *Drosophila* proto-oncogenes and tumor suppressor genes was used. Furthermore, two lines with the human epidermal growth factor receptor (*hEGFR*) fused to either the *Drosophila Egfr* (*dEgfr*) or the *Drosophila* PDGFR-/VEGFR-receptor related *Pvr* were used, to evaluate if the human gene can induce changes in the tracheal structure, too. By crossing with the different driver lines, an ectopic expression in the tracheal system at different time points was achieved. Crossing of the *ppk4*-Gal4 and *btl*-Gal4 driver lines with the w^{1118} wildtype served as control. The tracheae were dissected and analyzed under the microscope. The attention was paid to differences to the normal tracheal structure (Fig. A, G). The observed phenotypes were for example: an increased nuclei number and size (Fig. 8 H, I), a thickened epithelium (Fig. 8 B-F), melanization (Fig. 8 D), chitin deformation Fig. 8 C-F), aberrant structures (Fig. 8 C) as well as lethality in early larval stages because of too strong malformation of the trachea (Fig. 8 E, F). The summary of genes and the occurrence of the phenotype ranged from mild (+) to severe (+++) and is displayed in Tab. 4.

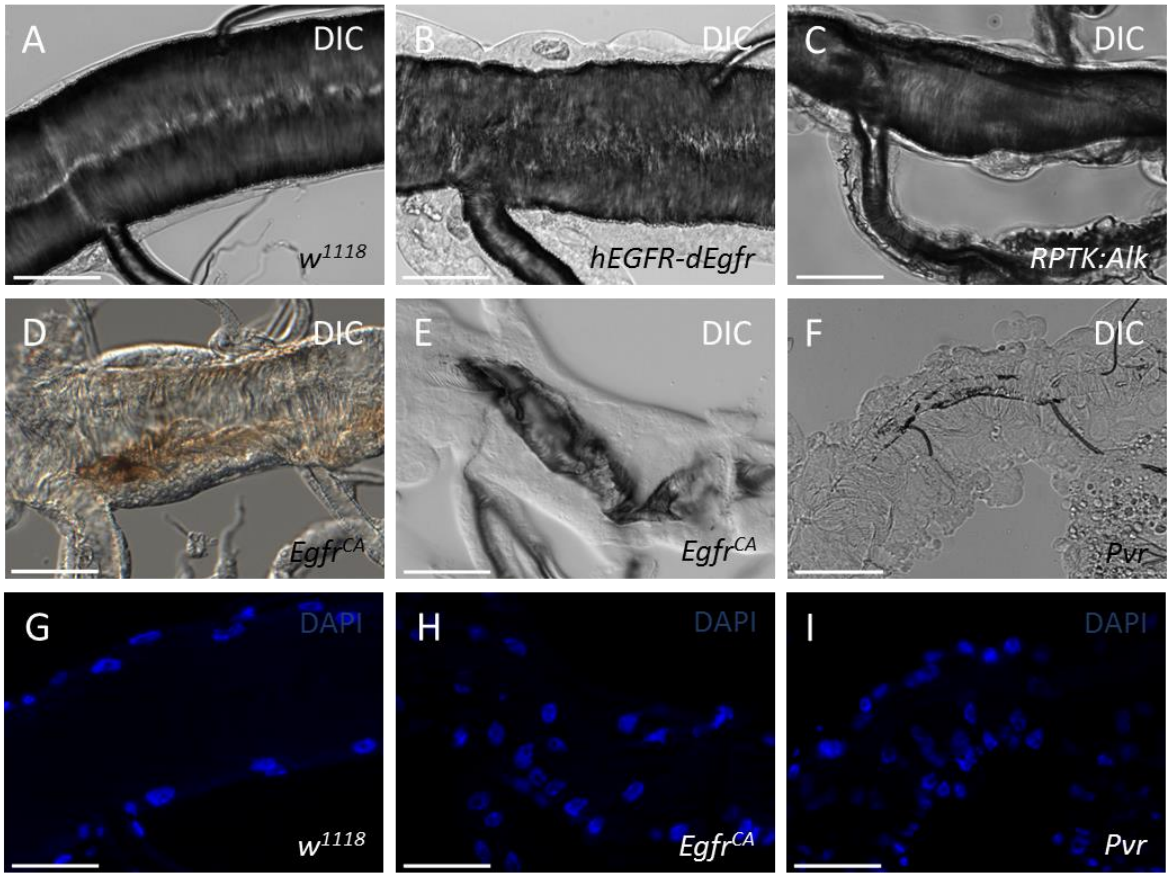

Figure 8: Ectopic expression of oncogenes in the larval tracheal system leads to severe phenotypes. Different oncogene containing UAS responder lines were crossed to either *ppk4*-Gal4 or *btl*-Gal4 trachea driver line. The tracheae of the larvae were dissected and analyzed under the microscope in DIC (**A**-**F**) and DAPI (**G**-**I**) channel. *Ppk4-Gal4 > w^{1118}* served as control (**A**, **G**). **B** *btl-Gal4 > UAS-hEGFR-dEgfr*. **C** *btl-Gal4 > UAS-RPTK:Alk*. **D, E, H** *ppk4-Gal4 > UAS-Egfr^{CA}*. **F**, **I** *btl-Gal4 > UAS-Pvr*. Scale = 50 µm.

A number of oncogenes are accordingly able to induce structural changes in the tracheal system of *Drosophila* larvae. Ectopic expression of *Btl*, *InR* and *Cdk* showed no tracheal phenotype, neither by crossing with the *ppk4-Gal4* driver line nor with the *btl-Gal4* driver line (Tab. 4). Expression of *hEGFR-dEgfr*, *hEGFR-Pvr*, *Sem* and *Akt* showed only a phenotype by expression with the *btl-Gal4* driver but not by expression with the *ppk4-Gal4* driver. Ectopic expression of *Egfr^{CA}*, *Pvr*, *Alk*, *Ras^{V12}*, *Raf^{GOF}*, *Rl*, *PI3K92E*, *Arm*, *p53*, *Apc* and *PGRP-LCx* showed a phenotype by weak expression and a stronger phenotype or even death by ectopic expression with *btl-Gal4*. The activated form of *Pvr* led to a massive thickening of the tracheal epithelium in L3 larvae by crossing with *ppk4*-Gal4, but no dead larvae were observed. The same was observed for *PGRP-LCx* expression. Ectopic expression of the constitutive active form of the *Drosophila Egfr* (*Egfr^{CA}*) in the trachea showed the strongest phenotype. Ectopic expression with both driver lines led to a strong tracheal malformation

and death. By use of the *ppk4-Gal4* driver line, the small early L3 larvae crawled out of the medium and died. Use of the *btl-Gal4* driver led to death in very early L1 larvae or even in the embryo.

Table 4: Expression of different oncogenes in the tracheal system and occurrence of the phenotypes.

***Drosophila* gene (human gene/pathway)**	**Isoform**	**Tracheal phenotype, larval death (x)**		
		ppk4-Gal4	***btl-Gal4* (20°C)**	***btl-Gal4* (30°C)**
Egfr (EGFR)	CA	+++ (x)	+++ (x)	+++ (x)
hEGFR-dEgfr	wt	-	+	++ (x)
hEGFR-Pvr	wt	-	+	+
Btl (FGFR)	CA	-	-	-
Pvr (VEGFR/PDGFR)	CA	++	+++ (x)	+++ (x)
InR (INSR)	CA	-	-	-
Alk (ALK)	fused to RPTK	+	+++ (x)	+++ (x)
Ras (RAS)	activated, (V12)	+	+++ (x)	+++ (x)
Raf (RAF)	GOF	+	+	+++ (x)
Sem (MAPK)	activated	-	+	+
Rl (MAPK)	wt	+	+	+++ (x)
PI3K92E (PI3K)	CA	+	+++ (x)	+++ (x)
Akt (AKT)	wt	-	+	+++ (x)
Arm (CTNNB1)	CA	+	+++ (x)	+++ (x)
Apc (APC)	RNAi	+	+	+
Cdk4 (CDK)	wt	-	-	-
P53 (TP53)	DN	+	+	+
PGRP-LCx (TNF pathway)	wt	++	+++ (x)	+++ (x)

CA = constitutive active; wt = wildtype; RPTK = receptor protein tyrosine kinase; GOF = gain of function; DN = dominant negative; +, ++, +++ = phenotypical occurrence from mild to severe; - = no phenotypical characteristics.

Further experiments were focused on the detailed characterization of $Egfr^{CA}$ expression driven by *ppk4* (3.2). In addition, expression of the oncogenes $Egfr^{CA}$, Ras^{V12}, *Sem* (3.5.1) and IMD pathway activation via *PGRP-LCx* expression (3.5.2) was investigated in the terminal cells (3.5).

3.2 Ectopic expression of *Egfr*^{CA} in the tracheal system

3.2.1 Death in early developmental stages and impaired tracheal structure

The ectopic expression of a constitutively activated isoform of the *Drosophila epidermal growth factor receptor* (*Egfr*^{CA}) by crossing with the trachea driver line *btl-Gal4* led to death in early developmental stages (3.1). Use of the *ppk4-Gal4* driver led to death in early L3 larvae directly after molt from L2 to L3. The larvae crawled out of the medium and died on day four after egg laying (Fig. 9 E, F). In contrast, the control larvae were able to develop from late L3 larvae into pupae on day five to six (Fig. 9 A, B).

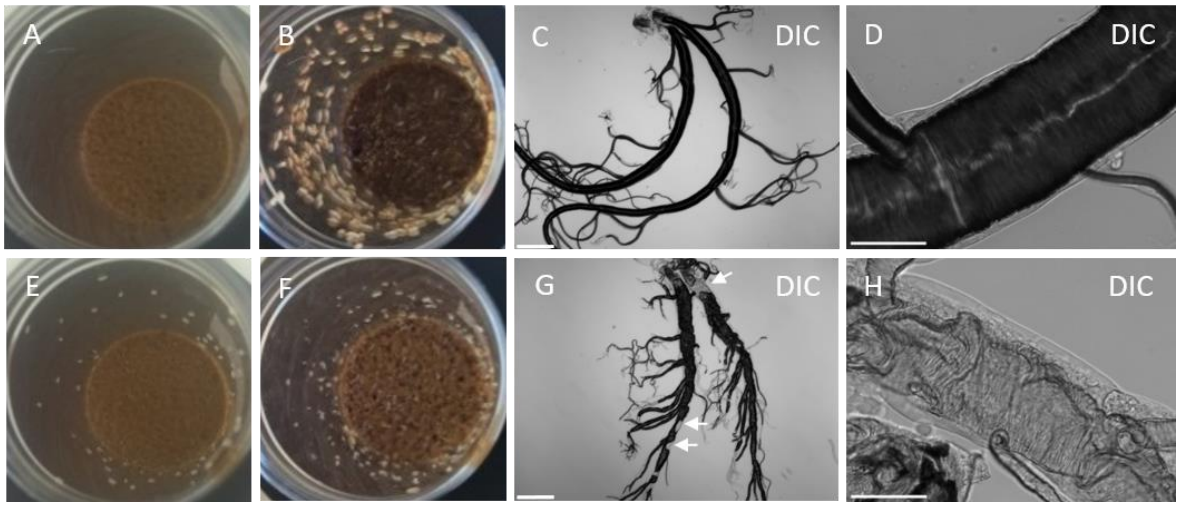

Figure 9: Development of control and *Egfr*^{CA} larvae and corresponding tracheal phenotype. Upper row: *ppk4-Gal4 > w*^{1118} control larvae and dissected trachea (**A**-**D**) after four days (**A, C, D**) and six days (**B**) of development. Lower row: *ppk4-Gal4 > UAS-Egfr*^{CA} larvae and dissected trachea (**E**-**H**) with constitutive activation of Egfr in the trachea after four days (**E**, **G**, **H**) and six days (**F**) of development. *Egfr*^{CA} larvae start to crawl out of the medium on day four and die, while control larvae undergo normal development into pupae. DIC pictures from the dissected tracheae were taken in two different magnifications (**C**, **D**, **G**, **H**). The white arrows indicate liquid filled areas (**G**). Scale = 50 µM.

This hypoxia escape response is known for animals with oxygen undersupply and gave evidence to an impaired tracheal structure and function. It seemed that the structural changes of the tissue occurred very fast and had severe consequences for the viability of the larvae. For further analysis only the *Egfr*^{CA} larvae from the wall of the food vials after manifestation of the hypoxia phenotype were used. Dissection of the tracheae from these larvae revealed a deformation of the dorsal trunks, the primary and the secondary

branches (Fig. 9 C, G). Furthermore, there were many liquid filled areas in these tracheae. More in detail, the dorsal drunks from *Egfr^{CA}* tracheae showed a massive increase in the thickness of the epithelium compared to the thin epithelium of the control tracheae (Fig. 9 D, H).

The development of the control crossings and the *Egfr^{CA}* crossing was observed over two weeks (Fig. 10).

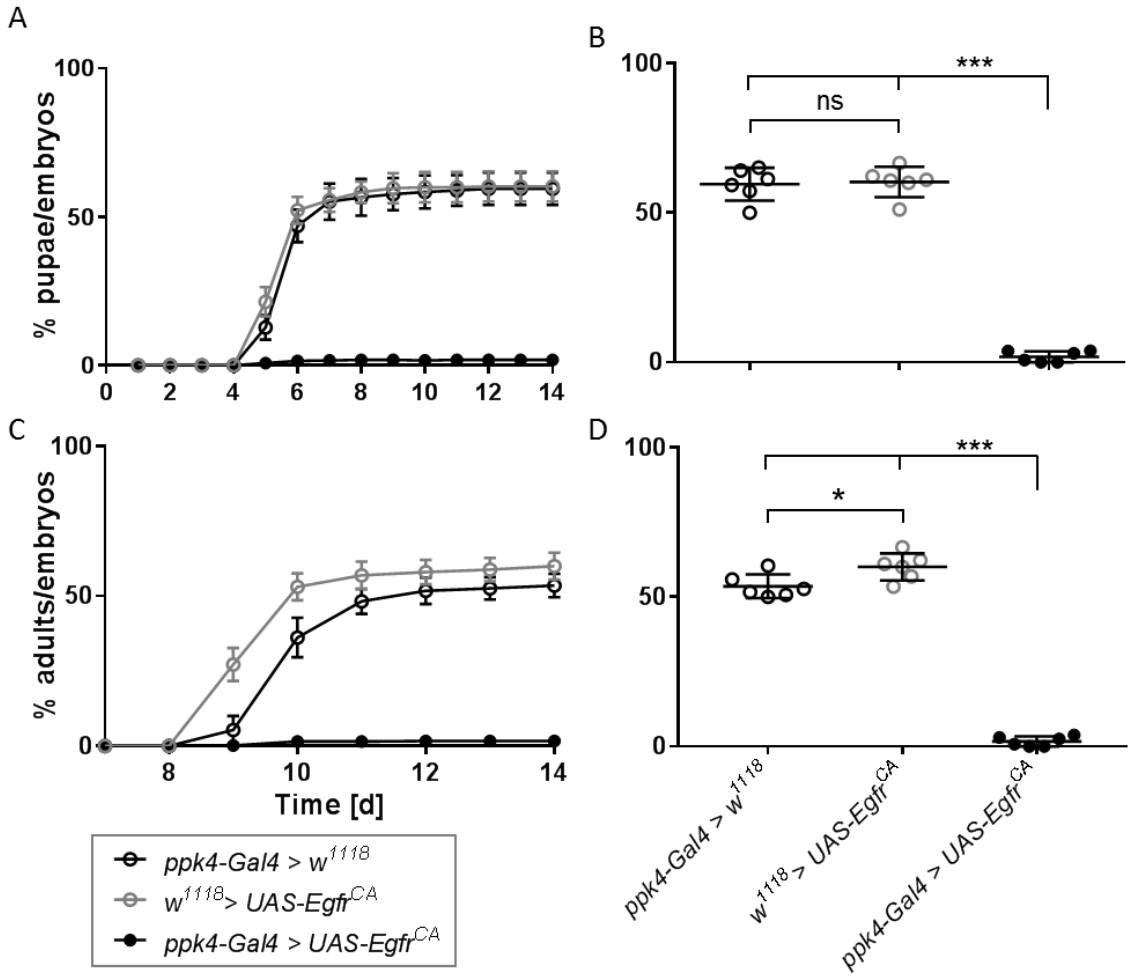

Figure 10: Death of *Egfr^{CA}* expressing animals in early larval stage. The embryos of *ppk4-Gal4 > w^{1118}*, *w^{1118} > UAS-Egfr^{CA}* (open circles) and *ppk4-Gal4 > UAS-Egfr^{CA}* (filled circles) were placed on low-melt CM prepared with DMSO [0.1 %] as the control medium for all experiments with compound treatment. The experiment was monitored daily over two weeks (**A**, **C**) in six replicates. The summary of pupae and adults after 14 days is represented in **B** and **D**. Represented are means ± SEM (**A**, **C**) or means ± SD (**B**, **D**). Statistical significance was tested with unpaired t-test. * p > 0.05, *** p > 0.001, ns = not significant.

Both, the larvae of the *Gal4* control and the larvae of the *UAS* control, started pupae formation equally on day four, whereas $Egfr^{CA}$ larvae showed significantly reduced pupae formation with almost no pupation rate (1.9 ± 1.8 %, p = <0.0001) (Fig. 10 A, B). The *Gal4* control showed a slight difference in the number of adult formation but for both lines the first adults eclosed on day nine (p = 0.0247) (Fig. 10 A, B). Correspondingly, there was a significantly reduced adult formation for $Egfr^{CA}$ (1.7 ± 1.7 %, p = <0.0001). Constitutive activation of the Egfr in the tracheal system led to death of the early L3 larvae and to severe structural changes in the respiratory system.

3.2.2 Tracheal phenotype caused by constitutive activation of the Egfr

To analyze the tracheal phenotype from $Egfr^{CA}$ larvae on a cellular level, an immunohistochemical analysis was performed. Antibodies directed against different components of the cell junctions were used. The septate junctions of the cell membranes were visualized by Coracle (Cora) and Disc large 1 (Dlg1) staining. Armadillo (Arm) is associated with the adherens junctions.

The control epithelium showed a regular cell shape and organized cell arrangement in all stainings (Fig. 11). The $Egfr^{CA}$ tracheal epithelium showed irregular cells with indistinct shape and curled membrane structures. The cell dimensions were anomalous and the epithelium showed a pseudo-stratified organization. Some cells appeared very large with more than one nucleus. The cell membranes appeared to be partially dissolved. All stainings showed a similar pattern with shift from the clear membrane assoziation (Fig. 11 A-C) to a consistant staining over the entire cells in $Egfr^{CA}$ (Fig. 11 A`-C`).

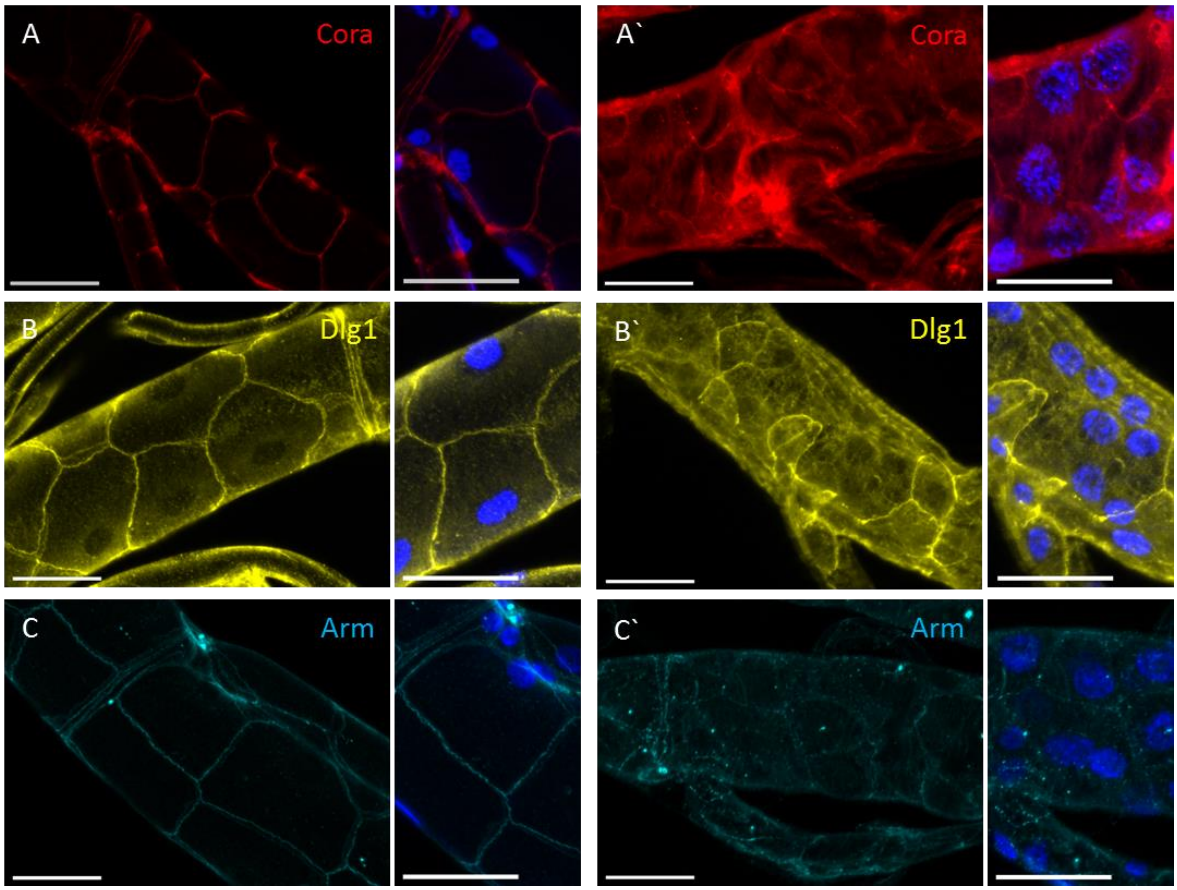

Figure 11: Tracheal *Egfr^{CA}* expression display severe changes in the cellular structure. Dissected and stained tracheae from *ppk4-Gal4 > w^{1118}* control larvae (**A**-**C**) and *ppk4-Gal4 > UAS-Egfr^{CA}* larvae with ectopic expression of *Egfr^{CA}* in the trachea (**A`-C`**). On the right of each picture a magnification including DAPI staining of the nuclei is shown. Coracle antibody staining (Cora) (**A, A`**), Armadillo antibody staining (Arm) (**B, B`**) and antibody staining of Disc large 1 (Dlg1) (**C, C`**). Scale = 50 µm.

The inner tube of the trachea is lined by a chitin layer. This chitin layer maintains the stability of the tube and the air conduction for oxygen supply. In the control tracheae the filaments were precisely ordered around the lumen of the tubes (Fig. 12 A). By tracheal expression of *Egfr^{CA}* the ordered arrangement of the chitin was completely lost (Fig. 12 A`). The chitin filaments formed loops and were not connected to each other anymore. The chitin layer formed holes to the inner of the lumen. The nuclei were enlarged compared to the control nuclei (Fig. 12 B).

Moreover, the DNA structure of the single nuclei looked decentralized and loosened. In contrast control nuclei were much smaller with condensed DNA. To confirm the mitotic activity, staining with the mitosis marker pospho-histone H3 (pH3) was performed

(Fig. 12 C). Nearly all nuclei of the *Egfr*^{CA} tracheae were positive for pH3, indicating a proliferative mitotic state of the tissue.

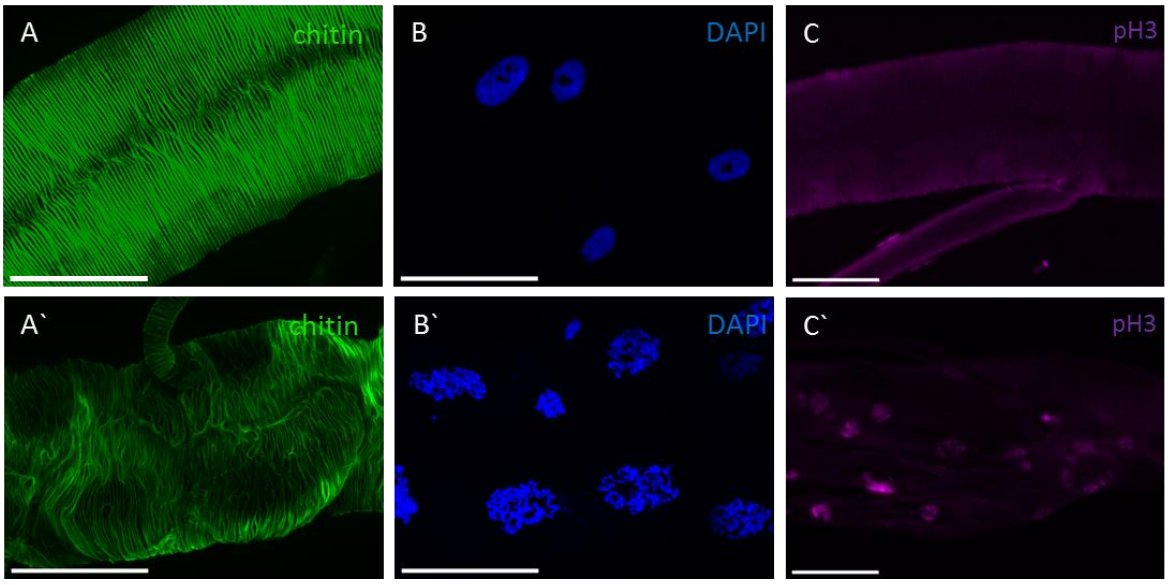

Figure 12: Chitin malformation, enlargement and mitotic state of the nuclei in *Egfr*^{CA} trachea. Dissected tracheae of *ppk4-Gal4 > w*^{1118} (**A**-**C**) and *ppk4-Gal4 > UAS-Egfr*^{CA} (**A`-C`**). Staining of the inner chitin tube by a conjugated chitin binding protein (**A, A`**), DAPI staining of the nuclei (**B, B`**) and staining with an antibody against the mitosis marker phospho-histone H3 (pH3) (**C, C`**). Scale = 50 µm.

To confirm the assumption of a tissue proliferation, the thickening of the epithelium, the nucleus number as well as the nucleus size were quantified in one segment of the dorsal trunks (Fig. 13). The thickness of the tracheal epithelium was significantly increased from a thickness of 5.9 ± 2.6 µm ($p = 0.003$) and 4.3 ± 1.7 µm ($p = <0.0001$) in the controls to 8.0 ± 2.7 µm in the *Egfr*^{CA} tracheae (Fig. 13 A).

Similarly, the number of nuclei was increased significantly in these animals. *Egfr*^{CA} tracheae showed a nucleus number of 22.5 ± 6.6 in the selected 8th segment of the dorsal trunks, while the two controls had a mean nucleus number of 18.2 ± 2.5 ($p = 0.0026$) and 14.2 ± 3.3 ($p = <0.0001$) (Fig. 13 B). Only the nucleus size (161.7 ± 47.1 µm²) showed no difference to the controls (123.4 ± 30.8 ($p = 0.001$) and 185.9 ± 49.5 µm², $p = 0.07$) (Fig. 13 C).

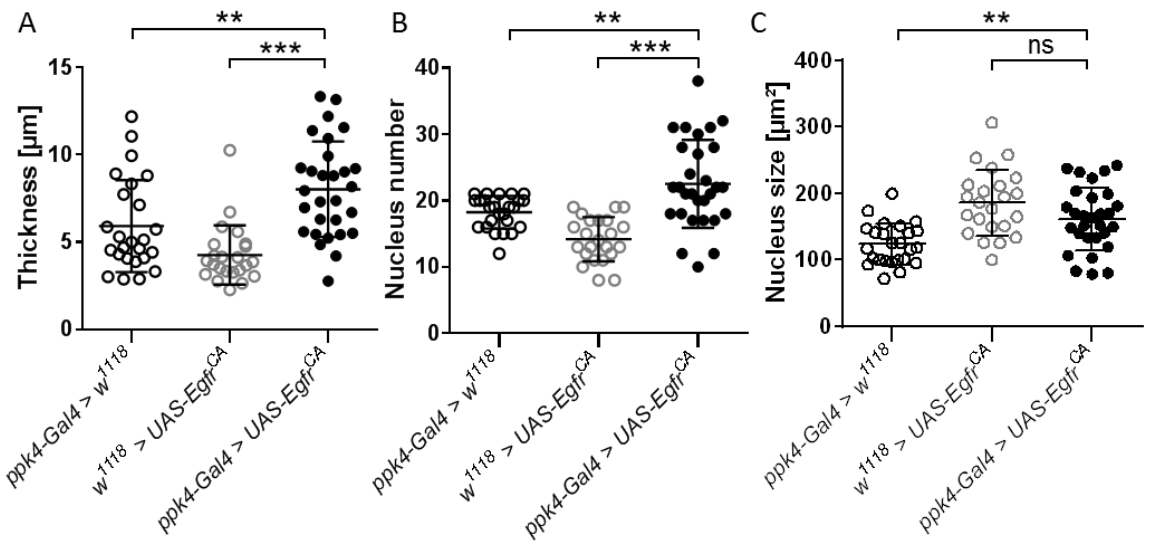

Figure 13: Quantification of epithelial thickness, nucleus number and nucleus size of *Egfr^{CA}* trachea. The tracheae of *ppk4-Gal4 > w^{1118}* (n = 25), *w^{1118} > UAS-Egfr^{CA}* (n = 23) and *ppk4-Gal4 > UAS-Egfr^{CA}* (n = 29) were dissected on day four after egg laying, stained with DAPI and analyzed under the microscope. Quantification of epithelial thickness (**A**), nucleus number (**B**) and nucleus size (**C**) occurred in AxioVision. For the measurement the 8th segment of the dorsal trunks was used. The controls are displayed in open black and grey circles, ectopic expression of *Egfr^{CA}* in the tracheal system is displayed in filled black circles. Statistical significance was tested with Mann-Whitney test (**A**, **B**) or unpaired t-test (**C**). ** = $p < 0.01$, *** = $p < 0.001$, ns = not significant.

3.3 Targeted drug screening for inhibiting effects on Egfr

3.3.1 Establishment of a whole animal high-throughput drug screening approach

The *Egfr^{CA}* larvae with this lethal phenotype described before, were intended to be used in order to identify specific compounds with an inhibitory effect in the Egfr pathway. Therefore, a screening method in a 96-well format was established.

To ensure the optimal supply with nutrients and humidity for embryos and larvae and to attain convenient conditions for plate preparation and compound application, concentrated medium with low-melt agarose was used. The embryos of *ppk4*-Gal4 > *w^{1118}* as control and *ppk4-Gal4 > UAS-Egfr^{CA}* (*Egfr^{CA}*) were placed on low-melt concentrated medium (CM) in a 96-well plate with deep wells (Fig. 14 A).

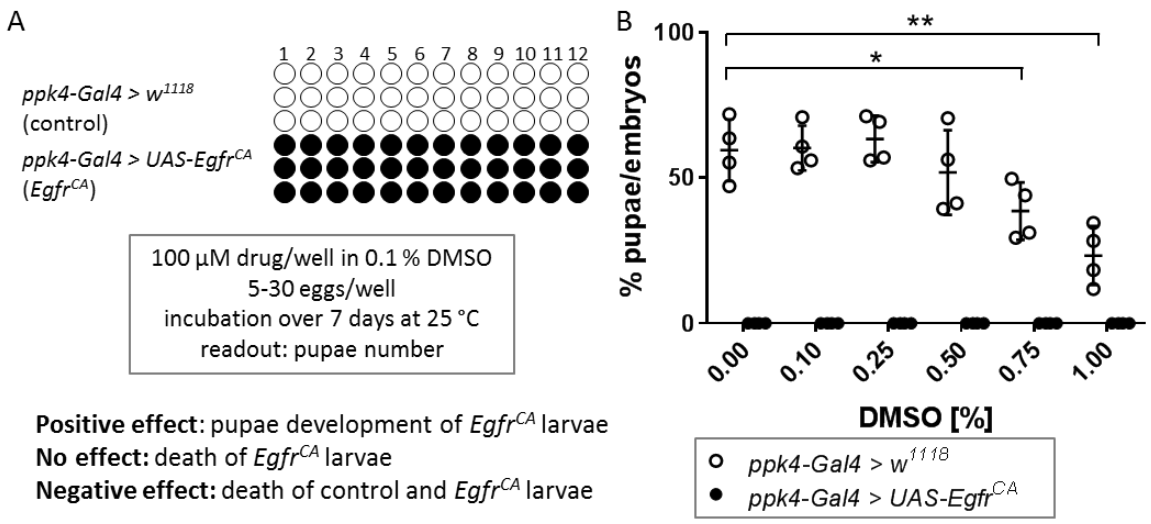

Figure 14: 96-well drug screening approach for compounds with an inhibiting effect on Egfr. **A** Embryos from *ppk4-Gal4 > w^{1118}* (control) and *ppk4-Gal4 > UAS-Egfr^{CA}* (Egfr^{CA}) are placed on a 96-well plate with low-melt CM. The medium is prepared with the compounds and the solvent as control (here DMSO), three wells for three technical replicates each. The plate is incubated for seven days at 25 °C before analysis. The number of pupae reflects the effect of the compound. A positive effect leads to pupae formation of *Egfr^{CA}* animals. No effect will result in death of early *Egfr^{CA}* L3 larvae. A negative effect will lead to death of both, control and *Egfr^{CA}* larvae. **B** Test of different DMSO concentrations (0-1 %) on pupae development of control (open circles) and *Egfr^{CA}* (filled circles) larvae. The experiment was performed as described in **A** in four replicates. Represented are means ± SD. Statistical significance was tested with unpaired t-test. * $p < 0.05$, ** $p < 0.01$.

The compound containing medium was prepared beforehand. The compounds were solved in DMSO, so the appropriate DMSO concentration served as control. The plates were closed with an air-permeable membrane and incubated at 25 °C for one week. The number of pupae on day seven was used as readout. Without any effect of a compound the *Egfr^{CA}* larvae died on day four. A positive effect of a compound turned out in the formation of pupae in these wells. A negative effect of a compound with general impact in the development of the larvae was assumed to lead to death of control and *Egfr^{CA}* larvae.

DMSO can have an inhibitory effect on larval development in high concentrations. Different DMSO concentrations were tested and the pupae development used as readout for viability (Fig. 14 B). Without DMSO, the pupae formation was 59.5 ± 10.7 %. On a DMSO concentration from 0.1-0.5 % the pupae formation was not impaired (51.9 ± 14.6 % to 63.4 ± 8.0 %). Starting from a DMSO concentration of 0.75 % the pupae formation of the control was reduced to 38.6 ± 9.9 % ($p = 0.028$). With 1 % DMSO the number of pupae

reached only half of the normal level without DMSO (23.3 ± 10.4 %, p = 0.0027). As expected, there was no pupae formation for all DMSO concentrations for *Egfr*^{CA} larvae.

To prove this screening approach, an initial screen with ten different receptor tyrosine kinase inhibitors and anti-proliferative reagents was carried out (Fig. 15). Three EGFR inhibitors (Afatinib, Gefitinib and Erlotinib), ALK inhibitors (Alectinib, Ceritinib and Crizotinib), one MEK/RAF inhibitor (Trametinib), a member of the statin drug class (Fluvastatin) and two anti-proliferative agents (Paclitaxel and Docetaxel) were tested. On day seven the pupae were counted and the pupae/embryos ratio was calculated.

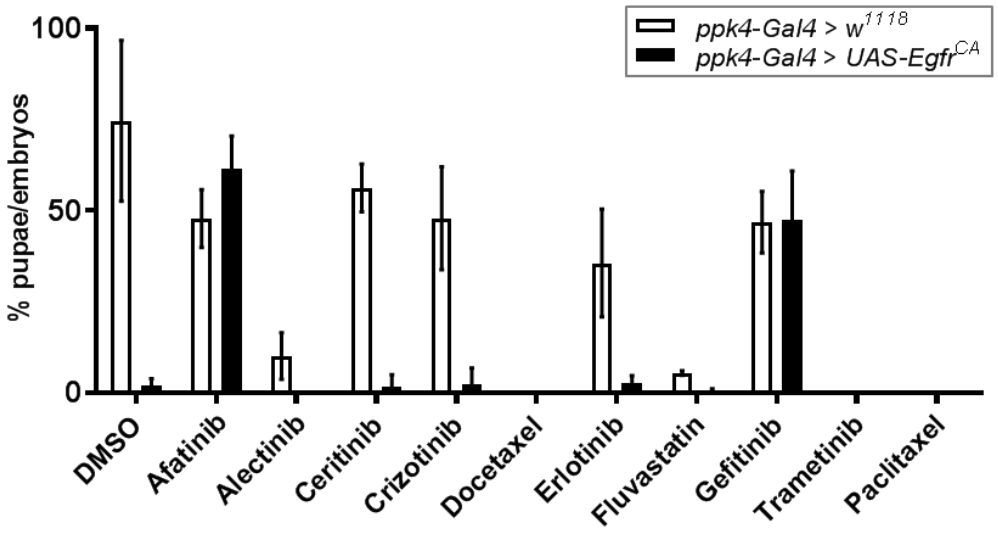

Figure 15: Initial screening with ten different compounds. The embryos of *ppk4-Gal4* > *w*^{1118} and *ppk4-Gal4 > UAS-Egfr*^{CA} were incubated with 100 µM of the different compounds in a 96-well plate on low-melt CM and incubated for seven days at 25 °C as described in Fig. 14. The experiment was performed in three replicates. 0.1 % DMSO served as control. Represented are means ± SD.

The DMSO control showed a normal development of the control crossing. The *Egfr*^{CA} larvae died before any pupae formation. Only the *Egfr*^{CA} larvae treated with the EGFR inhibitors Afatinib and Gefitinib could form pupae and were able to survive. Alectinib, Docetaxel, Fluvastatin, Trametinib and Paclitaxel had a lethal effect on control larval development, defined as negative effect. Ceritinib, Crizotinib and Erlotinib had no effect on both crossings.

3.3.2 FDA-approved drug library screening for *Egfr^{CA}* phenotype rescue

The successfully established 96-well screening approach (3.3.1) was used in a screening with 978 compounds from a commercial FDA-approved drug library. The screening was performed with *ppk4-Gal4 > UAS-Egfr^{CA}* (*Egfr^{CA}*) only. All compounds were tested in a concentration of 50 µM from a 10 mM stock solution (in DMSO). Each compound was tested in three technical replicates. 0.5 % DMSO served as negative control and 50 µM Afatinib as positive control on each plate. In this crossing no pupation was expected in general. In the screening with such large amounts of embryos an unspecific basic pupation level was observed. To avoid this high number of false positive counts a threshold of >3 pupae was set. All positive counts were confirmed by a second test.

Seven of the 978 compounds were positive in the first screening round (Tab. 5; App. Tab. 6). Three of them were confirmed by a second testing. The specific EGFR inhibitors Afatinib, Gefitinib, but also the Btk inhibitor Ibrutinib were able to induce pupae formation in *Egfr^{CA}* larvae (Tab. 5). Erlotinib turned out negative in the second testing.

Table 5: Positive hits from *Egfr^{CA}* animal treatment with compounds from a FDA approved drug library.

CatalogNumber	Item Name	#pupae	#2nd	#pupae (Afatinib)
S1011	Afatinib (BIBW2992)	9	7	12
S1023	Erlotinib HCl	6	0	10
S1025	Gefitinib (Iressa)	22	26	14
S1040	Sorafenib (Nexavar)	1	-	4
S1756	Enoxacin (Penetrex)	0	-	4
S1759	Pitavastatin calcium (Livalo)	1	-	6
S2098	Bexarotene	0	-	4
S2128	Bazedoxifene HCl	0	-	6
S2159	Tebipenem pivoxil (L0084)	0	-	7
S2586	Dimethyl Fumarate	4	0	1
S2589	Miglitol (Glyset)	4	0	1
S2680	PCI032765 (Ibrutinib)	5	7	10
S4172	Cetylpyridinium Chloride	4	0	0

Positive hits are highlighted in green. #pupae = number of counted pupae, #2nd = number of pupae after verification in a second testing, #pupae (Afatinib) = number of pupe after testing in combination with Afatinib [2 µM].

In a first test run for a more complex treatment regimen, all compounds of the library were tested together with a low Afatinib concentration (2 µM). This low Afatinib concentration alone showed no effect on pupae development (Fig. 19). It was assumed that Afatinib could have a synergistic effect with some other compounds, where no previous effect was shown in the first screening. The experiment was performed in the same way as the first one, except the addition of 2 µM Afatinib in each well. Ten compounds out of the 978 were positive (Tab. 5).

3.4 Rescue experiments with the specific EGFR inhibitors Afatinib and Gefitinib

Afatinib and Gefitinib were the first positively tested EGFR inhibitors in this study. After treatment, the *Egfr^{CA}* larvae were able to survive and to develop into pupae. To analyze how these two compounds operate on the meta- and hyperplasia phenotype of *Egfr^{CA}* tracheae and the development of the larvae, additional experiments were carried out. For all experiments *ppk4-Gal4 > w^{1118}* (control) and *ppk4-Gal4 > UAS-Egfr^{CA}* (*Egfr^{CA}*) embryos were treated with 100 µM Afatinib and Gefitinib. 0.1 % DMSO served as control.

3.4.1 Formation of larvae and adults

The development of a control crossing and the *Egfr^{CA}* crossing was observed over two weeks with and without treatment with the EGFR TKIs Afatinib and Gefitinib (Fig. 16).
The control larvae started to crawl out of the medium in L3 state on day five after egg laying to build pupae (Fig. 16 A). On day eight or nine after egg laying the adult flies eclosed from the pupae (Fig. 16 C). The untreated control had a pupation rate of 59.5 ± 5.5 % on day 14. The eclosion rate achieved 53.6 ± 4.0 % after two weeks.
The control larvae treated with Afatinib and Gefitinib formed a similar number of pupae. As expected, untreated (DMSO) *Egfr^{CA}* larvae hardly ever developed into pupae and adults (1.9 ± 1.8 %, p = <0.0001) (Fig. 16 B). In contrast Afatinib (63.4 ± 16.3 %) and Gefitinib (64.2 ± 8.4 %) treated *Egfr^{CA}* larvae formed nearly the same number of pupae like the controls. Afatinib and Gefitinib are able to rescue pupae development of *Egfr^{CA}* larvae. With regard to Afatinib treated larvae almost the same number adult flies hatched (57.4 ± 18.1 %), as seen for pupae development (Fig. 16 D).The number of adult flies was

just like in the controls. In case of the Gefitinib treatment, the amount of the adult flies in the control was significantly reduced and only reached a eclosion rate of 33.6 ± 6.0 % (p >0.0001). The number of adults in case of *Egfr*^{CA} was reduced even more to 13.72 ± 3.4 % (p = >0.0001).

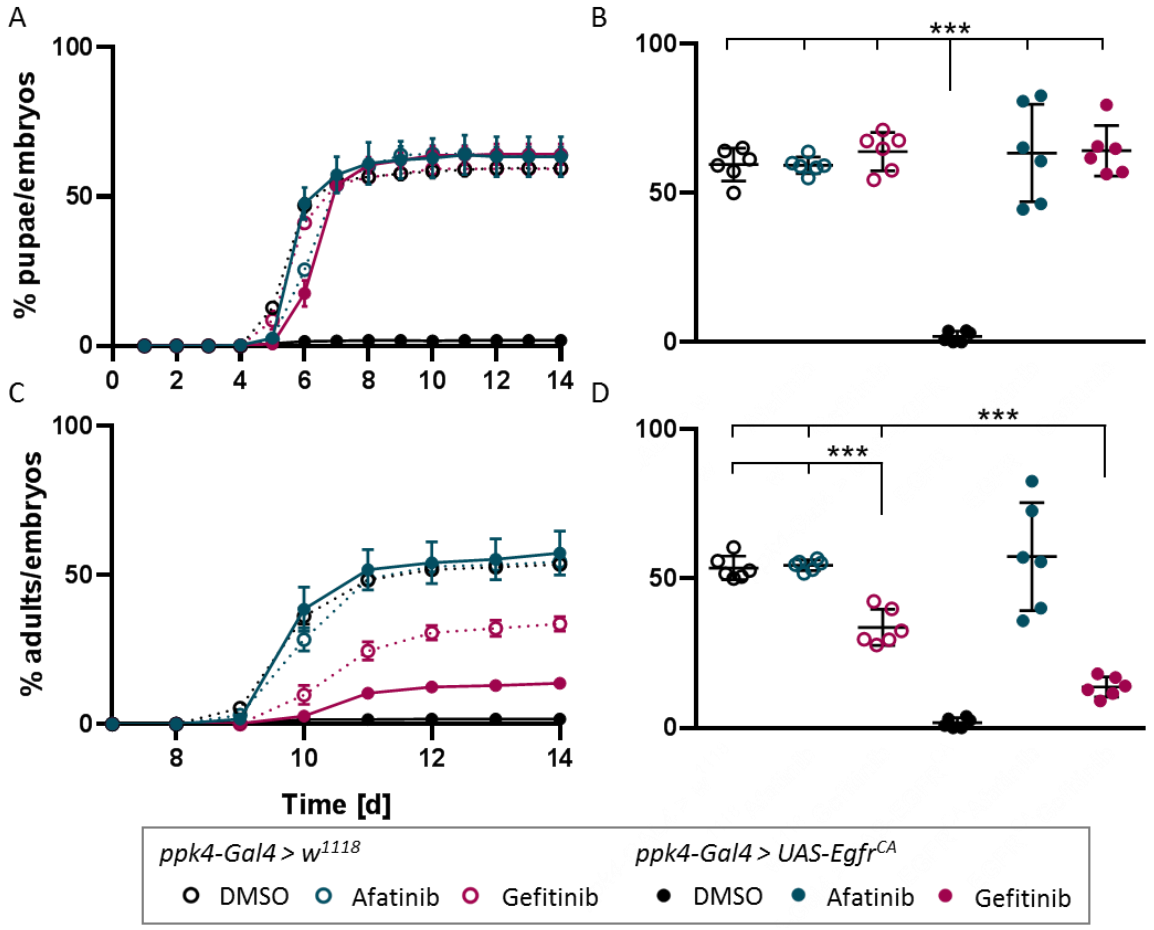

Figure 16: Afatinib and Gefitinib treated *Egfr*^{CA} embryos successfully develop into pupae and adult flies. The embryos of *ppk4-Gal4 > w*^{1118} (open circles) and *ppk4-Gal4 > UAS-Egfr*^{CA} (filled circles) were placed on low-melt CM prepared with either DMSO [0.1 %], Afatinib [100 µM] or Gefitinib [100 µM]. The experiment was monitored daily over two weeks (**A**, **C**) in six replicates. The summary of pupae and adults after 14 days is represented in **B** and **D**. Represented are means ± SEM (**A**, **C**) or means ± SD (**B**, **D**). Statistical significance was tested with unpaired t-test. *** p > 0.001.

3.4.2 Structural changes of the tracheal epithelium

The treatment of the *Egfr*^{CA} larvae with Afatinib and Gefitinib did not only rescue the lethality of the larvae. The rescue was also observed on a cellular level in the tracheal epithelium. For all experiments *ppk4-Gal4 > w*^{1118} (control) and *ppk4-Gal4 > UAS-Egfr*^{CA}

(*Egfr*^{CA}) embryos were treated with 100 µM Afatinib or Gefitinib. 0.1 % DMSO served as control. The tracheae were dissected on day four after egg laying.

The tracheae of the untreated *Egfr*^{CA} larvae showed a thickened epithelium, an increased number of nuclei, a complete loss of the cellular structure and a deformation of the stabilizing chitin structure (Fig. 17 B).

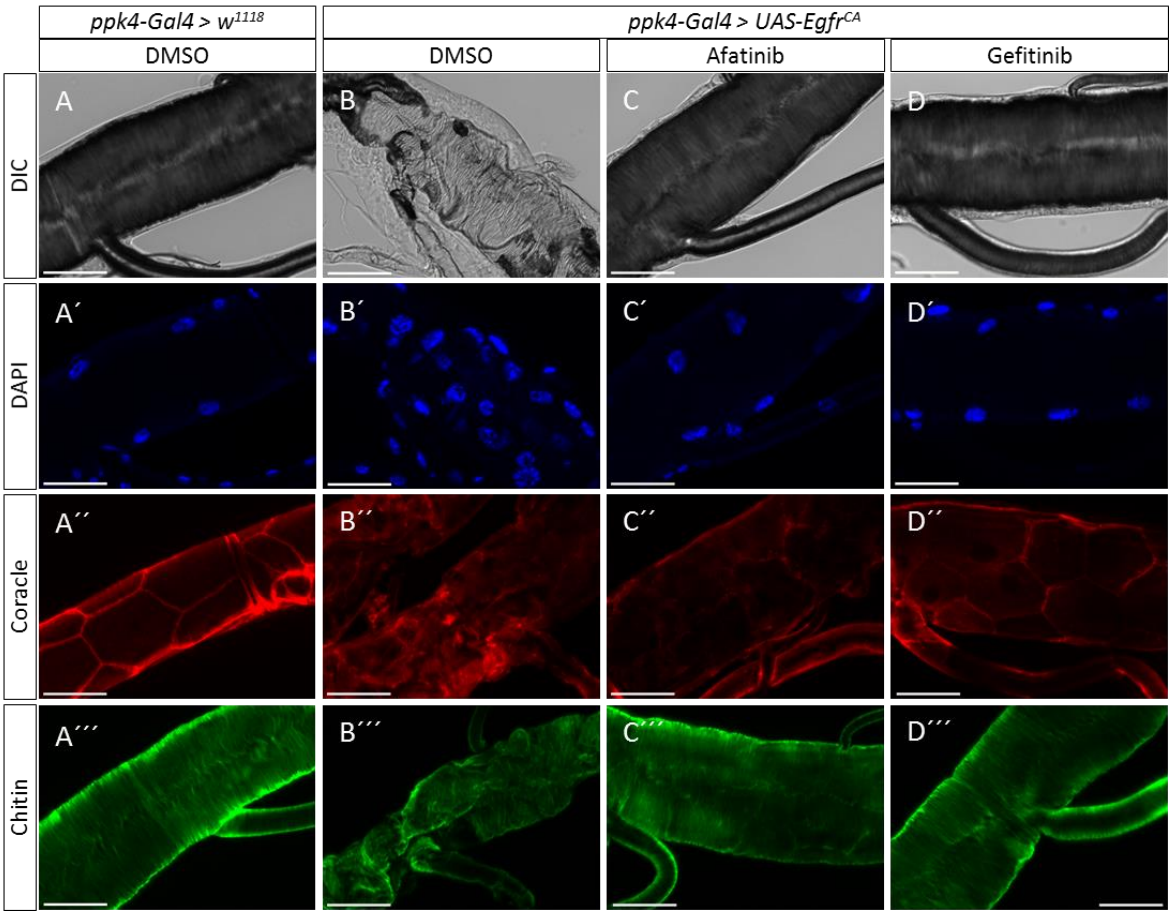

Figure 17: Rescue of the structural changes in *Egfr*^{CA} trachea by Afatinib and Gefitinib treatment. The embryos of *ppk4-Gal4 > w*^{1118} (**A**, control) and *ppk4-Gal4 > UAS-Egfr*^{CA} (**B-D,** *Egfr*^{CA}) were placed on low-melt CM prepared with either DMSO [0.1 %] (**A, B**), Afatinib [100 µM] (**C**) or Gefitinib [100 µM] (**D**). The tracheae were dissected on day four after egg laying and observed in DIC (**A-D**), stained with DAPI (**A`**-**D`**), an antibody against Coracle (**A``**-**D``**) and with a conjugated Chitin binding protein (**A```**-**D```**). Scale = 50 µM.

After treatment with Afatinib and Gefitinib this severe phenotype was completely reversed (Fig. 17 B-D). There was no thickening of the epithelium anymore and the tracheae were completely air-filled, like it was the case in the controls (Fig. 17 A-D). The DAPI staining obtained a reduced number of the nuclei (Fig. 17 A`-D`). The staining of the septate junctions of the epithelium showed signs of single cell boundaries with straight

organization in Afatinib treatment (Fig. 17 C``). This was even more obvious in tracheae from Gefitinib treated larvae (Fig. 17 D``). The staining of the inner chitin layer of the tracheal tubes showed a complete rescue of the deformed phenotype (Fig. 17 A```-D```). The chitin filaments are precisely ordered around the lumen of the trachea, like it was the case in the controls. Treatment with Afatinib and Gefitinib had no effect on the tracheal phenotype in the controls (App. Fig. 34). To quantify this phenotypical rescue, the tracheal epithelial thickening the nucleus number (Fig. 18) and the nucleus size was measured in treated controls and *Egfr*^{CA} larvae.

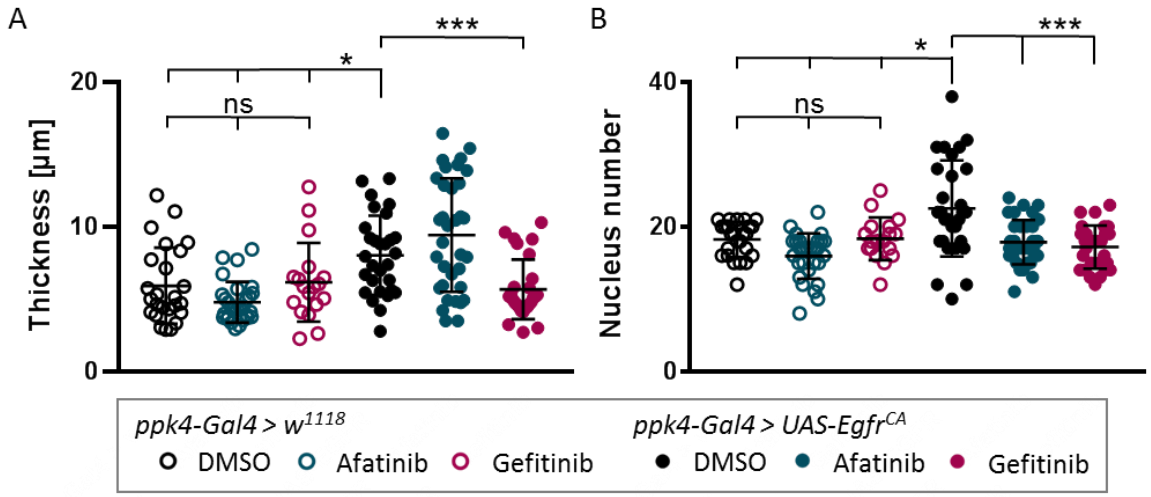

Figure 18: Tracheal epithelial thickness and nucleus number after Afatinib and Gefitinib treatment. The embryos of *ppk4-Gal4 > w*^{1118} (open circles) and *ppk4-Gal4 > UAS-Egfr*^{CA} (filled circles) were treated with either DMSO [0.1 %] (control n = 25, *Egfr*^{CA} n = 29), Afatinib [100 µM] (control n = 29, *Egfr*^{CA} n = 34) or Gefitinib [100 µM] (control n = 18, *Egfr*^{CA} n = 28) and dissected on day four after egg laying. The tracheae were stained with DAPI and analyzed under the microscope in DIC and DAPI channel. Quantification of epithelial thickness (**A**) and nucleus number (**B**) occurred in AxioVision. For the measurement the 8th segment of the dorsal trunks was used. Represented are means ± SD. Statistical significance was tested with Mann-Whitney test. * = $p < 0.05$, *** = $p < 0.001$, ns = not significant.

Treatment of the controls had no effect on the epithelial thickness and the nuclei number in the selected segment of the dorsal trunk. Both, the epithelial thickness and the nucleus number, was significantly increased in untreated *Egfr*^{CA} tracheae (8 ± 2.7 µm, p = 0.0165; 22.5 ± 6.6, p = 0.0100) compared to the untreated control (5.9 ± 2.6 µm, 18.2 ± 2.5). After treatment with Gefitinib both was significantly reduced to a control level (5.7 ± 2.1 µm, p = >0.0001; 17.2 ± 3, p = >0.0001). For Afatinib treatment it was the same in nucleus number (17.9 ± 3.1, p = >0.0001) but there was still a thickening of the epithelium

(9.4 ± 3.9 µm, p = 0.2137) compared to the untreated *Egfr*^{CA} tracheae. Nucleus size of *Egfr*^{CA} tracheae was not reduced after treatment with both compounds (App. Fig. 35)

3.4.3 Concentration dependency of the rescue effect

To determine the Afatinib and Gefitinib concentrations from which the lethal phenotype can be rescued, different concentrations between 0.1 µM and 100 µM were tested for *ppk4-Gal4 > w*^{1118} (control) and *ppk4-Gal4 > UAS-Egfr*^{CA} (*Egfr*^{CA}) larvae (Fig. 19). 0.1 % DMSO served as control. After seven days, the pupation rate was determined.

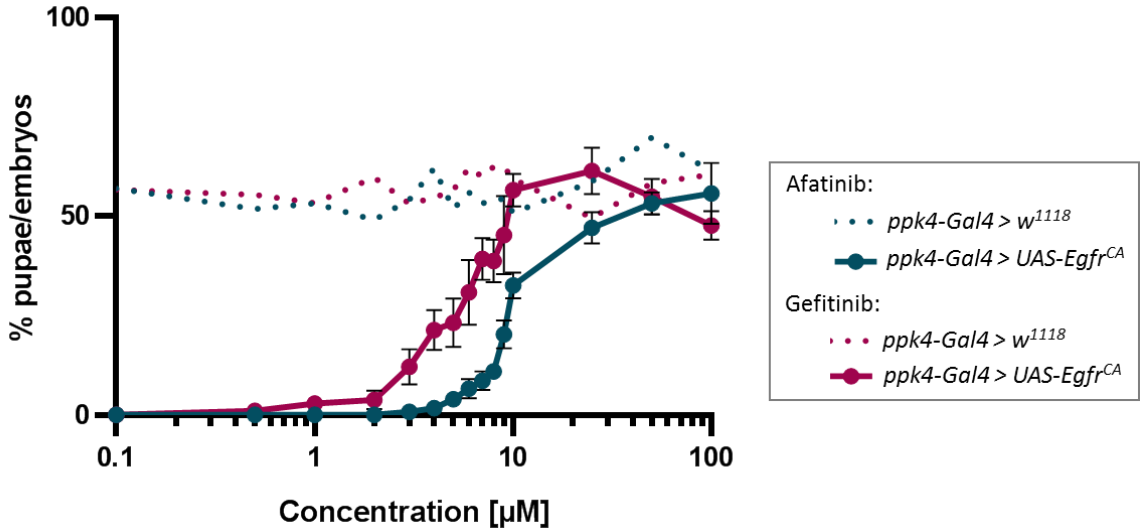

Figure 19: Dose-response relationship of Afatinib and Gefitinib concentration and *Egfr*^{CA} pupation. The embryos of *ppk4-Gal4 > w*^{1118} (control, dotted lines) and *ppk4-Gal4 > UAS-Egfr*^{CA} (*Egfr*^{CA}, filled circles) were placed on low-melt CM prepared with Afatinib or Gefitinib in different concentrations from 0.1 to 100 µM. 0.1 % DMSO served as control. The experiment was incubated at 25 °C and analyzed after seven days in four replicates. Represented are means (control) and means ± SEM (*Egfr*^{CA}).

The control shows a continuous mean pupation rate in all concentrations around 49-70 %. For Afatinib the first *Egfr*^{CA} pupae were observed at 3 µM. The pupation rate rose slowly and reached the control level between 25 µM and 100 µM. For Gefitinib the first *Egfr*^{CA} pupae were already observed at 0.5 µM. The pupation rate increased steadily and reached the control level at 10 µM. Gefitinib had already an effect in very low concentrations. 10 µM would be sufficient to rescue the lethal phenotype of the *Egfr*^{CA} larvae completely.

3.4.4 Adult formation after treatment with different Gefitinib concentrations

In order to find out if the impaired formation of adults after Gefitinib treatment (3.4.1) was concentration dependent or if Gefitinib had an effect on the adult flies in general, different concentrations were investigated. Pupae and adult formation of *ppk4-Gal4 > w^{1118}* (control) and *ppk4-Gal4 > UAS-Egfr^{CA}* (*Egfr^{CA}*) embryos were monitored by treating them with five different Gefitinib concentrations between 1 µM and 100 µM over 14 days (App. Fig. 36). The summary of pupae and adults after 14 days from control and *Egfr^{CA}* is displayed in Fig. 20.

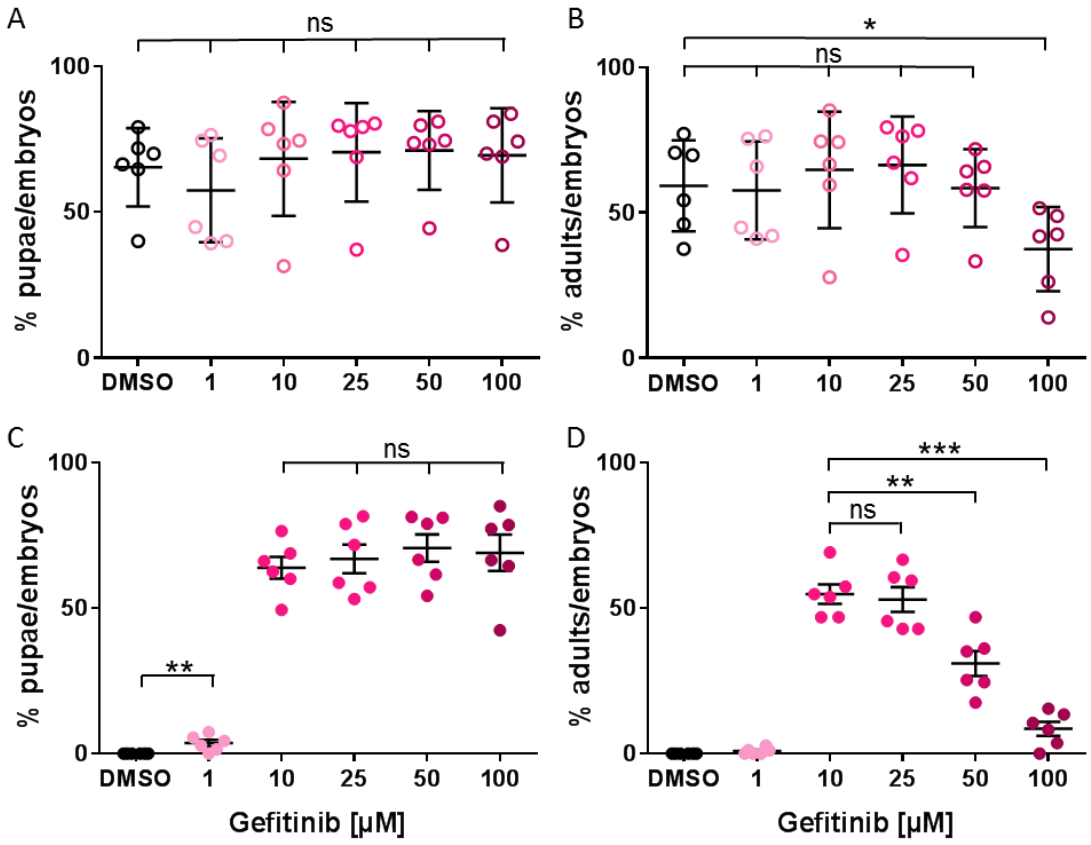

Figure 20: *Egfr^{CA}* animals show differences in the formation of adult flies by treatment with different Gefitinib concentrations. The embryos of *ppk4-Gal4 > w^{1118}* (**A**, **B**, open circles) and *ppk4-Gal4 > UAS-Egfr^{CA}* (**C**, **D**, filled circles) were placed on low-melt CM prepared with either DMSO [0.1 %] or five different Gefitinib concentrations from 1 µM to 100 µM. The experiment was monitored daily over two weeks in six replicates. The summary of pupae (**A**, **C**) and adults (**B**, **D**) after 14 days is represented. Represented are means ± SD. Statistical significance was tested with unpaired t-test (**A**, **B**, **D**) or Mann-Whitney test (**C**). * p > 0.05, ** p > 0.01, *** p > 0.001, ns = not significant.

As already shown before, the treatment of the control with Gefitinib had no effect on pupae formation, at all concentrations mean pupation rates between 57.4 ± 17.8 % and 71.1 ± 13.5 % were measured (Fig. 20 A). For the adult formation it looked different. By treatment between 1 µM and 50 µM Gefitinib no differences were observed (57.6 ± 16.8 % to 66.4 ± 16.6 %). The number of adults dropped at 100 µM (37.5 ± 14.5 %, p = 0.0320) (Fig. 20 B).

For *Egfr*^{CA} there was no difference in the rescued pupae formation between 10 µM and 100 µM (63.9 ± 9.1 % to 70.6 ± 11.5 %) (Fig. 20 C). For treatment with 1 µM Gefitinib there was only a less number of pupae (3.6 ± 2.7 %, p = 0.0089). This was due to the low rescue effect at this low concentration. Regarding the rescued *Egfr*^{CA} adult flies there was no difference between 10 µM and 25 µM (54.8 ± 8.2 % and 53 ± 10.5 %). At 50 µM and 100 µM the number of adult flies dropped significantly (30.9 ± 10.5 %, p = 0.0014 and 8.6 ± 5.9 %, p = <0.0001) (Fig. 20 D).

3.4.5 Gefitinib concentration dependent wing deformation in adult flies

Gefitinib treatment with higher concentrations had an effect on control and *Egfr*^{CA} adult formation. It was noticed, that many of the adults could not eclose out of the pupae properly or did not eclose at all. Many of the eclosed flies had a conspicuous wing phenotype (Fig. 21). The wings looked deformed and clotted and were not functional anymore. For Afatinib this wing phenotype could not be observed.

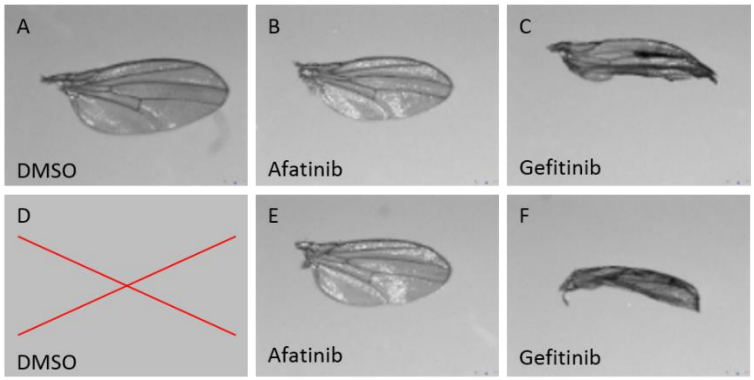

Figure 21: Wing phenotype of the adult flies after treatment with Afatinib and Gefitinib. The embryos of *ppk4-Gal4 > w*^{1118} (**A**-**C**) and *ppk4-Gal4 > UAS-Egfr*^{CA} (**D**-**F**) were placed on low-melt CM prepared with 100 µM Afatinib (**B**, **E**) or Gefitinib (**C**, **F**). 0.1 % DMSO served as control (**A**, **D**). The phenotype of the wings from the eclosed flies were monitored in brightfield. The DMSO treated *Egfr*^{CA} larvae died before the development into the adult flies in early L3 state (**D**).

In order to investigate if this wing phenotype is concentration dependent, the eclosed flies were analyzed after the treatment with different Gefitinib concentrations. The flies were sorted as flies with no observed phenotype (0), flies with one deformed wing (1) or flies with two deformed wings (2). The proportion of deformed wings increased consistently with the Gefitinib concentration for both, control and *Egfr*^{CA} in the same manner (Fig. 22). The number of analyzed flies decreased with increased Gefitinib concentration due to the fact that the number of adult flies was reduced in general.

For 1 µM Gefitinib there were only a few rescued flies. This was due to the low rescue effect at this low concentration. All flies showed hardly ever a phenotype for 1 µM and 10 µM in control and *Egfr*^{CA}. From a concentration of 25 µM the formation of the wing phenotype started. At a concentration of 50 µM more than 50 % of the flies had at least one deformed wing in control and *Egfr*^{CA}. This rate raised to 80-100 % at a concentration of 100 µM Gefitinib.

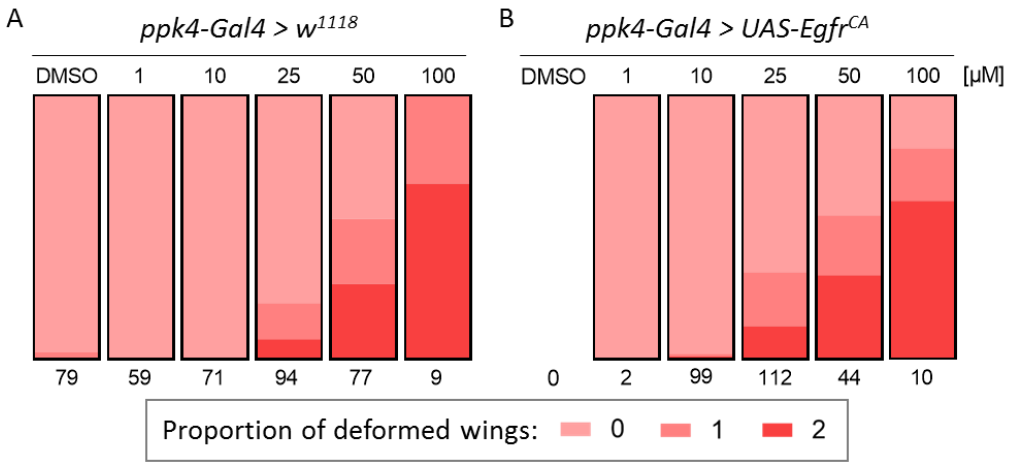

Figure 22: Wing phenotype after treatment with different Gefitinib concentrations. The embryos of *ppk4-Gal4 > w*^{1118} (**A**) and *ppk4-Gal4 > UAS-Egfr*^{CA} (**B**) were placed on low-melt CM prepared with either DMSO [0.1 %] or different Gefitinib concentrations from 1 µM to 100 µM. The eclosed flies of this experiment were counted and the wing phenotype documented: flies without a wing phenotype (0), flies with one deformed wing (1) or flies with both deformed wings (2). The proportion of the wing phenotype is shown in different colors in each Gefitinib concentration. The used Gefitinib concentrations are shown above the columns. The numbers of the observed flies are shown below the columns.

3.5 Ectopic expression of oncogenes in the tracheal terminal cells

The tracheal terminal cells of the larval tracheal system are known for their plasticity and capability to adopt to different circumstances. Different oncogenes that provoked larval death by use of the *btl* driver line (3.1) for the expression in the whole trachea were selected for investigation in the terminal cells. For gene expression in the terminal cells, the *DSRF-GFP-Gal4* driver line was used. The animals were analyzed regarding terminal cell morphology and hypoxia sensitivity.

3.5.1 Ectopic expression of different components of the MAPK signaling pathway

In order to investigate how the terminal cells respond to the activation of the MAPK signaling pathway, three of the core components of this pathway were expressed exclusively in the terminal cells. The constitutively active forms of the genes were used (*Egfr^{CA}*, *Ras^{V12}* and *Sem* (*Rolled*).

3.5.1.1 Branching and cell morphology

The *DSRF-Gal4* driver line for the tracheal terminal cells was used for the experimental crossings. In this line *Gal4* is fused to GFP. This makes it easy to trace and document the branches of the terminal cells under fluorescence light (Fig. 23).

The numbers and lengthes of the branches were determined by using the ImageJ plugin NeuronJ. The control crossing showed a mean number of branches of 15.9 ± 4.1 and a mean length of 1681 ± 472.6 µm in total (Fig. 23 A, E, F). By the ectopic expression of *Egfr^{CA}* no significant change in number (12.9 ± 2.7, p = 0.0639) and length (1357 ± 304.9 µm, p = 0.0593) of the branches could be observed in the terminal cells (Fig. 23 B, E, F).

The ectopic expression of the constitutively active form of the Ras protein (*Ras^{V12}*) showed the strongest branching phenotype (Fig. 23 C, E, F). *Ras^{V12}* led to a massive increase in terminal cell branch number (36 ± 7, p = <0.0001). Accordingly, the total length of all branches was increased, too (2794 ± 523.3 µm, p = <0.0001). The cells with the ectopic expression of *Ras^{V12}* showed a different cell shape compared to the control (Fig. 24 A, C).

Ectopic expression of *Sem* in the terminal cells led to a significantly increased number (22.9 ± 7.7, p = 0.0013) and total length (2266 ± 651.6 µm, p =0.0021) of all branches (Fig. 23 D, E, F).

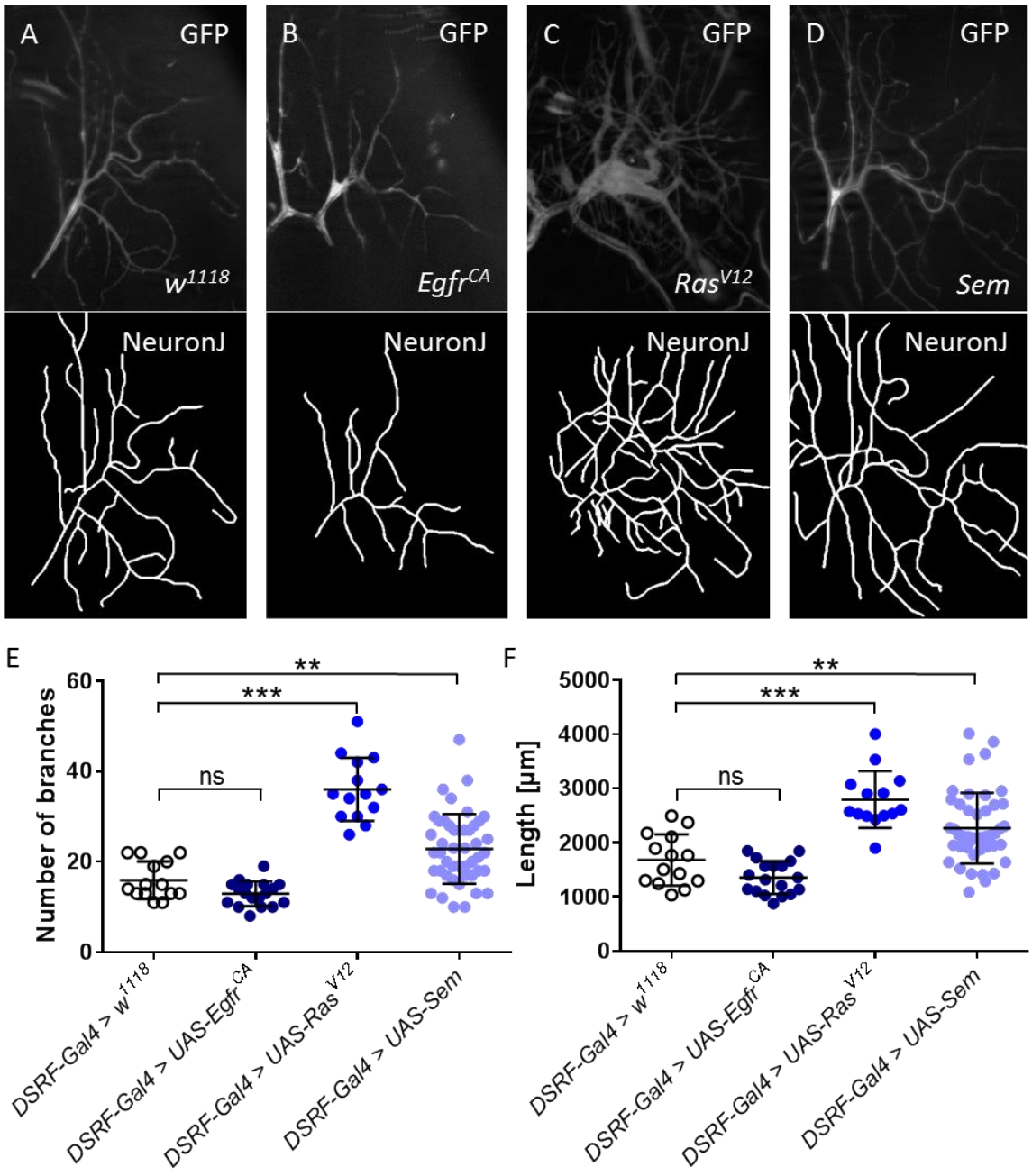

Figure 23: Branching analysis of the terminal cells after activation of MAPK signaling in these cells. The pictures for the analysis of the tracheal terminal cells were taken in the GFP channel. The right dorsal terminal cell of the 3rd segment was chosen. **A** *DSRF-Gal4 > w^{1118}* (n = 14). **B** *DSRF-Gal4 > UAS-Egfr^{CA}* (n = 18). **C** *DSRF-Gal4 > UAS-Ras^{V12}* (n = 14). **D** *DSRF-Gal4 > UAS-Sem* (n = 46). Quantification and tracing of the branches was performed with the ImageJ plugin NeuronJ. The terminal cells were analyzed regarding number (**E**) and length (**F**) of the branches. Represented are means ± SD. Statistical significance was tested with Mann-Whitney test. ** p < 0.01, *** p < 0.001, ns = not significant.

Most of the *Ras^{V12}* cells were not air-filled anymore and the cell body appeared thickened (Fig. 24). This was likely due to a massive increase of the nucleus in these cells, while the nuclei in the control cells were as small as the other nuclei in the tracheal epithelium (Fig. 24 A`, B`).

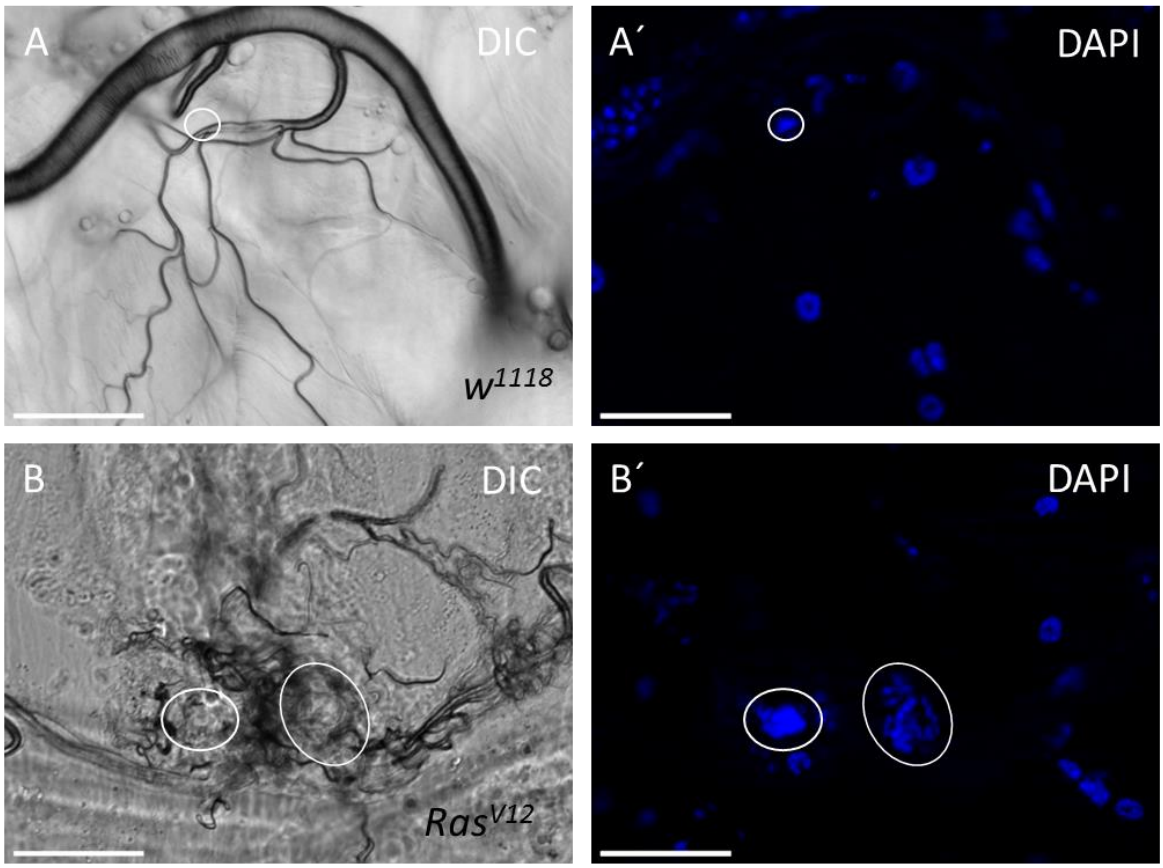

Figure 24: Deformation of the cell shape and nucleus enlargement by *Ras^{V12}* expression in the terminal cells. The L3 larvae of *DSRF-Gal4 > w^{1118}* (**A**) and *DSRF-Gal4 > UAS-Ras^{V12}* (**B**) were dissected in a filet preparation and the lateral terminal cells documented in DIC and DAPI. The circles indicate the nuclei of the terminal cells. Scale = 50 µM.

3.5.1.2 MAPK pathway alteration changes hypoxia sensitivity

Ectopic expression of three core components of the MAPK signaling in the tracheal terminal cells led to alterations in the cells. To test if these structural changes have any effect on the physiology and on the oxygen supply of the larvae, a hypoxia sensitivity assay was performed (Fig. 25). It is a natural response of the larvae to escape from the medium under hypoxic conditions (2-3 % O_2). With structural changes of the tracheae it was expected, that the larvae will show differences in behavior. To test this, the larvae were placed in a new

tube and observed over 25 min. The escaped larvae were counted every five minutes. After 5 min a mean of 35.8 ± 4.3 % of the control larvae left the medium. After 10 min the rate increased to 53.3 ± 4.2 % and to 64.1 ± 2.6 after 15 min. After 20 min 68.3 ± 3.8 % of the larvae left the medium followed by 74.2 ± 3.1 % after 25 min under hypoxic conditions (Fig. 25 A-D).

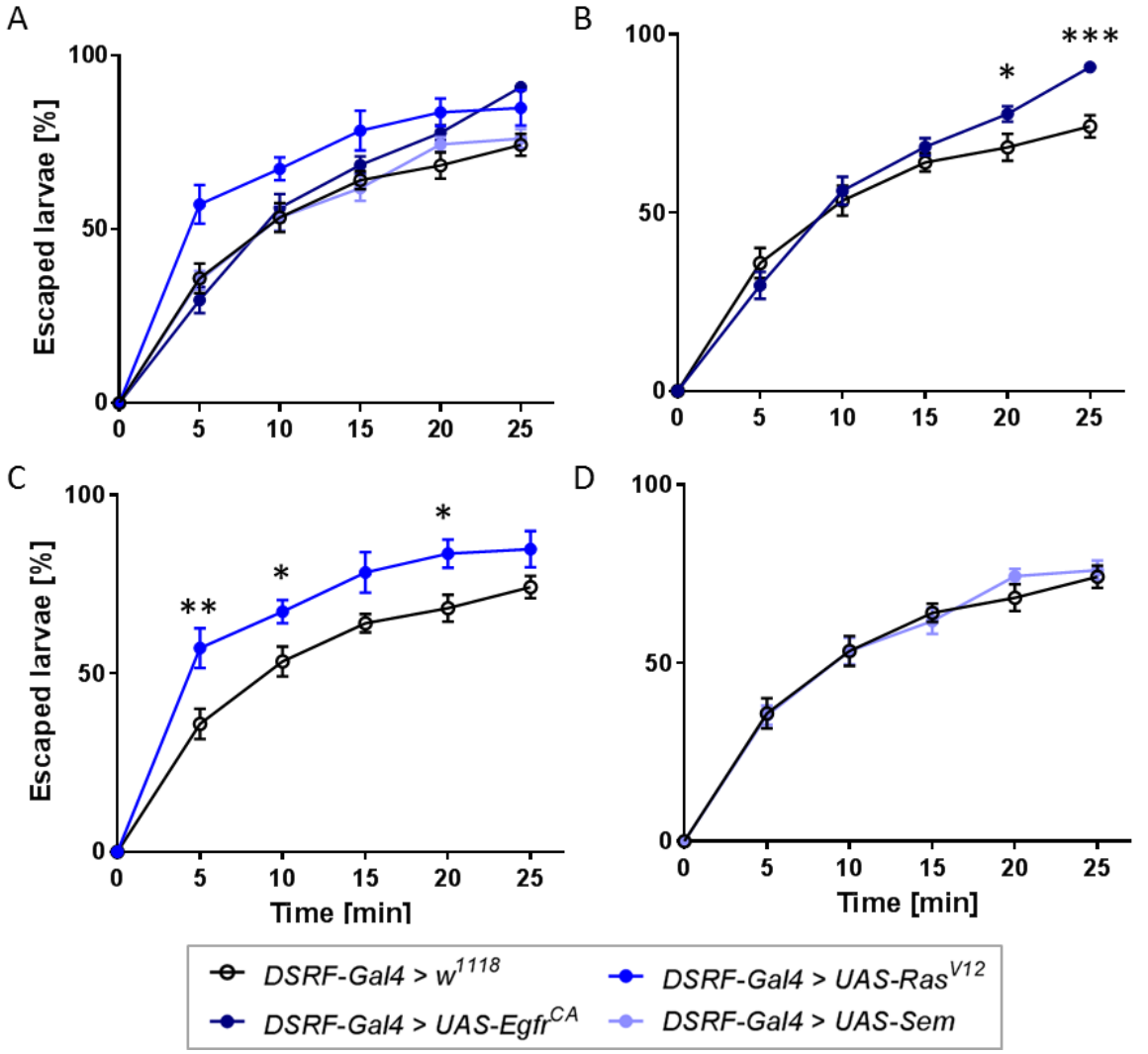

Figure 25: Hypoxia sensitivity of L3 larvae after activation of MAPK signaling in the tracheal terminal cells. The larvae were placed in a food vial under hypoxic conditions (2-3 % O_2) and monitored over 25 min. The escaped larvae were counted every 5 min. **B** *DSRF Gal4 > w^{1118}* (n = 12) and *DSRF-Gal4 > UAS-$Egfr^{CA}$* (n = 13) **C** *DSRF-Gal4 > w^{1118}* (n = 12) and *DSRF-Gal4 > UAS-Ras^{V12}* (n = 6) **D** *DSRF-Gal4 > w^{1118}* (n = 12) and *DSRF-Gal4 > UAS-Sem* (n = 15) **A** Summary of all experiments. Represented are means ± SEM. Statistical significance was tested with Mann-Whitney test. * $p < 0.05$, *** $p < 0.001$, ns = not significant.

The *$Egfr^{CA}$* larvae showed no increase in hypoxia sensitivity in the first 15 min. From 20 min on there was a slight increase (77.7 ± 2.2 %, p = 0.0374), which was even higher after 25

min (90.8 ± 1.4 %, p = <0.0001) (Fig. 25 B). The *Ras*^{V12} larvae crawled out of the medium faster than the control immediately (57.1 ± 5.6 %, p = 0.0089) (Fig. 25 C). The difference was significantly higher than the control almost over the whole 25 min period compared to the control. The treatment of the *Sem* larvae with this low oxygen content led to no effect on the hypoxia response of the larvae (Fig. 25 D).

3.5.2 Activation of the IMD pathway in the terminal cells

In order to investigate the influence of the activation of the *Drosophila* homolog of the TNF pathway in the tracheal terminal cells, the IMD receptor PGRP-LCx was used and ectopically overexpressed in these cells.

3.5.2.1 Shrinking of the terminal cells

The larvae with activated IMD in the terminal cells showed no impairment. A closer evaluation of the tracheal terminal cells obtained a decreased branching of very small and shrunken cells. In some cases they were not even present anymore. The GFP signal was obviously reduced. This phenotype was quantified with the ImageJ plugin NeuronJ by tracing of the branches of the terminal cells in control and *PGRP-LCx* larvae (Fig. 26).
A distinct significant decreased branching of the terminal cells in PGRP-LCx larvae was observed. The cells showed only between one and five (2.7 ± 1.4, p = <0.0001) branches adjacent to the controls with branch number of 14.3 ± 3.6. The length of these branches was significantly decreased to a length of 238.8 ± 111.4 µm (p = <0.0001), while the control branches where more than six times longer (1592 ± 451.6 µm).
IMD activation in the tracheal terminal cells by PGRP-LCx overexpression led to a distinct shrinkage and change in number and length of the branches.

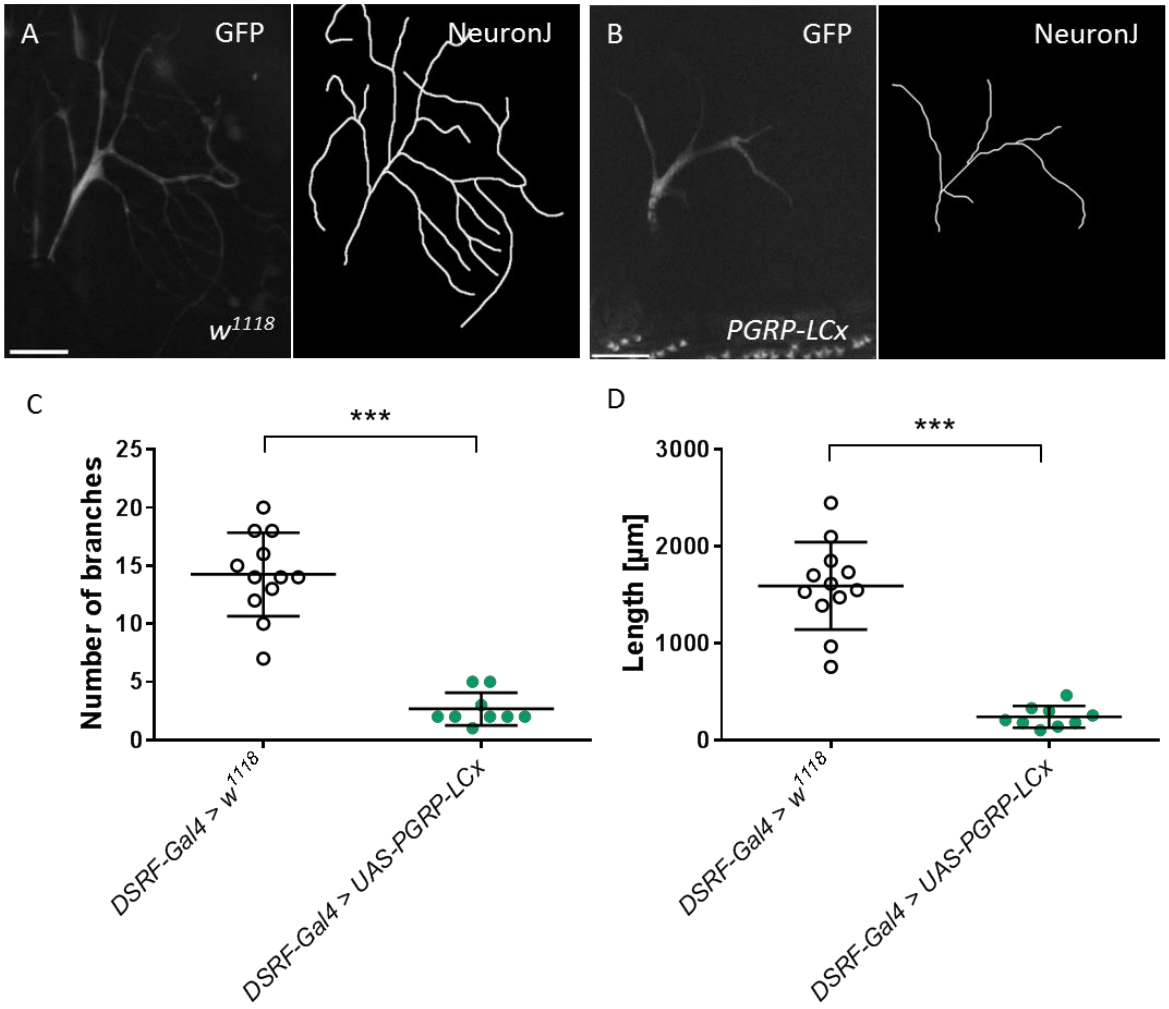

Figure 26: Decreased branching of the terminal cells by *PGRP-LCx* overexpression. The dorsal tracheal terminal cells from the 3rd segment of *DSRF*-Gal4 > w^{1118} (**A**, n = 12), and *DSRF-Gal4* > *UAS-PGRP-LCx* (**B**, n = 9) in the whole larvae were documented and quantified regarding the number (**C**) and length (**D**) of branches in the GFP channel. Tracing and quantification of the branches was performed with NeuronJ. Represented are means ± SD. Statistical significance was tested with Mann-Whitney test (**C**) or unpaired t-test (**D**), *** = $p < 0.001$.

3.5.2.2 PGRP-LCx expression alters hypoxia sensitivity

The IMD pathway activation via *PGRP-LCx* overexpression in the terminal cells led to decreased branching and shrinking of the cells (3.5.2). To investigate this severe phenotype of the terminal cells on a physiological level, a hypoxia sensitivity assay was performed (Fig. 27). Therefore, the L3 larvae were placed in a new tube and treated with 2-3 % O_2 over a period of 25 min. The escaped larvae were counted every five minutes.

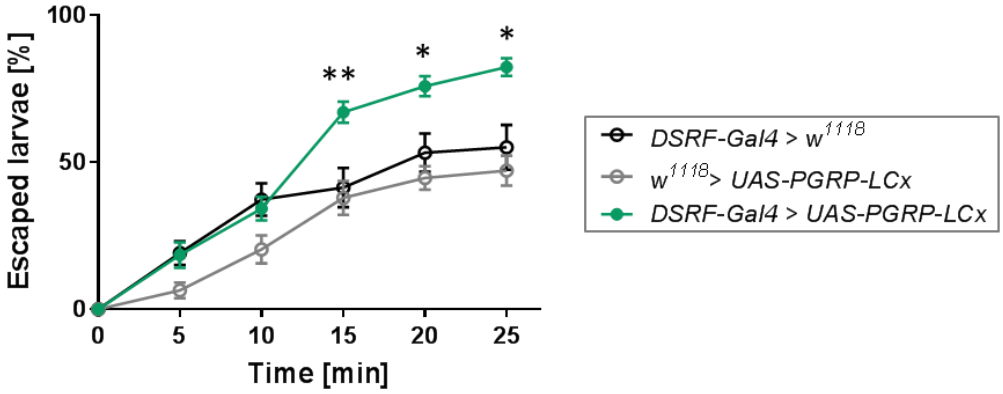

Figure 27: Hypoxia sensitivity induced by *PGRP-LCx* overexpression in terminal tracheal cells. Hypoxia sensitivity assay with *DSRF-Gal4 > w^{1118}* (n = 11), *w^{1118} > UAS-PGRP-LCx* (n = 14) and *DSRF-Gal4 > UAS-PGRP-LCx* (n = 13). The L3 larvae were placed in a food vial under hypoxic conditions (2-3 % O^2) and monitored over 25 min. The escaped larvae were counted every 5 min. Represented are means ± SEM. Statistical significance was tested with Man-Whitney test. * $p < 0.05$, ** $p < 0.01$.

The controls showed an escape rate of 19.1 ± 4 and 5.8 ± 2.8 % at 5 min and 37.3 ± 5.5 % and 19.2 ± 5 % at 10 min. After 15 min the escape rate rose slowly to 41.4 ± 6.7 % and 36.2 ± 5.9 %. At 20 min 53.2 ± 6.5 % and 43.1 ± 4 % of the control larvae escaped the medium. These values increased to 55 ± 7.6 % and 45.8 ± 5.3 % after 25 min under hypoxic conditions. In the first ten minutes there was no difference observed between *PGRP-LCx* larvae and both of the controls (Fig. 27). After 15 minutes significantly more *PGRP-LCx* larvae left the medium than control larvae (66.5 ± 4.5 %, $p = 0.0090$). These values increased further in the last ten minutes of the experiment with means of 77 ± 3.8 % ($p = 0.0192$, 20 min) and 83 ± 3.4 % at 25 min ($p = 0.0160$).

3.5.2.3 Initiation of apoptosis in the terminal cells

The phenotype of the shrunk cells at *PGRP-LCx* overexpression was compared to the terminal cells after initiation of apoptosis. Terminal cell death was achieved by ectopic expression of two mediators of programmed cell death, *head involution defective* (*Hid*) and *reaper* (*Rpr*). The expression of *Hid* and *Rpr* in the tracheal terminal cells by crossing with the *DSRF* driver line resulted in early death of the larvae. They started to crawl out of the medium very early and died presumably due to oxygen undersupply. Normally the terminal cells are connected to all organs to ensure the oxygen supply of the whole larval body. The

branches of the terminal cells in the controls were spread over broad parts of the organs in the control (Fig. 28 A). Dissection of the intestine of the *Hid* and *Rpr* expressing larvae obtained a complete loss of the terminal cells (Fig. 28 B). The few residual cells were small, shrunk and showed a similar phenotype to the cells with IMD activation via *PGRP-LCx* expression in the terminal cells (Fig. 28 C).

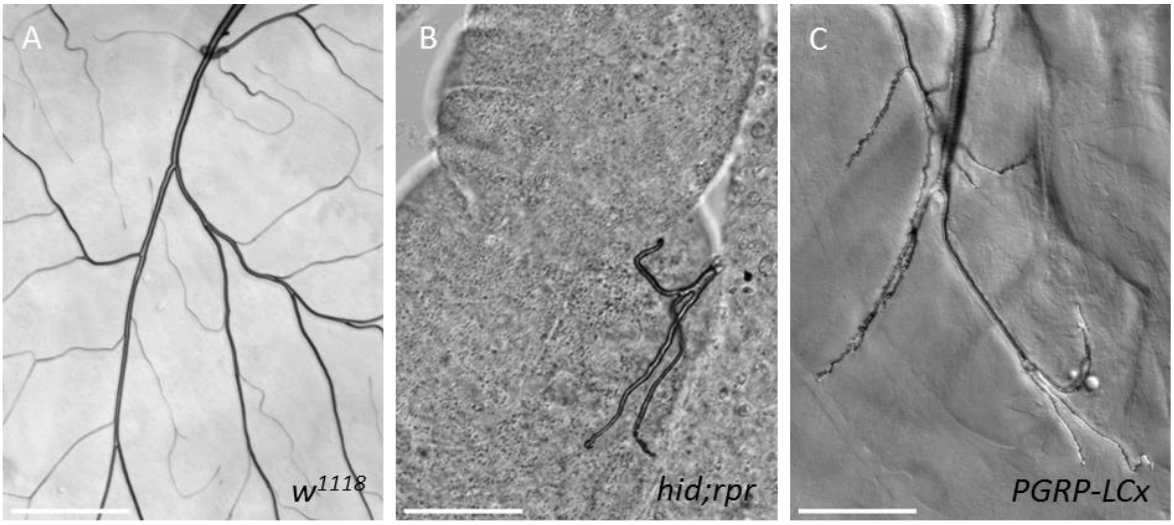

Figure 28: Tracheal terminal cells after induction of apoptosis and IMD pathway activation. Dissected intestines from L3 or L2 (**B**) larvae with the connected tracheal terminal cells of *DSRF-Gal4 > w^{1118}* (**A**) *DSRF-Gal4 > UAS-hid;rpr* (**B**) and *DSRF-Gal4 > UAS-PGRP-LCx* (**C**) in the DIC channel. Scale = 50 µM.

To evaluate if there is an induced apoptosis in the terminal cells with PGRP-LCx expression, an antibody staining for cleaved *Drosophila* Dcp-1 was performed (Fig. 29).

The control terminal cells of *DSRF-Gal4 > w^{1118}* are completely visible through the GFP signal. No evidence for cleaved Dcp-1 could be detected in the terminal cells (Fig. 29 A).

The terminal cells of *DSRF-Gal4 > UAS-PGRP-LCx* were positive for Dcp-1 staining (Fig. 29 B). Some of the cells showed an inconsistent result (App. Fig. 37). With an increased GFP signal in the cells, the Dcp-1 staining was decreased. All cells with a distinct Dcp-1 staining showed only a weak GFP signal.

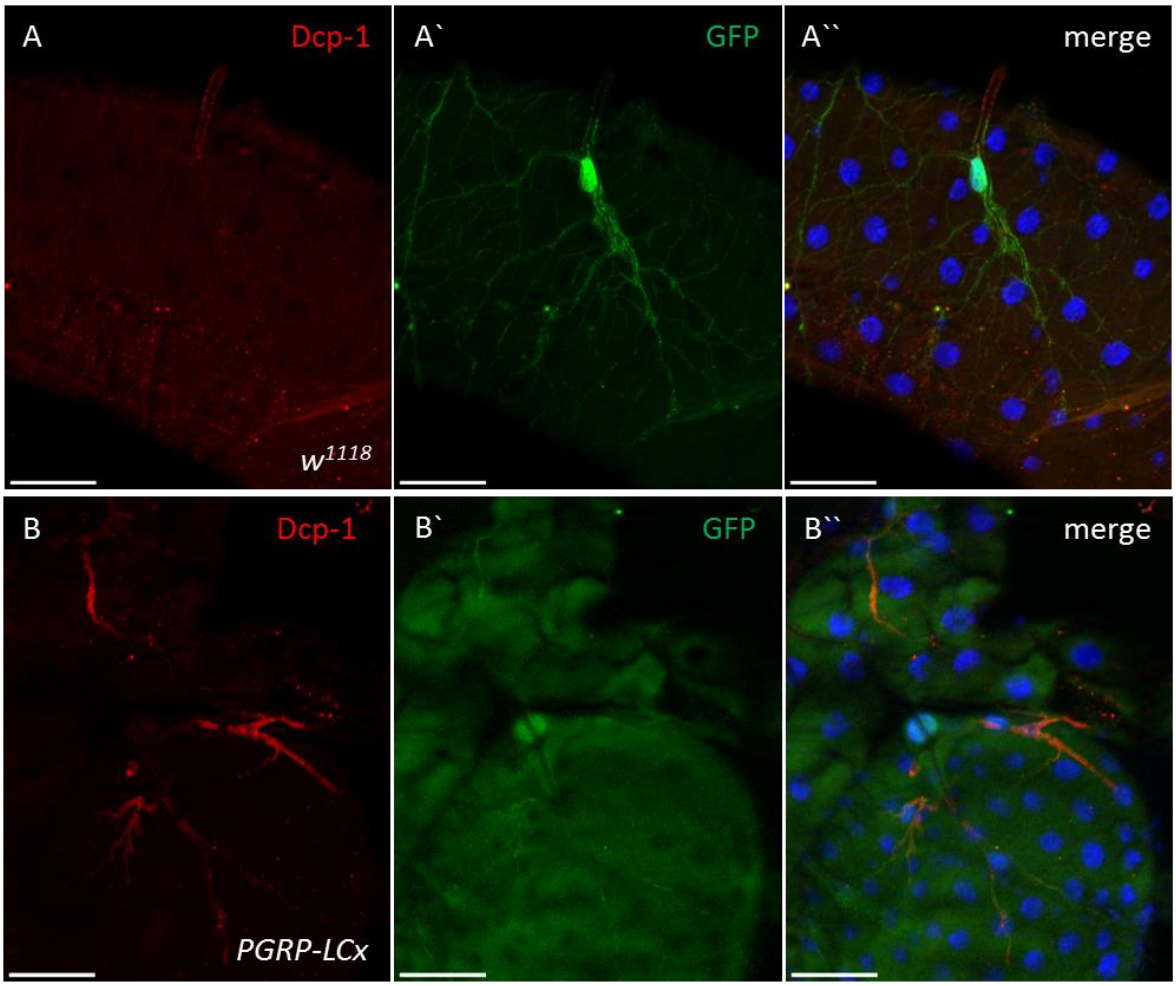

Figure 29: Dcp-1 staining of the terminal cells with *PGRP-LCx* expression. Dissected intestines of *DSRF-Gal4 > w^{1118}* (**A**) and *DSRF-Gal4 > UAS-PGRP-LCx* (**B**) with the connected terminal cells were stained with cleaved *Drosophila* Dcp-1 antibody (**A**, **B**). The terminal cells were counterstained with a GFP antibody (**A`**, **B`**). The merge of both is shown with DAPI staining of the cell nuclei (**A``**, **B``**). Scale = 50 µM.

3.5.2.4 AMP expression in the tracheal terminal cells

To get to know what role the IMD pathway plays in the terminal cells, the *ppk4* driver line for the whole trachea was used to express the secreted IMD receptor *PGRP-LE*. In this line the gene for the antimicrobial peptide *drosomycin* (*Drs*) is fused to GFP. Accordingly, the activation of the IMD pathway can be followed by the visualized AMP expression in the tissue (Fig. 30).

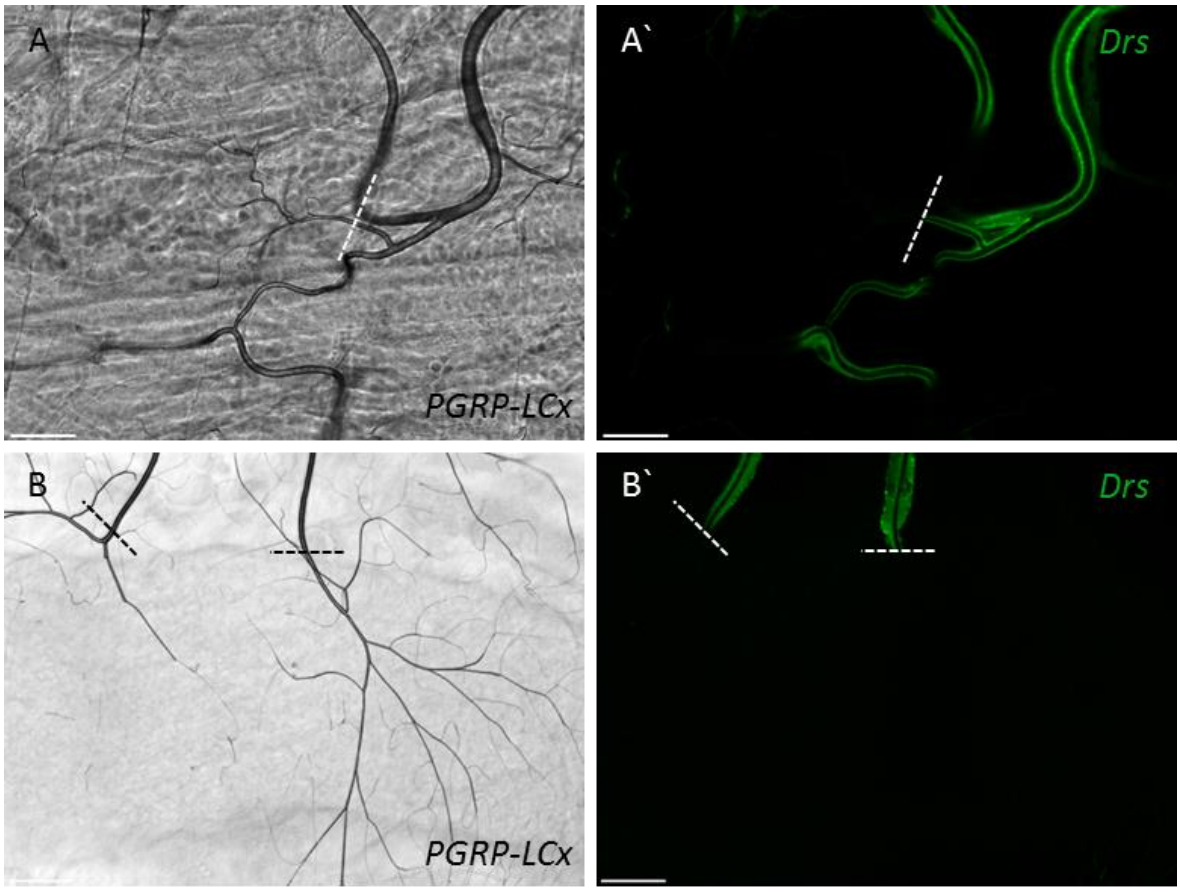

Figure 30: Ectopic expression of *PGRP-LE* in the trachea reveal no IMD pathway activation in the terminal cells. IMD pathway was activated in the trachea by ectopic expression of the IMD receptor *PGRP-LE*. The activation was visualized by the downstream antimicrobial peptide drosomycin (Drs) fused to GFP (*ppk4-Gal4 > UAS-PGRP-LE; GFP-Drs*). The tracheal terminal cells of the L3 larvae were either observed in a filet preparation (A) or on the dissected intestine (B). The dashed line displays the proximal end of the terminal cell. Scale = 50 µM.

Remarkably the GFP signal was observed in the whole trachea except in the terminal ells. The signal stopped exactly where the terminal cell started. It was observed in the terminal cells connected to the cuticle as well as on the intestine (Fig. 30 B, D).

3.5.2.5 Ectopic overexpression of *PGRP-LCx* in the whole tracheal system

It was already shown in 3.1 that IMD pathway activation led to a different phenotype by *PGRP-LCx* overexpression in the whole tracheal system. This IMD pathway influence on the whole tracheal system was investigated in detail by using the *ppk4-Gal4* driver line. *PGRP-LCx* expression in the whole trachea led to a massive thickening of the epithelium of 14.2 ± 2.9 µm ($p = <0.0001$), compared to the controls with mean thicknesses of 3.3 ± 0.7 µm and 3.5 ± 0.5 µm (Fig. 31).

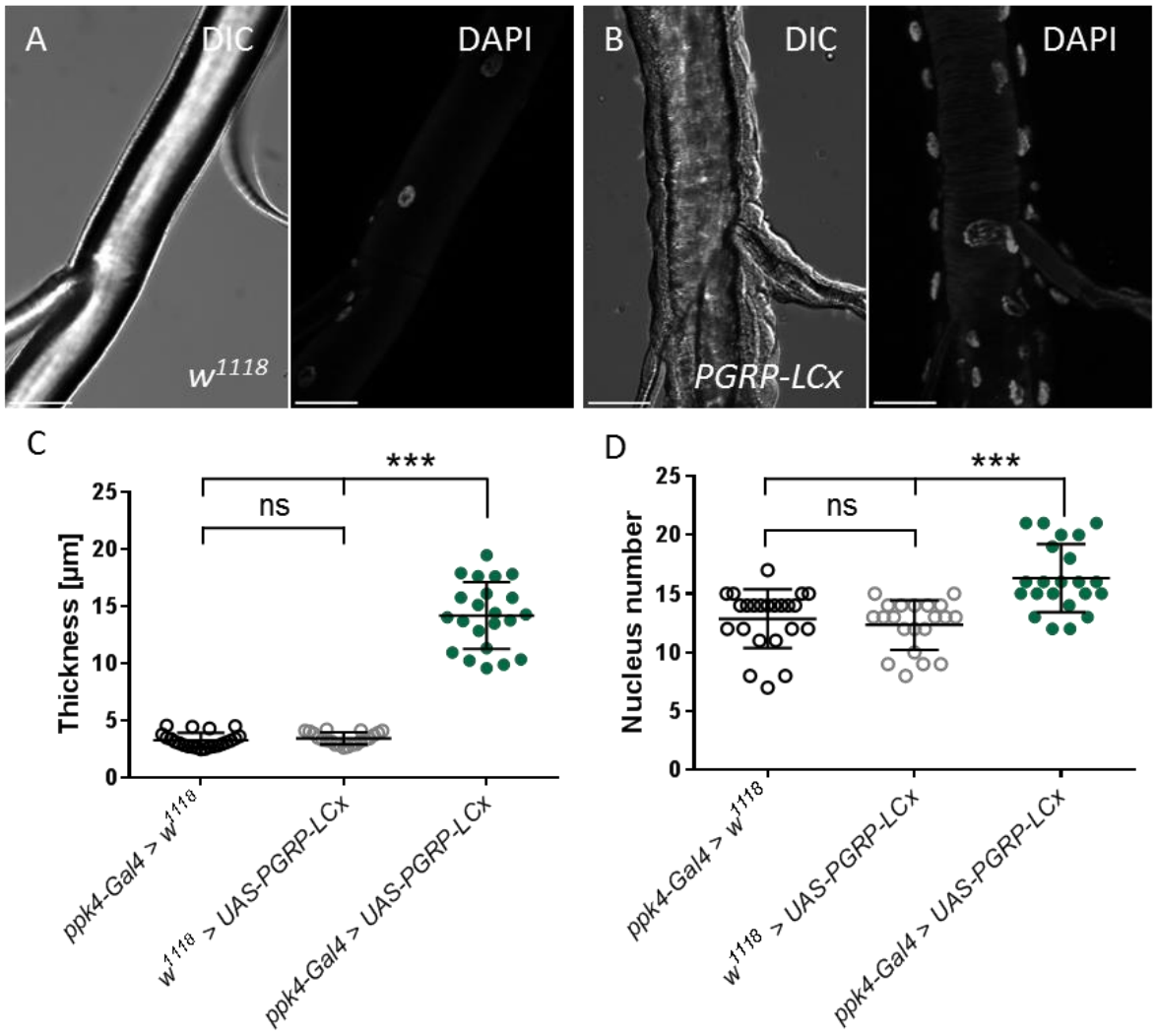

Figure 31: Quantification of epithelial thickness and nucleus number at overexpression of *PGRP-LCx* in the trachea. The tracheae of *ppk4-Gal4 > w*^{1118} (**A**) (n = 23), *w*^{1118} *> UAS-EGFR*^{CA} (n = 21) and *ppk4-Gal4 > UAS-PGRP-LCx* (**B**) (n = 22) were dissected, stained with DAPI and analyzed under the microscope (**A**, **B**). Quantification of epithelial thickness (**C**) and nucleus number (**D**) occurred in AxioVision. For the measurement the 8th segment of the dorsal trunks was used. The controls are displayed in open black and grey circles, the over expression of PGRP-LCx in the tracheal system is displayed in filled green circles. Statistical significance was tested with Mann-Whitney test, *** = $p < 0.001$, ns = not significant.

Adapted to this observation the number of nuclei in *PGRP-LCx* tracheae was increased, too (16.3 ± 2.9, controls = 12.9 ± 2.5 and 12.3 ± 2.1, p = <0.0001).

Besides the thickness of the epithelium, a melanization of the dorsal trunks was observed in nearly all larvae (Fig. 32). The brownish discoloration showed up mostly in the upper (posterior) part of the dorsal trunks, near the posterior spiracular openings.

In general, it was conspicuous, that the tracheae were very fragile and sensitive upon dissection. Staining of the cell membranes with an antibody against the septate junction protein Coracle revealed a distinct change in the cell shape (Fig. 32).

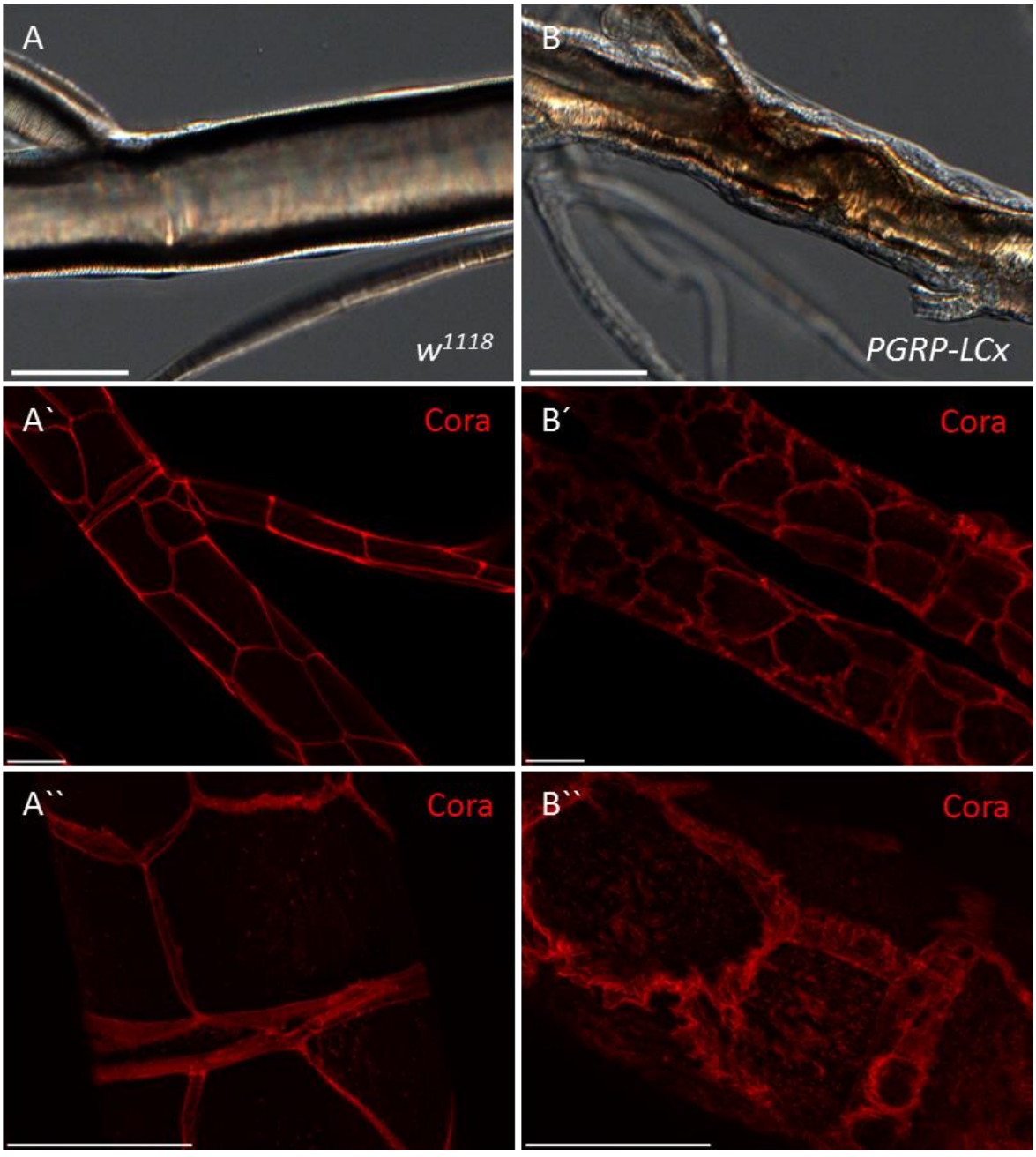

Figure 32: Melanization and cell membranes in the dorsal trunks with activated IMD pathway. The tracheae were dissected from *ppk4-Gal4 > w^{1118}* (**A-A``**) and *ppk4-Gal4 > UAS-PGRP-LCx* (**B-B``**) and observed in brightfield (**A, B**) or under fluorescence light. Antibody staining against the cell membrane protein coracle (Cora). Fluorescence pictures were taken in 20x (**A`-B`**) and 63x (**A``-B``**). Scale = 50 µm.

The cells in *PGRP-LCx* tracheae looked smaller and rounded. The thickening of the epithelium was visible in this staining. The cell membranes looked unraveled and irregular but the general structure of the tissue and the particular segments were still maintained.

3.6 Generation of a new driver line for the tracheal terminal cells

It is known, that some of the *pickpocket* (*ppk*) genes are expressed in the trachea. The promotor region of the *ppk* gene 11 was cloned into a *Gal4* expression vector, to generate a new driver line for the tracheal system in larvae (App. pBPGUw-*ppk11* sequence map). A sequence from 1424 bp directly upstream of the gene was chosen. The construct was prepared for injection into early embryos. After injection of the constructs the corresponding fly lines with the integrated constructs were analyzed. These lines were crossed with a *UAS-GFP* line to visualize, if the cloned promotor region had an activity in the tracheal system.

The view on the whole larvae showed a GFP expression in the tracheal terminal cells on the body wall of the whole larvae (Fig. 33 A-C). It seems, that the expression is restricted to the terminal cells (Fig. 33 A`-C`).

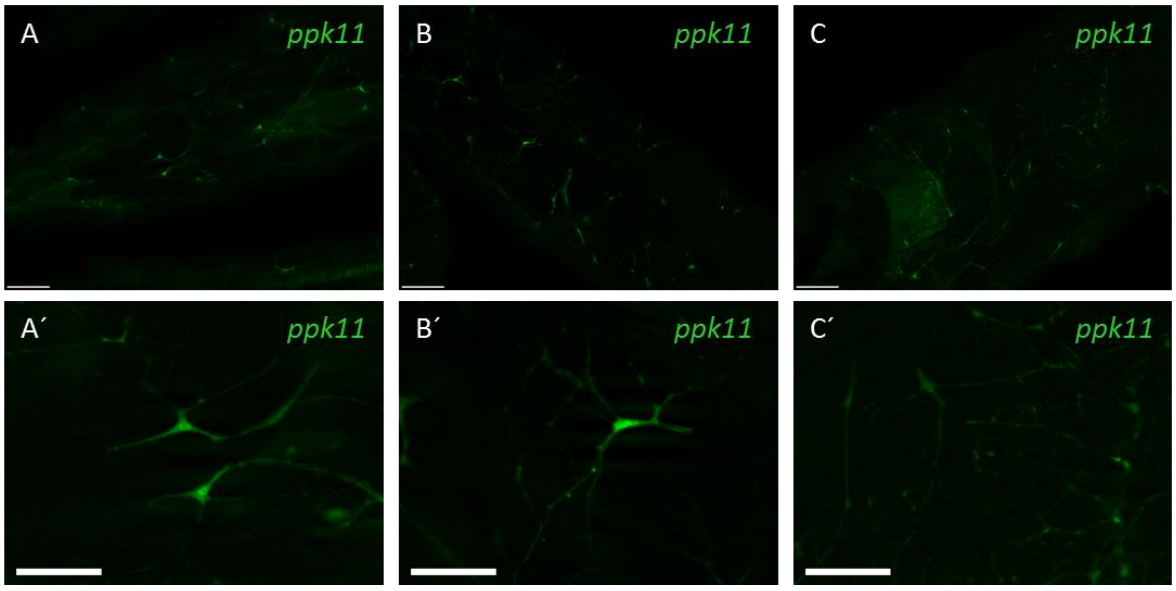

Figure 33: Activity pattern of the *ppk11* promotor in the larval tracheal system. *ppk11-Gal4* was crossed to a *UAS-GFP* line to visualize the activity of the *ppk11* promotor. The *ppk11* promotor showed an activity pattern in the terminal cells visible in the whole larvae from dorsal (**A**), lateral (**B**) and ventral (**C**). Scale = 200 µm (**A**-**C**), 100 µM (**A`**-**C`**).

4 Discussion

The tracheal system of *Drosophila* consists of a thin monolayer of epithelial cells that supplies all parts of the body with oxygen. It shares structural and functional similarities with the human lung. Moreover, the development, gene expression profile and immune response are surprisingly similar. Because of the presence of orthologes to most asthma-susceptibility genes in *Drosophila*, the tracheal system became a model for lung diseases like asthma in the recent years (Roeder *et al.*, 2009). Moreover, the tracheal system of the fruit fly was already used as a cancer model for drug screenings (Levine and Cagan, 2016). In this study the impact of the ectopic expression of different oncogenes in the respiratory system of *Drosophila* was investigated. The genes were either expressed in the whole tracheal system or in the specialized cells for the oxygen supply to the organs, the terminal cells. Several pathways whose alterations are known in human lung cancers were addressed. This includes RTK pathways (Egfr, Fgfr, Pvr, InR, Alk) with the downstream effectors (Ras, Raf, Sem/Rl, PI3K92E, Akt), Wnt/β-catenin signaling (Arm, Apc) and cell cycle regulators like p53 and Cdk4. Moreover, activation of the the IMD pathway, homolog to the TNF pathway known for dual anti-apoptotic and pro-apoptotic roles in carcinogenesis, was analysed.

4.1 Expression of different oncogenes provokes structural changes in the tracheal system

Most parts of the development of the trachea occurs in the embryo, only the differentiation of terminal cells is accomplished in larval stages. From stage 11 onwards, no cell division takes place anymore. The further growth occurs without generation of new cells by migration, rearrangement and elongation of the existing cells (Samakovlis *et al.* 1996a). Accordingly, results obtained with the two different tracheal driver lines used in this study led to different outcome by expression of the selected oncogenes. Most of the experiments with ectopic overexpression of oncogenes driven by the *btl* driver line led to death in very early developmental stages most likely in the embryo or the first instar larvae. This line drives the expression in embryonic and all larval stages in the whole tracheal system. Moreover, the level of expression is relatively high. Intervention in a critical period of the

tracheal development may be one reason for this severe phenotypes. The *ppk4* driver is active through the larval stages. At this stage the tracheal development is fully terminated and most of the cells are differentiated. The occurring phenotypes by the expression with this driver line were less severe. The observed phenotypes comprise thickening of the epithelium, enlarged and increased number of nuclei, melanization, but also aberrant structures and the even strongest result – death of the larvae in early developmental stages (Fig. 8, Tab. 4). In human cancers, histological characteristics of the tissue are extremely important to determine tumor class and stage. For example, the nucleus size is used as one of the prognostic factors for worse outcomes in LUSC (Kadota *et al.*, 2014).

Ectopic expression of the fusion genes comprising the human *EGFR* gene and the matching *Drosophila* orthologes showed a mild phenotype if driven by both driver lines. The *Drosophila* fusion domains are the wildtype domains of the proteins and do not comprise activating mutations. The simple overexpression of the proteins could explain the mild phenotype by ectopic expression with the strong *btl* driver line, while constitutively activated Egfr and Pvr showed a strong phenotype. For *Akt*, only an overexpression of the wildtype protein was used, which could explain the mild phenotype. This could also explain the complete absence of a phenotype by ectopic *Cdk4* expression. There was no visible phenotype by activating the human FGFR homolog *breathless* (*Btl*) which plays an important role in tracheal branching and development of the respiratory system (Klämbt *et al.*, 1992).

In contrast, most of the other oncogenes were able to induce a phenotypical change in the tracheal epithelium by expression in the tracheal system. Most of the genes, which showed a phenotype if either of both driver lines was used, are constitutively activated isoforms ($Egfr^{CA}$, *Pvr*, *Alk*, Ras^{V12}, Raf^{GOF}, *PI3K92E*, *Arm*). All these genes are relevant in human lung cancer and represent each a known driver gene in cancer development (Ding *et al.*, 2008; CGARN, 2012; CGARN, 2014). These genes encode for kinases that display prospective targets in targeted cancer therapy (Shtivelman *et al.*, 2014). Especially mutations in *EGFR*, *KRAS* and the *ALK* are of importance in lung cancer of never smokers (Govindan *et al.*, 2012). *P53* is an important tumor suppressor gene in all lung cancer types (Peifer *et al.,* 2012; CGARN, 2012; CGARN, 2014). Nevertheless, it was not possible to provoke any phenotype by depletion of the single *p53* gene.

In the approach presented here, only single genes were altered in the corresponding models. In human cancer at least three driver mutations have to occur, to drive the tumor progression into a malignant state (Tomasetti *et al.*, 2015). Alteration of multiple genes and combinations of activation of an oncogene and depletion of a tumor suppressor gene in *Drosophila* can lead to neoplastic hyperproliferation of a tissue (Brumby and Richardson, 2005; Wu *et al.*, 2010; Herranz *et al.*, 2012). This may depict the real situation in human tumors in a more representative picture and produce a stronger phenotype.

PGRP-LCx, Pvr and $Egfr^{CA}$ were the only genes that could produce a severe phenotype of the already differentiated tracheal cells of L3 larvae, alone. This reflects the enormous potential of this genes to convert a normal differentiated cell into a cell with completely different characteristics. Pvr and Egfr belong to the group of receptor tyrosine kinases that initiate several downstream signaling cascades involved in important cellular processes.

Drosophila PDGF/VEGF receptor related (Pvr) is homologous to the mammalian platelet derived growth factor (PDGFR) and to the vascular endothelial growth factor receptor (VEGFR). Mutations in both receptors were found in cancers and are known to play a role in tumor angiogenesis (Sakurai and Kudo, 2011). There are therapeutics available that directly target the receptors and thereby should inhibit signaling and block proliferation and angiogenesis.

Because of the high relevance of EGFR mutations in lung cancer, this tracheal phenotype was characterized in detail.

4.2 Characterization of the tracheal phenotype caused by $Egfr^{CA}$ expression

As shown in 3.1, ectopic expression of a constitutively activated isoform of the *Egfr* ($Egfr^{CA}$) in the *Drosophila* trachea leads to death in early L3 larvae. The larvae start to crawl out of the medium and die (Fig. 9). Lethality was the most obvious phenotype. The hypoxia response phenotype appears due to the metaplasia phenotype of the tracheal epithelium and the resulting lack of oxygen supply to the organs. Owing to the extremely thickened epithelium there was no air filling of the dorsal trunks anymore, which excluded any gas exchange in the downstream parts of the tracheal system. Thus, almost no pupae and adult flies could be observed in $Egfr^{CA}$ animals (Fig. 10).

Immunohistochemical analysis of the tracheal structure revealed epithelial dysplasia with irregular cell sizes and curled cell membranes (Fig. 11; Fig. 12). Partially, big cells with more than one nucleus were observed. The weak membrane associated Arm staining and the diffuse signal over the whole tissue could point to a cytoplasmic localization of the protein. Additionally, the diffuse appearance of Cora and Dlg1 could point to a loss of the septate junctions and thereby the cell polarity. This may accommodate with an induced EMT-like process in the tracheal epithelium. The EMT-like phenotype and accompanying loss of polarity of the cells comprise possibly enabled metastatic behavior of these enlarged cells. In human breast cancer, polyploid giant cancer cells and epithelial-mesenchymal transition (EMT) are associated with invasion and metastasis (Fei *et al.*, 2015). It was shown, that increased EGFR signaling in the airway epithelium leads to goblet cell hyperplasia, squamous metaplasia, decreased epithelial junctional barrier integrity and an EMT-like phenotype in the cells of the human lung (Shaykhiev *et al.*, 2013). EMT is a process by which epithelial cells lose their apical-basal cell polarity and the tight junctions between cells. The cells gain mesenchymal characteristics and get invasive and metastatic properties (Nieto *et al.*, 2016). Dlg1 is located in the septate junctions of the membrane and is known to function as a tumor suppressor gene in *Drosophila* (Fig. 11). Loss of Dlg1 lead to defects in proliferation control and cell polarity, adhesion and differentiation (Woods and Bryant, 1991). Arm is the β-catenin orthologue in *Drosophila* (Fig. 11). Localization of β-catenin is Wnt/β-catenin signaling dependent. Without Wnt signaling, cytoplasmic free β-catenin levels are low because of a constitutive degradation process (Valenta *et al.*, 2012). In this case β-catenin is bound to E-cadherin and localizes at the membrane as part of the adherens junction complex (Gottardi *et al.*, 2001). Activated Wnt signaling inhibits β-catenin degradation and leads to accumulation in the cytoplasm and translocation to the nucleus (Valenta *et al.*, 2012). Loss or relocalization of β-catenin from the cell membrane into the cytoplasm and transcriptional activity in the nucleus are associated with EMT and were found in cancer cells (Kim, Daniels and Hay, 1998). It is known that MAPK signaling is required for Wnt signaling and β-catenin activity (Hall and Verheyen, 2015).

Morphological changes of the nuclei are associated with numerous cancer types and are common characteristics of cancer cells. Nucleus size and atypia are accepted as diagnostic and prognostic factors (Jevtić *et al.*, 2014). In this study, quantification of the nucleus size comprised significant differences between Gal4 control and $Egfr^{CA}$ (Fig. 13). Furthermore,

the nuclei number in the analyzed dorsal trunk metamere was increased indicating a proliferation of the cells. Egfr is involved in embryonic control of tube length by restricting the elongation of the tracheal dorsal trunk. Ectopic expression in the developing embryo leads to decreased tube length but with unaltered cell number (Olivares-Castiñeira and Llimargas, 2017).

Ectopic expression of *Egfr*^{CA} in the tracheal system of *Drosophila* leads to a distinct change in the epithelial structure with similarities to the changes in human tissues provoked by increased Egfr activity. Together with the size and structure and the mitotic activity of the nuclei a proliferative state and meta- and hyperplasia of the tracheal epithelium, induced by the constitutive activation of Egfr, can be assumed.

4.3 Establishment of a whole animal drug screening approach by using *Egfr*^{CA} animals

Mutations in the EGFR gene are common in NSCLC and are commonly found in tumors that are sensitive to the treatment with Gefitinib (Pao *et al.*, 2004). Treatment with specific TKIs, such as Erlotinib exhibited impressive results with prolonged survival. The response rate range from 65 to 94 % with a median survival of 2 years (Janne, 2006). In comparison untreated NSCLC patients have a median survival rate of only 17 weeks (Rapp *et al.*, 1988). The human and the *Drosophila* Egfr comprise 59 % identity in the protein sequences of the tyrosine kinase domain and 99 % sequence identity in the ATP binding pocket of the protein. This leads to a similar mode of action by binding inhibiting compounds like Erlotinib and Gefitinib and highlight the possibility to test EGFR TKIs in *Drosophila* to identify personal treatment options (Aritakula and Ramasamy, 2008).

By using the lethal phenotype caused by the expression of a constitutively active isoform of *Egfr* (*Egfr*^{CA}) in the tracheal tissue of L3 larvae, a drug screening approach was established (Fig. 14). The readout was a simple life-death screening by determining the pupation rate as a positive outcome. First testing of different TKIs obtained the selectivity of the system to identify specific EGFR TKIs (Fig. 15). As expected, there was no positive response to the ALK inhibitors. Additionally it is not suited to test anti-proliferative agents like Docetaxel and Paclitaxel. Even the control larvae die on this treatment, what is not surprising because of the effect on proliferating cells. This was also observed for Fluvastatin

and the MEK inhibitor Trametinib. In a recent study with a *btl > Ras,PTENi* tumor model in *Drosophila* trachea a positive synergistic effect of both compounds with lower concentrations was shown (Levine and Cagan, 2016). Here the control larvae died, demonstrating an overall negative effect on larval viability at high concentrations.

There are several other established drug screening systems published, that utilize *Drosophila*. Most of these testing systems have the need of relatively high investment in time and effort to obtain reproducible results. This includes the use of adult flies, dissection of the target tissue, luciferase assays or measurement of GFP signal intensities (Willoughby *et al.*, 2013; Markstein *et al.*, 2014). The here established system is convincing because of its simplicity, similar to the *btl > Ras,PTENi* tumor model presented by Levine & Cagan (Levine and Cagan, 2016). In the future, automated readouts by registration of movements in single wells would transform the established system to an even more convenient level, suitable for high-throughput applications.

A screening of 978 FDA-approved drugs from a drug library was performed (App. Tab. 6). With this approach it was possible to identify four specific EGFR inhibitors which are already commonly used as EGFR inhibitors in targeted lung cancer therapy. The specific EGFR inhibitors Afatinib, Erlotinib and Gefitinib were identified as positive hits. The Btk inhibitor Ibrutinib, turned out to be positive in this screening (Tab. 5). It binds irreversible to the Bruton's tyrosine kinase (Btk) and is clinically used in treatment of malignant B cells. For this TKI a high efficiency on Btk and less potency on EGFR in cell free assays is reported. Here it shows a comparable effect to Afatinib and Gefitinib in rescuing the lethality of $Egfr^{CA}$ (Tab. 5). Thus, further *in vivo* testing might detect a higher unknown effect of Ibrutinib on inhibiting EGFR. Lapatinib another TKI for EGFR positive tumors is approved in breast cancer treatment but turned out to be ineffective in this screening. The results show the possibility to identify novel specific EGFR TKIs with this approach used in this study.

Surprisingly, embryonic Egfr activity and functions in different developmental steps in the embryo seems to be unimpaired by the treatment presented here. This could be caused by the robust envelope of the *Drosophila* embryo. It might be impossible for the positive tested TKIs to permeate through the chorion of the embryo. Thus, specific EGFR inhibitors like the ones already used in cancer therapy including Afatinib and Gefitinib seems to have no adverse effect on the embryonic development and throughout the larval stages. This is

a great advantage in this testing approach. It is not necessary to wait until larval hatching and to handle larvae or adult flies, one can directly treat the embryos.

Mutations that promote the resistance against first or second generation TKI lead to the need of more effective solutions. Furthermore, it is known that not only single mutations promote tumor development. There is more than one driver mutation and many passenger mutations that are known to support tumor progression. One promising approach to overcome these problems could be the combination of low dosed TKIs with a synergistically acting drug (Tong *et al.*, 2017). The suitability of the here established approach for combinational testing of different compounds was investigated in a second screening (Tab. 5, App. Tab. 6). The combination of all 978 compounds with a low dose of Afatinib showed a synergistic effect of the TKI on some of the compounds besides the aforementioned positive hits. This includes: Sorafenib Tosylate, Enoxacin, Pitavastatin Calcium, Bexarotene, Bacedoxifene and Tebipenem pivoxil. These hits should be confirmed in further testings. For none of these compounds a direct effect on EGFR is reported. Sorafanib Tosylate is a multiple kinase inhibitor with activity on RAF, VEGFR, PDGFR, Flt3, c-Kit and FGFR and weak activity against MEK and ERK phosphorylation but not against EGFR, at least in cell-free assays. Enoxacin is an antibacterial agent that acts by inhibiting bacterial DNA gyrase and topoisomerase IV. It was already tested as an anti-tumor agent in prostate cancer cells with high effectiveness. Enoxacin was able to decrease cell viability, induce apoptosis, cause cell cycle arrest and inhibit cell cycle arrest of the cell lines (Sousa *et al.*, 2013). Pitavastatin Calcium is a highly effective HMG-CoA reductase inhibitor and belongs to the family of statins. Statins were shown to have an effect on cancer cells (Wong *et al.*, 2002). Statins are commonly used as cholesterol lowering drugs. Recent studies revealed a potency in cancer treatment. Pitavastatin decreased tumor growth and improved survival in tumor bearing mice (You *et al.*, 2016). Levine and Cagan (2016) showed a positive effect of the statin group corresponding Fluvastatin in a *Ras, PTEN Drosophila* model, as well. Bexarotene is a retinoid specifically selective for retinoid X receptors and is used as antineoplastic agent in the treatment of cutaneous T-cell lymphoma. It was shown to inhibit proliferation of mammary epithelial cells in mice (Li *et al.* 2008). Bazedoxifene is a non-steroidal, indol-based estrogen receptor modulator (SERM) binding to ERα and ERβ. It is used for prevention and treatment of osteoporosis.

Tebipenem pivoxil is an oral carbapenem antibiotic used to treat otolaryngologic and respiratory infections.

The drug screening approach established in this study emerged not only as a possibility to identify single compounds with inhibiting effects on EGFR but may also identify compounds with a synergistic effect in combinational applications. By this it will be possible to analyze all kinds of combinations with all promising compounds in different concentrations. This could result into new treatment options for lung cancer with mutations in *EGFR*. The third-generation of TKIs are advanced for T790M mutations in *EGFR* (Russo *et al.*, 2017). It should be confirmed, that this screening approach is also suitable for compounds with an effect on *EGFR* harboring a T790M mutation. Furthermore, it should be ascertained, if the screening system is suitable for testing of monoclonal antibodies targeting EGFR.

It was possible to verify specific compounds with an EGFR inhibiting effect. These compounds are already known and used in human cancer therapy in tumors with EGFR activating mutations. Thus, a whole animal single gene screening approach for compunds with inhibiting effect on mutated Egfr was successfully established.

4.4 Afatinib and Gefitinib rescue the $Egfr^{CA}$ phenotype in the tracheal system

First-generation TKIs, like Erlotinib and Gefitinib, competitively interact with the ATP-binding site of EGFR preventing autophosphorylation and consequently inhibit downstream signaling. They are successfully applied as treatment for tumors with mutations in the *EGFR* gene (Fry, 2003). Second-generation TKIs bind covalently to the tyrosine kinase domain. The covalent binding comprises an advantage over first-generation TKIs and the acquiring T790M and other resistance causing mutations (Yu and Riely, 2013). Exon 19 deletions and exon 21 mutations are the most common mutations in EGFR positive tumors (Eberhard *et al.*, 2005). Treatment with Erlotinib and Gefitinib is often associated with tumor recurrence and a second mutation in T790M in the EGFR gene (Pao *et al.* 2005b). Afatinib belongs to the second-generation TKIs and is an irreversible inhibitor of EGFR, HER2 and HER4 suited for the treatment of NSCLC harboring exon 19 deletions or exon 21 (L858R) mutations. Additionally, Afatinib showed a 100-fold higher effectiveness on T790M mutated EGFR than Gefitinib. It was a promising alternative to first-generation TKIs like Erlotinib and Gefitinib to overcome the acquired resistance (Li *et al.* 2008). Now,

treatment with Afatinib turned out in a similar mutation rate in T790M compared to treatment with Erlotinib and Gefitinib (Tanaka *et al.*, 2017).

Afatinib and Gefitinib turned out as positive hits in the screening (3.3.2) and were selected for detailed characterization in the treatment of $Egfr^{CA}$ animals. Both were able to rescue the phenotypes, lethality and impaired tracheal structure, to ensure survival of the larvae and successful development into the adult flies (Fig. 16; Fig. 17). Moreover, the thickness of the epithelium and the nucleus number was decreased to a control level (Fig. 18). This indicates an inhibition of proliferation of the tracheal cells. Gefitinib treated embryos showed a reduced number of hatching adults at higher concentrations (Fig. 20). This occurs presumably due to EGFR inhibition in important developmental steps in morphogenesis from larvae into adult flies (Shilo, 2003). The Gefitinib treated adults showed a concentration dependent atypical wing phenotype (Fig. 21; Fig. 22). It was already published in 2008, that larval treatment with Gefitinib has a negative effect on the development of several adult tissues (Aritakula and Ramasamy, 2008). The impact of the reversible EGFR TKI Gefitinib lasts until the pupal stages and impairs adult formation. In contrast, the treatment with the irreversible TKI Afatinib showed no visible changes in the adult flies.

Afatinib and Gefitinib showed differences in the required concentrations that rescue the phenotype (Fig. 19). Gefitinib was more effective than Afatinib at lower concentrations without showing an impaired adult formation. This does not reflect the real situation in lung cancer treatment where Afatinib is lower dosed than Gefitinib (Burotto *et al.*, 2015). It is certainly not feasible to adopt this outcome in the fly to the situation in human. In humans the dose dependency is closely related to the patient tolerance to the treatment. Afatinib shows in fact more side effects compared to Gefitinib, but improved outcome in patients with EGFR mutations (Park *et al.*, 2016). Thus, the search for new compounds for combined therapy of low-dose Afatinib with another compound with synergistic effects could be a promising approach to overcome side effects by low dosing but without loss in treatment efficiency.

4.5 Activation of the MAPK pathway leads to changes in the terminal cells

The tracheal terminal cells are characterized by their plasticity in response to different conditions such as hypoxia or differences in the supply with nutrients. Terminal cell sprouting is dependent on FGF and HIF signaling (Jarecki, Johnson and Krasnow, 1999; Centanin *et al.*, 2008). An additional dependency on insulin signaling was described as another factor for terminal cell remodeling (Linneweber *et al.*, 2014). The branching process is regulated by FGF signaling. Ras and rolled/sem act downstream of the FGF receptor and induce branching during embryonal tracheal development (Imam *et al.*, 1999). In larvae, FGFR signaling requires the Ras/MAPK pathway and Pointed for formation/outgrowth of the adult tracheal air sacs from the air sac precursor on the wing disc (Cabernard and Affolter, 2005).

Ectopic expression of several compounds of the Egfr pathway in the tracheal terminal cells lead to certain structural changes in these cells and a correlative change in hypoxia sensitivity was observed (Fig. 23; Fig. 24). The structural phenotype was distinct from the expression of downstream Ras^{V12} and *Sem*, while expression of *Egfr* showed a rather reverse outcome. In case of Ras^{V12} and *Sem* expression, branching of the cells was increased, but only Ras^{V12} animals showed an increased hypoxia sensitivity (Fig. 25). This is presumably caused by the fact, that cells with Ras^{V12} expression seem not to be air filled (Fig. 24). Due to this, the oxygen supply is not guaranteed anymore. The shape of the cells is extremely altered which is accompanied with enlarged nuclei. The human *KRAS* is the most frequently activated oncogene in LUAD (32 %) (CGARN, 2014). Oncogenic *Ras* (Ras^{V12}) expression in the terminal cells can induce a massive phenotype with similarities to neovascularization in humans.

EGFR and FGFR are both tyrosine kinases sharing the same downstream components of MAPK signaling in general. While FGF signaling is restricted to particular tissues, EGFR is broadly expressed. EGFR signaling is activated by ligand binding and is regulated by three induceable feedback loops (Shilo, 2014). The intracellular protein Sprouty acts in the cytoplasm by inhibiting RAS/MAPK pathway. It binds to Drk and Gap1 downstream of the receptor and thereby blocks signal transduction to Ras (Casci *et al.*, 1999). It is known as an antagonist of EGF and FGF signaling (Kramer *et al.* 1999).

Although Egfr is upstream of Ras and has that impact of proliferation initiation on the cells of the dorsal trunks (3.2), no response was observed in the terminal cells. In contrast, a rather contrary effect was seen. The functionality of the cells was slightly impaired, as shown in the hypoxia sensitivity test (Fig. 25). Intracellular inhibition of components between the receptor and Ras could be the reason why the phenotype of $Egfr^{CA}$ and Ras^{V12} expression is so different. Sprouty could be a possible regulator. It is known, that loss of Sprouty leads to overactivity of the FGF pathway and induces branching (Hacohen *et al.*, 1998). FGF and VEGF signaling are important pathways in angiogenesis regulation, as well as PDGF signaling is (Sakurai and Kudo, 2011). FGF is known to regulate terminal cell branching in the larvae. The genome of *Drosophila* comprises one PDGF/VEGF related receptor gene (*Pvr*). Sprouting of the terminal cells seems strongly regulated by intracellular action of sprouty. Sprouty is discussed as angiogenesis inhibitor and as a possible target for angiostatic agents (Sabatel *et al.*, 2010).

4.6 Activation of the IMD pathway leads to impairment of the terminal cells

The epithelium of the tracheal system is able to launch an innate immune response in terms of the expression of antimicrobial peptides upon infection. The responsible transduction pathways comprise IMD, JNK and JAK/STAT whereas essential components of the Toll pathway are missing (Wagner *et al.*, 2008). It was found, that infection of the tracheal system with gram-negative bacteria leads to the expression of a cell-death promoting factor, but counteracting processes seem to prevent apoptosis of the cells (Wagner *et al.*, 2009). The *Drosophila* IMD pathway is homologous to the TNF pathway in mammals. Activation of both pathways result in NF-κB signaling (Silverman *et al.*, 2003; Park *et al.*, 2004).

IMD pathway activation via overexpression of the membrane bound peptidoglycan recognition receptor *PGRP-LCx* exclusively in the tracheal terminal cells leads to shrinking and decreased functionality of these cells (Fig. 26; Fig. 27). They show structural similarities to apoptotic cells. Staining with the *Drosophila* cleaved Death caspase-1 (Dcp-1) confirmed this assumption (Fig. 29). Dcp-1 staining correlates negatively with the *DSRF* driven GFP signal of the terminal cells (App. Fig. 37). This could imply, that a terminal cell with a GFP signal is still functional whereas a disappearing GFP signal points to apoptosis of the cell

confirmed by the more distinct Dcp-1 staining. This was consistent with the size of the cells. Most cells with a GFP signal seem larger than the cells positive for Dcp-1. This could explain why these animals are still alive, while animals with *Hid* and *Rpr* expression in the terminal cells die in earlier stages.

Reaper (Rpr) is sufficient to induce apoptosis in *Drosophila*. Head involution defective (Hid) is a second apoptosis promoting factor (White *et al.*, 1994; Grether *et al.*, 1995). Here, both factors were activated in the terminal cells of the tracheal system to induce apoptosis. The emerging larvae had no terminal cells anymore (Fig. 28). They died and showed the typical response to hypoxia by crawling out of the medium. Obviously, the terminal cells are essential for the larvae to supply oxygen to all organs and ablation of the terminal cells makes this impossible and leads to death. The emerging cell phenotype was similar to the phenotype induced by IMD activation. The terminal cells shrank and increased hypoxia sensitivity was observed presumably due to impaired structure and functionality of the cells. It was shown, that IMD signaling leads to the expression of *Rpr* and thereby induces cell death (Georgel *et al.*, 2001). This supports the assumption of IMD mediated cell death of the terminal cells by overexpression of *PGRP-LCx*. Activation of the IMD homologuous TNF pathway in endothelial cells by continuous stimulation with TNF and sustained signaling blocks proliferation and sprouting *in vitro* and inhibits angiogenesis *in vivo* (Sainson *et al.*, 2008). This displays similarities to the continuous activation of IMD signaling in the terminal cells resulting in decreased branching of the terminal cells.

IMD pathway activation via the secreted receptor PGRP-LE in the whole trachea and tracing of the *drosomycin* expression showed no AMP expression in the terminal cells (Fig. 30). This implies, that no IMD signaling is operative in these cells naturally. In contrast IMD activation in the tracheal trunks leads to a thickening of the epithelium and an increase in cell number (Fig. 31). Obviously, activation of IMD signaling has a dual effect in the different parts of the tracheal system. While a general activation of the immune response in the trunks is possible, it seems suppressed in the terminal cells. This could be a form of a protective mechanism against a damage of the terminal cells because of suplurious immune activity. Formation of the tracheal terminal cells starts in late embryogenesis and completes in early larval stages. Loss of these cells leads to death of the early larvae (Fig. 28). The tracheal terminal cells are important for the oxygen supply of all organs by branching over broad areas of the tissues. The immune response as reaction to infections can obviously lead to

impairment of the cells, this could be avoided by local immune suppression. It is possible, that one or multiple parts of the IMD pathway are missing in the terminal cells. This assumption needs to be confirmed. An identification of the transcripts of all essential properties for a functional signaling could be achieved by PCR. It is not possible to dissect the terminal cells, thus another possibility for specific RNA isolation of this cells is needed.
NF-κB activation in endothelial cells promotes pro-apoptotic and immune signaling whereas NF-κB activity in tumor cells comprise anti-apoptotic and pro-angiogenic features (Tabruyn and Griffioen, 2007). NF-κB response is cell type, stimulus and context dependent (Radhakrishnan and Kamalakaran, 2006). It is assumed, that the dual pro-apoptotic and and anti-apoptotic role of NF-κB signaling is dependent on the activity of the different transcription factor subunits (Chen *et al.*, 2003). NF-κB is activated by chemotherapy or radiation and is therefore often associated with resistance to apoptosis. But activation of NF-κB was also shown to induce the expression of apoptosis promoting genes in certain situations. Angiostatic agents induce NF-κB activation in endothelial cells. In addition NF-κB inhibition impairs the ability of angiostatic agents to block sprouting of endothelial cells (Tabruyn *et al.*, 2009). Activation of IMD signaling in the terminal cells leads to decreased branching and apoptotic phenotype of the cell possibly because of the extraordinary expression of AMPs. This seems similar to the situation of NF-κB activation in endothelial cells. In contrast, activated IMD signaling in the cells of the whole tracheal system induces an increase in cell number and probably resistance to apoptosis as NF-κB activation causes in tumor cells.
With the here presented phenotypes in the different parts of the tracheal system, further investigations of NF-κB signaling could lead to new insights into the dual role of this pathway for carcinogenesis and cancer treatment.

4.7 Summary and future perspective

Expression of different oncogenes was effective to induce structural phenotypes in the tracheal system of *Drosophila* larvae. The experiments were performed by ectopic expression of the single genes in the whole tissue. Expression of $Egfr^{CA}$ induces proliferation of the tissue. The larvae die in early developmental stages and display structural changes of the cells. Unfortunately, it was not possible to analyze the further processing and

progression of the tissue proliferation, because of the early death of the larvae. The use of a driver line with GFP expression in the trachea would be a good opportunity to trace the tracheal cells and to investigate their potential to leave the tissue formation. Substitution of the Gal4 repressor Gal80 can delay the expression of *Egfr*^{CA} to the adult fly. This would enable a larger time frame for the investigation of the tissue changes. Death of the larvae in early stages was successfully used to establish a drug screening system in a 96-well format. It was possible to identify specific inhibitors for the EGF receptor that are already used in cancer treatment. The established drug screening approach emerged not only as a good possibility to identify single compounds with inhibiting effect on EGFR but may also identify compounds with a synergistic effect in combinational application. It might by possible to adapt the system to the other oncogenes which can provoke a phenotype in the trachea, too. This would provide different tailored *Drosophila* models for drug screenings for the personalized therapy in cancer treatment.

The reversible first-generation TKI Gefitinib and the irreversible second-generation TKI Afatinib inhibit proliferation of the tissue and thereby not only rescue lethality but also the cellular tracheal phenotype. Nevertheless, treatment with Gefitinib showed a negative effect on adult structures. Search for new compounds for combined therapy of low-dose TKIs with another compound with synergistic effects could be a promising way to overcome negative effects. The here established approach may display a promising approach in this direction.

Whereas *Egfr*^{CA} expression in the whole tracheal system leads to proliferation of the cells, there was no visible phenotype in the terminal cells. The downstream signaling seems to be inhibited. Though, activation of downstream Ras and MAPK leads to increased branching of the cells. RNA isolation exclusively from the terminal cells would be a good possibility to investigate the impact of the altered gene expression in these cells on a transcriptional level. On one hand there is the branching initiation by activation of components from the Ras/MAPK pathway. On the other hand, activation of one of the major immune signaling pathways in the trachea leads to cell death of the terminal cells. However, *PGRP-LCx* expression in the whole tracheal system leads to proliferation of the tissue. Furthermore, it should be investigated if the terminal cell death is intiated by NF-κB activation or other connected pathways and if other factors like hypoxia play a role.

5 References

Adams MD, Celniker SE, Holt RA, Evans CA, Gocayne JD, Amanatides PG, Scherer SE, Li PW, Hoskins RA, Galle RF, George RA, Lewis SE, Richards S, Ashburner M, Henderson SN, Sutton GG, Wortman JR, Yandell MD, Zhang Q, Chen LX, Brandon RC, Rogers YH, Blazej RG, Champe M, Pfeiffer BD, Wan KH, Doyle C, Baxter EG, Helt G, Nelson CR, Gabor GL, Abril JF, Agbayani A, An HJ, Andrews-Pfannkoch C, Baldwin D, Ballew RM, Basu A, Baxendale J, Bayraktaroglu L, Beasley EM, Beeson KY, Benos PV, Berman BP, Bhandari D, Bolshakov S, Borkova D, Botchan MR, Bouck J, Brokstein P, Brottier P, Burtis KC, Busam DA, Butler H, Cadieu E, Center A, Chandra I, Cherry JM, Cawley S, Dahlke C, Davenport LB, Davies P, de Pablos B, Delcher A, Deng Z, Mays AD, Dew I, Dietz SM, Dodson K, Doup LE, Downes M, Dugan-Rocha S, Dunkov BC, Dunn P, Durbin KJ, Evangelista CC, Ferraz C, Ferriera S, Fleischmann W, Fosler C, Gabrielian AE, Garg NS, Gelbart WM, Glasser K, Glodek A, Gong F, Gorrell JH, Gu Z, Guan P, Harris M, Harris NL, Harvey D, Heiman TJ, Hernandez JR, Houck J, Hostin D, Houston KA, Howland TJ, Wei MH, Ibegwam C, Jalali M, Kalush F, Karpen GH, Ke Z, Kennison JA, Ketchum KA, Kimmel BE, Kodira CD, Kraft C, Kravitz S, Kulp D, Lai Z, Lasko P, Lei Y, Levitsky AA, Li J, Li Z, Liang Y, Lin X, Liu X, Mattei B, McIntosh TC, McLeod MP, McPherson D, Merkulov G, Milshina NV, Mobarry C, Morris J, Moshrefi A, Mount SM, Moy M, Murphy B, Murphy L, Muzny DM, Nelson DL, Nelson DR, Nelson KA, Nixon K, Nusskern DR, Pacleb JM, Palazzolo M, Pittman GS, Pan S, Pollard J, Puri V, Reese MG, Reinert K, Remington K, Saunders RD, Scheeler F, Shen H, Shue BC, Sidén-Kiamos I, Simpson M, Skupski MP, Smith T, Spier E, Spradling AC, Stapleton M, Strong R, Sun E, Svirskas R, Tector C, Turner R, Venter E, Wang AH, Wang X, Wang ZY, Wassarman DA, Weinstock GM, Weissenbach J, Williams SM, WoodageT, Worley KC, Wu D, Yang S, Yao QA, Ye J, Yeh RF, Zaveri JS, Zhan M, Zhang G, Zhao Q, Zheng L, Zheng XH, Zhong FN, Zhong W, Zhou X, Zhu S, Zhu X, Smith HO, Gibbs RA, Myers EW, Rubin GM, Venter JC (2000) The genome sequence of *Drosophila melanogaster*. Science 287, 2185-2195.

Affolter M & Caussinus E (2008) Tracheal branching morphogenesis in *Drosophila*: New insights into cell behaviour and organ architecture. Development 135, 2055-2064.

Aritakula A & Ramasamy A (2008) *Drosophila*-based in vivo assay for the validation of inhibitors of the epidermal growth factor receptor/ Ras pathway. J. Biosc. 33, 731–742.

Bell DW, Gore I, Okimoto RA, Godin-Heymann N, Sordella R, Mulloy R, Sharma SV, Brannigan BW, Mohapatra G, Settleman J, Haber DA (2005) Inherited susceptibility to lung cancer may be associated with the T790M drug resistance mutation in EGFR. Nat. Genet. 37, 1315–1316.

Bellusci S, Grindley J, Emoto H, Itoh N, Hogan BL (1997) Fibroblast growth factor 10 (FGF10) and branching morphogenesis in the embryonic mouse lung. Development 124, 4867–4878.

Bilder D, Li M, Perrimon N. (2000) Cooperative regulation of cell polarity and growth by *Drosophila* tumor suppressors. Science 289, 113–116.

Bivona TG, Hieronymus H, Parker J, Chang K, Taron M, Rosell R, Moonsamy P, Dahlman K, Miller VA, Costa C, Hannon G, Sawyers CL (2011) FAS and NF-κB signalling modulate dependence of lung cancers on mutant EGFR. Nature 471, 523–526.

Bozic I, Antal T, Ohtsuki H, Carter H, Kim D, Chen S, Karchin R, Kinzler KW, Vogelstein B, Nowak MA (2010) Accumulation of driver and passenger mutations during tumor progression. Proc. Natl. Acad. Sci. USA. 107,18545–18550.

Brand AH & Perrimon N (1993) Targeted gene expression as a means of altering cell fates and generating dominant phenotypes. Development 118, 401–415.

Brumby AM & Richardson HE (2005) Using *Drosophila melanogaster* to map human cancer pathways. Nat. Rev. Cancer 5, 626–639.

Burotto M, Manasanch EE, Wilkerson J, Fojo T (2015) Gefitinib and Erlotinib in metastatic non-small cell lung cancer: A meta-analysis of toxicity and efficacy of randomized clinical trials. Oncologist 20, 400–410.

Cabernard C & Affolter M (2005) Distinct roles for two receptor tyrosine kinases in epithelial branching morphogenesis in *Drosophila*. Dev. Cell 9, 831–842.

Cancer Genome Atlas Research Network (2012) Comprehensive genomic characterization of squamous cell lung cancers. Nature 489, 519–525.

Cancer Genome Atlas Research Network (2014) Comprehensive molecular profiling of lung adenocarcinoma. Nature 511, 543–550.

Casci T, Vinós J, Freeman M (1999) Sprouty, an intracellular inhibitor of Ras signaling. Cell 96, 655–665.

Centanin L, Dekanty A, Romero N, Irisarri M, Gorr TA, Wappner P (2008) Cell autonomy of HIF effects in *Drosophila*: Tracheal cells sense hypoxia and induce terminal branch sprouting. Dev. Cell 14, 547–558.

Chang CI, Chelliah Y, Borek D, Mengin-Lecreulx D, Deisenhofer J (2006) Structure of tracheal cytotoxin in complex with a heterodimeric pattern-recognition receptor. Science 311, 1761–1764.

Chen W, Li Z, Bai L, Lin Y (2011) NF-kappaB, a mediator for lung carcinogenesis and a target for lung cancer prevention and therapy. Front. Biosci. 1, 1172–1185.

Chen X, Kandasamy K, Srivastava RK (2003) Differential roles of RelA (p65) and c-Rel subunits of nuclear factor kappaB in tumor necrosis factor-related apoptosis-inducing ligand signaling. Cancer Res. 63, 1059–1066.

Choe KM, Lee H, Anderson KV (2005) *Drosophila* peptidoglycan recognition protein LC (PGRP-LC) acts as a signal-transducing innate immune receptor. Proc. Natl. Acad. Sci. USA.102, 1122–1126.

Das TK & Cagan RL (2013) A *Drosophila* approach to thyroid cancer therapeutics. Drug Discov. Today Technol. 10, e65–e71.

De Craene B and Berx G (2013) Regulatory networks defining EMT during cancer initiation and progression. Nat Rev Cancer 13, 97-110.

Dietzl G, Chen D, Schnorrer F, Su KC, Barinova Y, Fellner M, Gasser B, Kinsey K, Oppel S, Scheiblauer S, Couto A, Marra V, Keleman K, Dickson BJ (2007) A genome-wide transgenic RNAi library for conditional gene inactivation in *Drosophila*. Nature 448, 151–156.

Ding L, Getz G, Wheeler DA, Mardis ER, McLellan MD, Cibulskis K, Sougnez C, Greulich H, Muzny DM, Morgan MB, Fulton L, Fulton RS, Zhang Q, Wendl MC, Lawrence MS, Larson DE, Chen K, Dooling DJ, Sabo A, Hawes AC, Shen H, Jhangiani SN, Lewis LR, Hall O, Zhu Y, Mathew T, Ren Y, Yao J, Scherer SE, Clerc K, Metcalf GA, Ng B, Milosavljevic A, Gonzalez-Garay ML, Osborne JR, Meyer R, Shi X, Tang Y, Koboldt DC, Lin L, Abbott R, Miner TL, Pohl C, Fewell G, Haipek C, Schmidt H, Dunford-Shore BH, Kraja A, Crosby SD, Sawyer CS, Vickery T, Sander S, Robinson J, Winckler W, Baldwin J, Chirieac LR, Dutt A, Fennell T, Hanna M, Johnson BE, Onofrio RC, Thomas RK, Tonon G, Weir BA, Zhao X, Ziaugra L, Zody MC, Giordano T, Orringer MB, Roth JA, Spitz MR, Wistuba II, Ozenberger B, Good PJ, Chang AC, Beer DG, Watson MA, Ladanyi M, Broderick S, Yoshizawa A, Travis WD, Pao W, Province MA, Weinstock GM, Varmus HE, Gabriel SB, Lander ES, Gibbs RA, Meyerson M, Wilson RK (2008) Somatic mutations affect key pathways in lung adenocarcinoma. Nature 455, 1069–1075.

Dushay MS, Asling B, Hultmark D (1996) Origins of immunity: Relish, a compound Rel-like gene in the antibacterial defense of *Drosophila*. Proc. Natl. Acad. Sci. USA. 93, 10343–10347.

Eberhard DA, Johnson BE, Amler LC, Goddard AD, Heldens SL, Herbst RS, Ince WL, Jänne PA, Januario T, Johnson DH, Klein P, Miller VA, Ostland MA, Ramies DA, Sebisanovic D, Stinson JA, Zhang YR, Seshagiri S, Hillan KJ (2005) Mutations in the epidermal growth factor receptor and in KRAS are predictive and prognostic indicators in patients with non-small-cell lung cancer treated with chemotherapy alone and in combination with erlotinib. J. Clin. Oncol. 23, 5900–5909.

Eberhard DA, Johnson BE, Amler LC, Goddard AD, Heldens SL, Herbst RS, Ince WL, Jänne PA, Januario T, Johnson DH, Klein P, Miller VA, Ostland MA, Ramies DA, Sebisanovic D, Stinson JA, Zhang YR, Seshagiri S, Hillan KJ (2010) Structural and mechanistic underpinnings of the differential drug sensitivity of EGFR mutations in non-small cell lung cancer. Biochim. Biophys. Acta 1804, 559–566.

Falschlehner C, Boutros M (2012) Innate immunity: Regulation of caspases by IAP-dependent ubiquitylation. EMBO Journal, 31, 2750–2752.

Fei F, Zhang D, Yang Z, Wang S, Wang X, Wu Z, Wu Q, Zhang S (2015) The number of polyploid giant cancer cells and epithelial-mesenchymal transition-related proteins are associated with invasion and metastasis in human breast cancer. J. Exp. Clin. Cancer Res. 34, 1–13.

Fry DW (2003) Mechanism of action of erbB tyrosine kinase inhibitors. Exp. Cell Res. 284, 131–139.

Gabay L, Scholz H, Golembo M, Klaes A, Shilo BZ, Klämbt C (1996) EGF receptor signaling induces pointed P1 transcription and inactivates Yan protein in the *Drosophila* embryonic ventral ectoderm. Development 122, 3355–3362.

Garcia J, Dusserre E, Cheynet V, Bringuier PP, Brengle-Pesce K, Wozny AS, Rodriguez-Lafrasse C, Freyer G, Brevet M, Payen L, Couraud S (2017) Evaluation of pre-analytical conditions and comparison of the performance of several digital PCR assays for the detection of major EGFR mutations in circulating DNA from non-small cell lung cancers: The CIRCAN_0 study. Oncotarget 8, 87980–87996.

Garg A & Aggarwal BB (2002) Nuclear transcription factor-kappaB as a target for cancer drug development. Leukemia 16, 1053–1068.

Gateff E, Schneiderman HA (1974) Developmental capacities of benign and malignant neoplasms of *Drosophila*. Wilhelm Roux' Arch. Entwickl. Mech. Org. 176, 23–65.

Georgel P, Naitza S, Kappler C, Ferrandon D, Zachary D, Swimmer C, Kopczynski C, Duyk G, Reichhart JM, Hoffmann JA (2001) *Drosophila* Immune Deficiency (IMD) Is a death domain protein that activates antibacterial defense and can promote apoptosis. Dev. Cell 1, 503–514.

Gervais L & Casanova J (2011) The *Drosophila* homologue of SRF acts as a boosting mechanism to sustain FGF-induced terminal branching in the tracheal system. Development, 138, 1269–1274.

Ghabrial A, Luschnig S, Metzstein MM, Krasnow MA (2003) Branching Morphogenesis of the *Drosophila* Tracheal System. Annual Review of Cell and Developmental Biology 19, 623–647.

Ghiglione C, Carraway KL, Amundadottir LT, Boswell RE, Perrimon N, Duffy JB (1999) The transmembrane molecule Kekkon 1 acts in a feedback loop to negatively regulate the activity of the *Drosophila* EGF receptor during oogenesis. Cell 96, 847–856.

Glazer L & Shilo BZ (1991) The *Drosophila* FGF-R homolog is expressed in the embryonic tracheal system and appears to be required for directed tracheal cell extension. Genes Dev. 5, 697–705.

Gottardi CJ, Wong E, Gumbiner BM (2001) E-cadherin suppresses cellular transformation by inhibiting β-catenin signaling in an adhesion-independent manner. J Cell Biol. 153, 1049–1059.

Govindan R, Ding L, Griffith M, Subramanian J, Dees ND, Kanchi KL, Maher CA, Fulton R, Fulton L, Wallis J, Chen K, Walker J, McDonald S, Bose R, Ornitz D, Xiong D, You M, Dooling DJ, Watson M, Mardis ER, Wilson RK (2012) Genomic landscape of non-small cell lung cancer in smokers and never-smokers. Cell 150, 1121–1134.

Gratz SJ, Wildonger J, Harrison MM, O'Connor-Giles KM (2013) CRISPR/Cas9-mediated genome engineering and the promise of designer flies on demand. Fly 12, 249–255.

Greenman C, Stephens P, Smith R, Dalgliesh GL, Hunter C, Bignell G, Davies H, Teague J, Butler A, Stevens C, Edkins S, O'Meara S, Vastrik I, Schmidt EE, Avis T, Barthorpe S, Bhamra G, Buck G, Choudhury B, Clements J, Cole J, Dicks E, Forbes S, Gray K, Halliday K, Harrison R, Hills K, Hinton J, Jenkinson A, Jones D, Menzies A, Mironenko T, Perry J, Raine K,

Richardson D, Shepherd R, Small A, Tofts C, Varian J, Webb T, West S, Widaa S, Yates A, Cahill DP, Louis DN, Goldstraw P, Nicholson AG, Brasseur F, Looijenga L, Weber BL, Chiew YE, DeFazio A, Greaves MF, Green AR, Campbell P, Birney E, Easton DF, Chenevix-Trench G, Tan MH, Khoo SK, Teh BT, Yuen ST, Leung SY, Wooster R, Futreal PA, Stratton MR (2007) Patterns of somatic mutation in human cancer genomes. Nature 446, 153–158.

Grether ME, Abrams JM, Agapite J, White K, Steller H (1995) The head involution defective gene of *Drosophila melanogaster* functions in programmed cell death. Genes Dev. 9, 1694–1708.

Groth AC, Fish M, Nusse R, Calos MP (2004) Construction of transgenic *Drosophila* by using the site-specific integrase from Phage phiC31. Genetics 166, 1775–1782.

Guillemin K, Groppe J, Ducker K, Treisman R, Hafen E, Affolter M, Krasnow MA (1996) The pruned gene encodes the *Drosophila* serum response factor and regulates cytoplasmic outgrowth during terminal branching of the tracheal system. Development 122, 1353–1362.

Hacohen N, Kramer S, Sutherland D, Hiromi Y, Krasnow MA (1998) Sprouty encodes a novel antagonist of FGF signaling that patterns apical branching of the *Drosophila* airways. Cell 92, 253–263.

Hall ET, Verheyen EM (2015) Ras-activated Dsor1 promotes Wnt signaling in *Drosophila* development. J. Cell Sci. 128, 4499–4511.

Hanahan D & Weinberg RA (2011) Hallmarks of cancer: The next generation. Cell 144(5), pp.646–674.

Harris RC, Chung E, Coffey RJ (2003) EGF receptor ligands. Experimental Cell Research 284, 2–13.

Hedengren M, Asling B, Dushay MS, Ando I, Ekengren S, Wihlborg M, Hultmark D (1999) Relish, a central factor in the control of humoral but not cellular immunity in *Drosophila*. Mol. Cell 4, 827–37.

Herbst RS, Morgensztern D, Boshoff C (2018) The biology and management of non-small cell lung cancer. Nature 553, 446–454.

Herranz H, Hong X, Hung NT, Voorhoeve PM, Cohen SM (2012) Oncogenic cooperation between SOCS family proteins and EGFR identified using a *Drosophila* epithelial transformation model. Genes Dev. 26, 1602–1611.

Hoadley KA, Yau C, Wolf DM, Cherniack AD, Tamborero D, Ng S, Leiserson MDM, Niu B, McLellan MD, Uzunangelov V, Zhang J, Kandoth C, Akbani R, Shen H, Omberg L, Chu A, Margolin AA, Van't Veer LJ, Lopez-Bigas N, Laird PW, Raphael BJ, Ding L, Robertson AG, Byers LA, Mills GB, Weinstein JN, Van Waes C, Chen Z, Collisson EA; Cancer Genome Atlas Research Network, Benz CC, Perou CM, Stuart JM (2016) Multi-platform analysis of 12 cancer types reveals molecular classification within and across tissues-of-origin. Cell 158, 929–944.

Howington JA, Blum MG, Chang AC, Balekian AA, Murthy SC (2013) Treatment of stage I and II non-small cell lung cancer: Diagnosis and management of lung cancer, 3rd ed: American college of chest physicians evidence-based clinical practice guidelines. Chest 143, e278S–e313S.

Hu S, Yang X (2000) dFADD, A novel death domain-containing adapter protein for the *Drosophila* caspase DREDD. J. Biol. Chem. 275, 30761–30764.

Imam F, Sutherland D, Huang W, Krasnow MA (1999) stumps, a *Drosophila* gene required for fibroblast growth factor (FGF)-directed migrations of tracheal and mesodermal cells. Genetics 152, 307–318.

Imielinski M, Berger AH, Hammerman PS, Hernandez B, Pugh TJ, Hodis E, Cho J, Suh J, Capelletti M, Sivachenko A, Sougnez C, Auclair D, Lawrence MS, Stojanov P, Cibulskis K, Choi K, de Waal L, Sharifnia T, Brooks A, Greulich H, Banerji S, Zander T, Seidel D, Leenders F, Ansén S, Ludwig C, Engel-Riedel W, Stoelben E, Wolf J, Goparju C, Thompson K, Winckler W, Kwiatkowski D, Johnson BE, Jänne PA, Miller VA, Pao W, Travis WD, Pass HI, Gabriel SB, Lander ES, Thomas RK, Garraway LA, Getz G, Meyerson M. (2012) Mapping the hallmarks of lung adenocarcinoma with massively parallel sequencing. Cell 150, 1107–1120.

Jänne PA, Johnson BE (2006) Effect of epidermal growth factor receptor tyrosine kinase domain mutations on the outcome of patients with non-small cell lung cancer treated with epidermal growth factor receptor tyrosine kinase inhibitors. Clin. Cancer Res. 12, 4416s–4420s.

Jarecki J, Johnson E, Krasnow MA (1999) Oxygen regulation of airway branching in *Drosophila* is mediated by Branchless FGF. Cell 99, 211–220.

Jevtić P, Edens LJ, Vuković LD, Levy DL (2014) Sizing and shaping the nucleus: Mechanisms and significance. Curr. Opin. Cell Biol. 28, 16–27.

Jin MH, Sawamoto K, Ito M, Okano H (2000) The interaction between the Drosophila secreted protein argos and the epidermal growth factor receptor inhibits dimerization of the receptor and binding of secreted spitz to the receptor. Mol. Cell. Biol. 20, 2098–2107.

Jones TA, Metzstein MM (2011) A novel function for the PAR complex in subcellular morphogenesis of tracheal terminal cells in *Drosophila melanogaster*. Genetics 189, 153–164.

Kadota K, Nitadori J, Woo KM, Sima CS, Finley DJ, Rusch VW, Adusumilli PS, Travis WD (2014) Comprehensive pathological analyses in lung squamous cell carcinoma: Single cell invasion, nuclear diameter, and tumor budding are independent prognostic factors for worse outcomes. J. Thorac. Oncol. 9, 1126–1139.

Kalluri R, Neilson EG (2003) Epithelial-mesenchymal transition and its implications for fibrosis. J. Clin. Invest. 112, 1776–1784.

Kalluri R, Weinberg RA (2009) The basics of epithelial-mesenchymal transition. J. Clin. Invest. 119, 1420–1428.

Kaneko T, Goldman WE, Mellroth P, Steiner H, Fukase K, Kusumoto S, Harley W, Fox A, Golenbock D, Silverman N (2004) Monomeric and polymeric gram-negative peptidoglycan but not purified LPS stimulate the *Drosophila* IMD pathway. Immunity 20, 637–649.

Kaneko T, Yano T, Aggarwal K, Lim JH, Ueda K, Oshima Y, Peach C, Erturk-Hasdemir D, Goldman WE, Oh BH, Kurata S, Silverman N (2006) PGRP-LC and PGRP-LE have essential yet distinct functions in the *Drosophila* immune response to monomeric DAP-type peptidoglycan. Nat. Immunol. 7, 715–723.

Kim K, Daniels KJ, Hay ED (1998) Tissue-specific expression of beta-catenin in normal mesenchyme and uveal melanomas and its effect on invasiveness. Exp. Cell Res. 245, 79–90.

Klämbt C, Glazer L, Shilo BZ (1992) breathless, a *Drosophila* FGF receptor homolog, is essential for migration of tracheal and specific midline glial cells. Genes Dev. 6, 1668–1678.

Lee T, Hacohen N, Krasnow M, Montell DJ (1996) Regulated breathless receptor tyrosine kinase activity required to pattern cell migration and branching in the *Drosophila* tracheal system. Genes Dev. 10, 2912–2921.

Lee T, Luo L (1999) Mosaic analysis with a repressible cell marker for studies of gene function in neuronal morphogenesis. Neuron 22, 451–461.

Lemjabbar-Alaoui H, Hassan OU, Yang YW, Buchanan P (2016) Lung cancer: Biology and treatment options. Biochim. Biophys. Acta. 1856, 189–210.

Levine BD, Cagan RL (2016) *Drosophila* lung cancer models identify trametinib plus statin as candidate therapeutic. Cell Rep. 14, 1–11.

Li D, Ambrogio L, Shimamura T, Kubo S, Takahashi M, Chirieac LR, Padera RF, Shapiro GI, Baum A, Himmelsbach F, Rettig WJ, Meyerson M, Solca F, Greulich H, Wong KK (2008) BIBW2992, an irreversible EGFR/HER2 inhibitor highly effective in preclinical lung cancer models. Oncogene 27, 4702–4711.

Li Y, Zhang Y, Hill J, Kim HT, Shen Q, Bissonnette RP, Lamph WW, Brown PH (2008) The rexinoid, bexarotene, prevents the development of premalignant lesions in MMTV-erbB2 mice. Br. J. Cancer 98, 1380–1388.

Linneweber GA, Jacobson J, Busch KE, Hudry B, Christov CP, Dormann D, Yuan M, Otani T, Knust E, de Bono M, Miguel-Aliaga I (2014) Neuronal control of metabolism through nutrient-dependent modulation of tracheal branching. Cell 156, 69–83.

Livneh E, Glazer L, Segal D, Schlessinger J, Shilo BZ (1985) The *Drosophila* EGF receptor gene homolog: Conservation of both hormone binding and kinase domains. Cell 40, 599–607.

Lusk JB, Lam VY, Tolwinski NS (2017) Epidermal growth factor pathway signaling in *Drosophila* embryogenesis: Tools for Understanding Cancer. Cancers 9, E16.

Lynch TJ, Bell DW, Sordella R, Gurubhagavatula S, Okimoto RA, Brannigan BW, Harris PL, Haserlat SM, Supko JG, Haluska FG, Louis DN, Christiani DC, Settleman J, Haber DA (2004) Activating mutations in the epidermal growth factor receptor underlying responsiveness of non–small-cell lung cancer to gefitinib. N. Engl. J. Med. 350, 2129–2139.

Mailleux AA, Tefft D, Ndiaye D, Itoh N, Thiery JP, Warburton D, Bellusci S (2001) Evidence that SPROUTY2 functions as an inhibitor of mouse embryonic lung growth and morphogenesis. Mech. Dev. 102, 81–94.

Markstein M, Dettorre S, Cho J, Neumüller RA, Craig-Müller S, Perrimon N (2014) Systematic screen of chemotherapeutics in *Drosophila* stem cell tumors. Proc. Natl. Acad. Sci. USA 111, 4530–4535.

McGuire SE, Le PT, Osborn AJ, Matsumoto K, Davis RL (2003) Spatiotemporal Rescue of Memory Dysfunction in *Drosophila*. Science 302, 1765–1768.

Meijering E, Jacob M, Sarria JC, Steiner P, Hirling H, Unser M (2004) Design and validation of a tool for neurite tracing and analysis in fluorescence microscopy images. Cytometry A. 58, 167–176.

Meinander A, Runchel C, Tenev T, Chen L, Kim CH, Ribeiro PS, Broemer M, Leulier F, Zvelebil M, Silverman N, Meier P (2012) Ubiquitylation of the initiator caspase DREDD is required for innate immune signalling. EMBO J. 31, 2770–2783.

Nieto MA, Huang RY, Jackson RA, Thiery JP (2016) EMT: 2016. Cell 166, 21–45.

Olivares-Castiñeira I, Llimargas M (2017) EGFR controls *Drosophila* tracheal tube elongation by intracellular trafficking regulation. PLoS Genet. 13, e1006882.

Paez JG, Jänne PA, Lee JC, Tracy S, Greulich H, Gabriel S, Herman P, Kaye FJ, Lindeman N, Boggon TJ, Naoki K, Sasaki H, Fujii Y, Eck MJ, Sellers WR, Johnson BE, Meyerson M (2004) EGFR mutations in lung cancer: Correlation with clinical response to gefitinib therapy. Science 304, 1497–1500.

Pandey UB, Nichols CD (2011) Human disease models in *Drosophila melanogaster* and the role of the fly in therapeutic drug discovery. Pharmacol. Rev. 63, 411–436.

Pao W, Miller V, Zakowski M, Doherty J, Politi K, Sarkaria I, Singh B, Heelan R, Rusch V, Fulton L, Mardis E, Kupfer D, Wilson R, Kris M, Varmus H (2004) EGF receptor gene mutations are common in lung cancers from “never smokers” and are associated with sensitivity of tumors to gefitinib and erlotinib. Proc. Natl. Acad. Sci. USA. 101, 13306–13311.

Pao W, Wang TY, Riely GJ, Miller VA, Pan Q, Ladanyi M, Zakowski MF, Heelan RT, Kris MG, Varmus HE (2005a) KRAS mutations and primary resistance of lung adenocarcinomas to gefitinib or erlotinib. PLoS Med. 2, 0057–0061.

Pao W, Miller VA, Politi KA, Riely GJ, Somwar R, Zakowski MF, Kris MG, Varmus H (2005b) Acquired resistance of lung adenocarcinomas to gefitinib or erlotinib is associated with a second mutation in the EGFR kinase domain. PLoS Med. 2, 0225–0235.

Papagiannouli F & Mechler BM (2013) Modeling tumorigenesis in *Drosophila* : Current advances and future perspectives. InTech 97–128.

Park JM, Brady H, Ruocco MG, Sun H, Williams D, Lee SJ, Kato T Jr, Richards N, Chan K, Mercurio F, Karin M, Wasserman SA (2004) Targeting of TAK1 by the NF- κ B protein Relish regulates the JNK-mediated immune response in *Drosophila* Targeting of TAK1 by the NF-kappa B protein Relish regulates the JNK-mediated immune response in *Drosophila*. Genes Dev. 18, 584–594.

Park K, Tan EH, O'Byrne K, Zhang L, Boyer M, Mok T, Hirsh V, Yang JC, Lee KH, Lu S, Shi Y, Kim SW, Laskin J, Kim DW, Arvis CD, Kölbeck K, Laurie SA, Tsai CM, Shahidi M, Kim M, Massey D, Zazulina V, Paz-Ares L (2016) Afatinib versus gefitinib as first-line treatment of patients with EGFR mutation-positive non-small-cell lung cancer (LUX-Lung 7): A phase 2B, open-label, randomised controlled trial. Lancet Oncol. 17, 577–589.

Park WY, Miranda B, Lebeche D, Hashimoto G, Cardoso WV (1998) FGF-10 is a chemotactic factor for distal epithelial buds during lung development. Dev. Biol. 201, 125–134.

Peifer M, Fernández-Cuesta L, Sos ML, George J, Seidel D, Kasper LH, Plenker D, Leenders F, Sun R, Zander T, Menon R, Koker M, Dahmen I, Müller C, Di Cerbo V, Schildhaus HU, Altmüller J, Baessmann I, Becker C, de Wilde B, Vandesompele J, Böhm D, Ansén S, Gabler F, Wilkening I, Heynck S, Heuckmann JM, Lu X, Carter SL, Cibulskis K, Banerji S, Getz G, Park KS, Rauh D, Grütter C, Fischer M, Pasqualucci L, Wright G, Wainer Z, Russell P, Petersen I, Chen Y, Stoelben E, Ludwig C, Schnabel P, Hoffmann H, Muley T, Brockmann M, Engel-Riedel W, Muscarella LA, Fazio VM, Groen H, Timens W, Sietsma H, Thunnissen E, Smit E, Heideman DA, Snijders PJ, Cappuzzo F, Ligorio C, Damiani S, Field J, Solberg S, Brustugun OT, Lund-Iversen M, Sänger J, Clement JH, Soltermann A, Moch H, Weder W, Solomon B, Soria JC, Validire P, Besse B, Brambilla E, Brambilla C, Lantuejoul S, Lorimier P, Schneider PM, Hallek M, Pao W, Meyerson M, Sage J, Shendure J, Schneider R, Büttner R, Wolf J, Nürnberg P, Perner S, Heukamp LC, Brindle PK, Haas S, Thomas RK (2012) Integrative genome analyses identify key somatic driver mutations of small cell lung cancer. Nat. Genet. 44, 1104–1110.

Peters K, Werner S, Liao X, Wert S, Whitsett J, Williams L (1994) Targeted expression of a dominant negative FGF receptor blocks branching morphogenesis and epithelial differentiation of the mouse lung. EMBO J. 13, 3296–3301.

Pfeiffer BD, Jenett A, Hammonds AS, Ngo TT, Misra S, Murphy C, Scully A, Carlson JW, Wan KH, Laverty TR, Mungall C, Svirskas R, Kadonaga JT, Doe CQ, Eisen MB, Celniker SE, Rubin GM (2008) Tools for neuroanatomy and neurogenetics in *Drosophila*. Proc. Natl. Acad. Sci. USA. 105, 9715–9720.

Radhakrishnan SK, Kamalakaran S (2006) Pro-apoptotic role of NF-kappaB: Implications for cancer therapy. Biochim. Biophys. Acta. 1766, 53–62.

Rapp E, Pater JL, Willan A, Cormier Y, Murray N, Evans WK, Hodson DI, Clark DA, Feld R, Arnold AM, *et al.* (1988) Chemotherapy can prolong survival in patients with advanced non-small-cell lung cancer--report of a Canadian multicenter randomized trial. J. Clin. Oncol. 6, 633–41.

Reich A, Shilo BZ (2002) Keren, a new ligand of the *Drosophila* epidermal growth factor receptor, undergoes two modes of cleavage. EMBO J 21, 4287–4296.

Roeder T, Isermann K, Kabesch M (2009) *Drosophila* in asthma research. Am. J. Respir. Crit. Care Med. 179, 979–983.

Rubin GM, Yandell MD, Wortman JR, Gabor Miklos GL, Nelson CR, Hariharan IK, Fortini ME, Li PW, Apweiler R, Fleischmann W, Cherry JM, Henikoff S, Skupski MP, Misra S, Ashburner M, Birney E, Boguski MS, Brody T, Brokstein P, Celniker SE, Chervitz SA, Coates D, Cravchik A, Gabrielian A, Galle RF, Gelbart WM, George RA, Goldstein LS, Gong F, Guan P, Harris NL, Hay BA, Hoskins RA, Li J, Li Z, Hynes RO, Jones SJ, Kuehl PM, Lemaitre B, Littleton JT, Morrison DK, Mungall C, O'Farrell PH, Pickeral OK, Shue C, Vosshall LB, Zhang J, Zhao Q, Zheng XH, Lewis S (2000) Comparative genomics of the eukaryotes. Science 287, 2204–2215.

Rudin CM, Avila-Tang E, Harris CC, Herman JG, Hirsch FR, Pao W, Schwartz AG, Vahakangas KH, Samet JM (2009) Lung cancer in never smokers: Molecular profiles and therapeutic implications. Clin. Cancer Res. 15, 5646–5661.

Russo A, Franchina T, Ricciardi GRR, Smiroldo V, Picciotto M, Zanghì M, Rolfo C, Adamo V (2017) Third generation EGFR TKIs in EGFR-mutated NSCLC: Where are we now and where are we going. Crit. Rev. Oncol. Hematol. 117, 38–47.

Rutledge BJ, Zhang K, Bier E, Jan YN, Perrimon N (1992) The *Drosophila* spitz gene encodes a putative EGF-like growth factor involved in dorsal-ventral axis formation and neurogenesis. Genes Dev. 6, 1503–1517.

Sabatel C, Cornet AM, Tabruyn SP, Malvaux L, Castermans K, Martial JA, Struman I (2010) Sprouty1, a new target of the angiostatic agent 16K prolactin, negatively regulates angiogenesis. Mol. Cancer 9, 1–13.

Sainson RC, Johnston DA, Chu HC, Holderfield MT, Nakatsu MN, Crampton SP, Davis J, Conn E, Hughes CC (2008) TNF primes endothelial cells for angiogenic sprouting by inducing a tip cell phenotype. Blood 111, 4997–5007.

Sakurai T, Kudo M (2011) Signaling pathways governing tumor angiogenesis. Oncology 81, 24–29.

Samakovlis C, Hacohen N, Manning G, Sutherland DC, Guillemin K, Krasnow MA (1996a) Development of the *Drosophila* tracheal system occurs by a series of morphologically distinct but genetically coupled branching events. Development 122, 1395–1407.

Samakovlis C, Manning G, Steneberg P, Hacohen N, Cantera R, Krasnow MA (1996b) Genetic control of epithelial tube fusion during *Drosophila* tracheal development. Development 122, 3531–3536.

Sangha R, Price J, Butts CA (2010) Adjuvant therapy in non-small cell lung cancer: current and future directions. Oncologist 15, 862–872.
Schnepp B, Grumbling G, Donaldson T, Simcox A (1996) Vein is a Novel Component in the Drosophila epidermal growth factor receptor pathway with similarity to the neuregulins. Genes Dev. 10, 2302–2313.

Segatto NV, Remião MH, Schachtschneider KM, Seixas FK, Schook LB, Collares T (2017) The oncopig cancer model as a complementary tool for phenotypic drug discovery. Front. Pharmacol. 8, 1–8.

Sekine K, Ohuchi H, Fujiwara M, Yamasaki M, Yoshizawa T, Sato T, Yagishita N, Matsui D, Koga Y, Itoh N, Kato S (1999) Fgf10 is essential for limb and lung formation. Nat. Genet. 21, 138–141.

Sharma SV, Bell DW, Settleman J, Haber DA (2007) Epidermal growth factor receptor mutations in lung cancer. Nat. Rev. Cancer 7, 169–181.

Shaykhiev R, Zuo WL, Chao I, Fukui T, Witover B, Brekman A, Crystal RG (2013) EGF shifts human airway basal cell fate toward a smoking-associated airway epithelial phenotype. Proc. Natl. Acad. Sci. USA. 110, 12102–12107.

Shilo BZ (1987) Proto-oncogenes in *Drosophila melanogaster*. Trends Genet. 4, 69–72.

Shilo BZ (2003) Signaling by the *Drosophila* epidermal growth factor receptor pathway during development. Exp. Cell Res. 284, 140–149.

Shilo BZ (2014) The regulation and functions of MAPK pathways in *Drosophila*. Methods 68, 151–159.

Shmueli A, Cohen-Gazala O, Neuman-Silberberg FS (2002) Gurken, a TGF-α-like protein involved in axis determination in *Drosophila*, directly binds to the EGF-receptor homolog Egfr. Biochem. Biophys. Res. Commun. 291, 732–737.
Shtivelman E, Hensing T, Simon GR, Dennis PA, Otterson GA, Bueno R, Salgia R (2014) Molecular pathways and therapeutic targets in lung cancer. Oncotarget 5, 1392–433.

Siegel RL, Miller KD, Jemal A (2017) Cancer statistics, 2017. CA Cancer J. C. 67, 7-30.

Silverman N, Zhou R, Stöven S, Pandey N, Hultmark D, Maniatis T (2000) A *Drosophila* IkappaB kinase complex required for relish cleavage and antibacterial immunity. Genes Dev. 14, 2461–2471.
Silverman N, Zhou R, Erlich RL, Hunter M, Bernstein E, Schneider D, Maniatis T (2003) Immune activation of NF-kappaB and JNK requires *Drosophila* TAK1. J. Biol. Chem. 278, 48928–48934.

Sousa E, Graça I, Baptista T, Vieira FQ, Palmeira C, Henrique R, Jerónimo C (2013) Enoxacin inhibits growth of prostate cancer cells and effectively restores microRNA processing. Epigenetics 8, 548–558.

St Johnston D (2002) The art and design of genetic screens: *Drosophila melanogaster*. Nat. Rev. Genet. 3, 176–188.

Stewart M, Murphy C, Fristrom JW (1972) The recovery and priliminary characterization of X chromosome mutants affecting imaginal discs of *Drosophila melanogaster*. Dev. Biol. 27, 71–83.

Stoven S, Silverman N, Junell A, Hedengren-Olcott M, Erturk D, Engstrom Y, Maniatis T, Hultmark D (2003) Caspase-mediated processing of the *Drosophila* NF- B factor Relish. Proc. Nat. Acad. Sci. 100, 5991–5996.

Subramanian J, Govindan R (2007) Lung cancer in never smokers: A review. J. Clin. Oncol. 25, 561–570.
Sutherland D, Samakovlis C, Krasnow MA (1996) branchless encodes a *Drosophila* FGF homolog that controls tracheal cell migration and the pattern of branching. Cell 87, 1091–1101.

Tabruyn SP, Mémet S, Avé P, Verhaeghe C, Mayo KH, Struman I, Martial JA, Griffioen AW (2009) NF-kappaB activation in endothelial cells is critical for the activity of angiostatic agents. Mol. Cancer Ther. 8, 2645–2654.

Tabruyn SP, Griffioen AW (2007) A new role for NF-kappaB in angiogenesis inhibition. Cell Death Differ. 14, 1393–1397.

Tanaka K, Nosaki K, Otsubo K, Azuma K, Sakata S, Ouchi H, Morinaga R, Wataya H, Fujii A, Nakagaki N, Tsuruta N, Takeshita M, Iwama E, Harada T, Nakanishi Y, Okamoto I (2017) Acquisition of the T790M resistance mutation during afatinib treatment in EGFR tyrosine kinase inhibitor – naïve patients with non – small cell lung cancer harboring EGFR mutations. Oncotarget 8, 68123–68130.

Tang X, Liu D, Shishodia S, Ozburn N, Behrens C, Lee JJ, Hong WK, Aggarwal BB, Wistuba II (2006) Nuclear factor-κB (NF-κB) is frequently expressed in lung cancer and preneoplastic lesions. Cancer 107, 2637–2646.

Tomasetti C, Marchionni L, Nowak MA, Parmigiani G, Vogelstein B (2015) Only three driver gene mutations are required for the development of lung and colorectal cancers. Proc. Nat. Acad. Sci. USA.112, 118–123.

Tong CWS, Wu WKK, Loong HHF, Cho WCS, To KKW (2017) Drug combination approach to overcome resistance to EGFR tyrosine kinase inhibitors in lung cancer. Cancer Lett. 405, 100–110.

Torre LA, Bray F, Siegel RL, Ferlay J, Lortet-Tieulent J, Jemal A (2012) Global Cancer Statistics, 2012. CA Cancer J. Clin. 65, 87–108.

Travis WD, Brambilla E, Nicholson AG, Yatabe Y, Austin JHM, Beasley MB, Chirieac LR, Dacic S, Duhig E, Flieder DB, Geisinger K, Hirsch FR, Ishikawa Y, Kerr KM, Noguchi M, Pelosi G, Powell CA, Tsao MS, Wistuba I; WHO Panel (2015) The 2015 World Health Organization Classification of Lung Tumors: Impact of genetic, clinical and radiologic advances since the 2004 classification. J. Thorac. Oncol. 10, 1243–1260.

Travis WD, Brambilla E, Riely GJ (2013) New pathologic classification of lung cancer: Relevance for clinical practice and clinical trials. J. Clin. Oncol. 31, 992–1001.

Uv A, Cantera R, Samakovlis C (2003) *Drosophila* tracheal morphogenesis: Intricate cellular solutions to basic plumbing problems. Trends Cell Biol. 13, 301–309.

Valenta T, Hausmann G, Basler K (2012) The many faces and functions of β-catenin. EMBO J. 31, 2714–2736.

Vidal M, Wells S, Ryan A, Cagan R (2005) ZD6474 suppresses oncogenic RET isoforms in a *Drosophila* model for type 2 multiple endocrine neoplasia syndromes and papillary thyroid carcinoma thyroid carcinoma. Cancer Res. 3538–3541.

Villaruz LC, Burns TF, Ramfidis VS, Socinski MA (2013) Personalizing therapy in advanced non–small cell lung cancer. Semin. Respir. Crit. Care Med. 34, 822–836.

Vincent S, Wilson R, Coelho C, Affolter M, Leptin M (1998) The *Drosophila* protein Dof is specifically required for FGF signaling. Cell 2, 515–525.

Vogelstein B, Papadopoulos N, Velculescu VE, Zhou S, Diaz LA Jr, Kinzler KW (2013) Cancer Genome Lanscapes. Science 339, 1546–1558.

Wagner C, Isermann K, Fehrenbach H, Roeder T (2008) Molecular architecture of the fruit fly's airway epithelial immune system. BMC Genomics 9, 446.
Wagner C, Isermann K, Roeder T (2009) Infection induces a survival program and local remodeling in the airway epithelium of the fly. FASEB J. 23, 2045–54.

Wells A (1999) EGF receptor. Int. J. Biochem. Cell Biol. 31, 637–643.

Werner T, Liu G, Kang D, Ekengren S, Steiner H, Hultmark D (2000) A family of peptidoglycan recognition proteins in the fruit fly *Drosophila melanogaster*. Proc. Natl. Acad. Sci. USA. 97, 13772–13777.

Werner T, Borge-Renberg K, Mellroth P, Steiner H, Hultmark D (2003) Functional diversity of the *Drosophila* PGRP-LC gene cluster in the response to lipopolysaccharide and peptidoglycan. J. Biol. Chem. 278, 26319–26322.

White K, Grether ME, Abrams JM, Young L, Farrell K, Steller H (1994) Genetic control of programmed cell death in *Drosophila*. Science 264, 677–83.

Wilk R, Weizman I, Shilo BZ (1996) trachealess encodes a bHLH-PAS protein that is an inducer of tracheal cell fates in *Drosophila*. Genes Dev. 10, 93–102.

Willoughby LF, Schlosser T, Manning SA, Parisot JP, Street IP, Richardson HE, Humbert PO, Brumby AM (2013) An in vivo large-scale chemical screening platform using *Drosophila* for anti-cancer drug discovery. Dis. Model Mech. 6, 521–9.

Wong WW, Dimitroulakos J, Minden MD, Penn LZ (2002) HMG-CoA reductase inhibitors and the malignant cell: The statin family of drugs as triggers of tumor-specific apoptosis. Leukemia 16, 508–519.

Woods DF, Bryant PJ (1991) The discs-large tumor suppressor gene of *Drosophila* encodes a guanylate kinase homolog localized at septate junctions. Cell 66, 451–464.

Wu M, Pastor-Pareja JC, Xu T (2010) Interaction between Ras(V12) and scribbled clones induces tumour growth and invasion. Nature 463, 545–548.

Xu-Welliver M, Carbone DP2 (2017) Blood-based biomarkers in lung cancer: Prognosis and treatment decisions. Transl. Lung Cancer Res. 6, 708–712.

Yarden Y, Schlessinger J (1987) Epidermal growth factor induces rapid, reversible aggregation of the purified epidermal growth factor receptor. Biochemistry 26, 1443–1451.

Yarden Y, Sliwkowski MX (2001) Untangling the ErbB signaling network. Nat. Rev. Mol. Cell Biol. 2, 127–137.

You HY, Zhang WJ, Xie XM, Zheng ZH, Zhu HL, Jiang FZ (2016) Pitavastatin suppressed liver cancer cells in vitro and in vivo. Onco. Targets Ther. 9, 5383–5388.

Yu HA, Riely GJ (2013) Second generation epidermal growth factor receptor tyrosine kinase inhibitors in lung cancer. J. Natl. Compr. Canc. Netw. 11, 161–169.

Internet references:

Creative Diagnostics (2009-2018) Figure 1: Life cycle of *Drosophila*. https://www.creative-diagnostics.com/Drosophila.htm.htm, last request: 12.02.2018.

Curriculum Vitae

Name	Judith Bossen
Date, place of birth	25.06.1987, 25899 Niebüll
Nationality	German

School education

1993-1997	Primary school: Hans-Momsen-Schule Fahretoft
1997-2003	Secondary school: Realschule Niebüll
2003-2006	Diploma: Fachgymnasium Niebüll
	Main focus: Nutrient sciences

Academic education

2007-2008	Agricultural sciences, Bachelor (1-Fach), Kiel University
2008-2011	Biology, Bachelor [Grade 1,8], Kiel University
	Thesis (Zoology, Comparative Immunolobiology): „Analyse der Lysozym-Synthese bei *Dictyostelium discoideum* in der Abhängigkeit von der Gegenwart von Bakterien“ [Grade 1,3]
2011-2014	Biology, Master [Grade 1,2], Kiel University
	Thesis (Zoology, Comparative Immunolobiology): „Physiologische Rolle der Acyloxyacylhydrolase in *Dictyostelium discoideum*“ [Grade 1,0]
07/2014-03/2018	Dissertation (Molecular Physiology, Kiel University): „Impact of oncogene expression in the respiratory system of *Drosophila melanogaster*“

Publications

2015	Uliczka K, Bossen J, Pfefferkorn R, Heine H, Roeder T. (2015) Etablierung eines *Drosophila*-Lungenkarzinom-Modells. Pneumologie. 69-A7.

Erklärung

Hiermit erkläre ich, Judith Bossen, dass diese Dissertation mit dem Titel: „Impact of oncogene expression in the respiratory system of *Drosophila melanogaster*“, sowie die darin beschriebenen Arbeiten, abgesehen von der Beratung durch meinen akademischen Lehrer, nach Inhalt und Form meine eigene Arbeit sind. Diese Arbeit wurde weder im Ganzen noch zum Teil an anderer Stelle im Rahmen eines Promotionsvorhabens eingereicht. Sie wurde nach den Regeln guter wissenschaftlicher Praxis der Deutschen Forschungsgemeinschaft angefertigt.

Kiel,

Judith Bossen

Danksagung

Danken möchte ich Prof. Dr. Thomas Roeder, für die Bereitstellung dieses Thema, die wissenschaftliche Unterstützung und die mir gewährte Betreuung während der gesamten Bearbeitungszeit. Ich bin wirklich froh, dass ich mich hierfür entschieden habe.

Dr. Christine Fink möchte ich danken, für die Unterstützung und Motivation, die sie mir über die gesamte Zeit gegeben hat. Danke Tinky, ich arbeite wirklich gern mit dir zusammen!

Ein besonders großer Dank an Britta und Christiane, die mich im Labor bei so vielen Dingen unterstützt haben! Außerdem danke ich auch allen anderen Mitgliedern der AG Roeder für die Unterstützung im Laboralltag. Dabei denke ich nicht nur an die methodischen Fragen, sondern auch an den Spaß, die Motivationshilfe und den Aufbau nach diversen Rückschlägen. Danke!

Dann danke ich allen anderen, die diese Arbeit für mich korrekturgelesen haben und die mich über die Arbeit im Labor hinaus während der ganzen Zeit immer wieder motiviert und unterstützt haben. Besonders danke ich da R!

Zu guter Letzt danke ich meinen geliebten Eltern und Geschwistern, ohne die mein ganzes Studium und auch diese Doktorarbeit nicht möglich gewesen wären.

Appendix

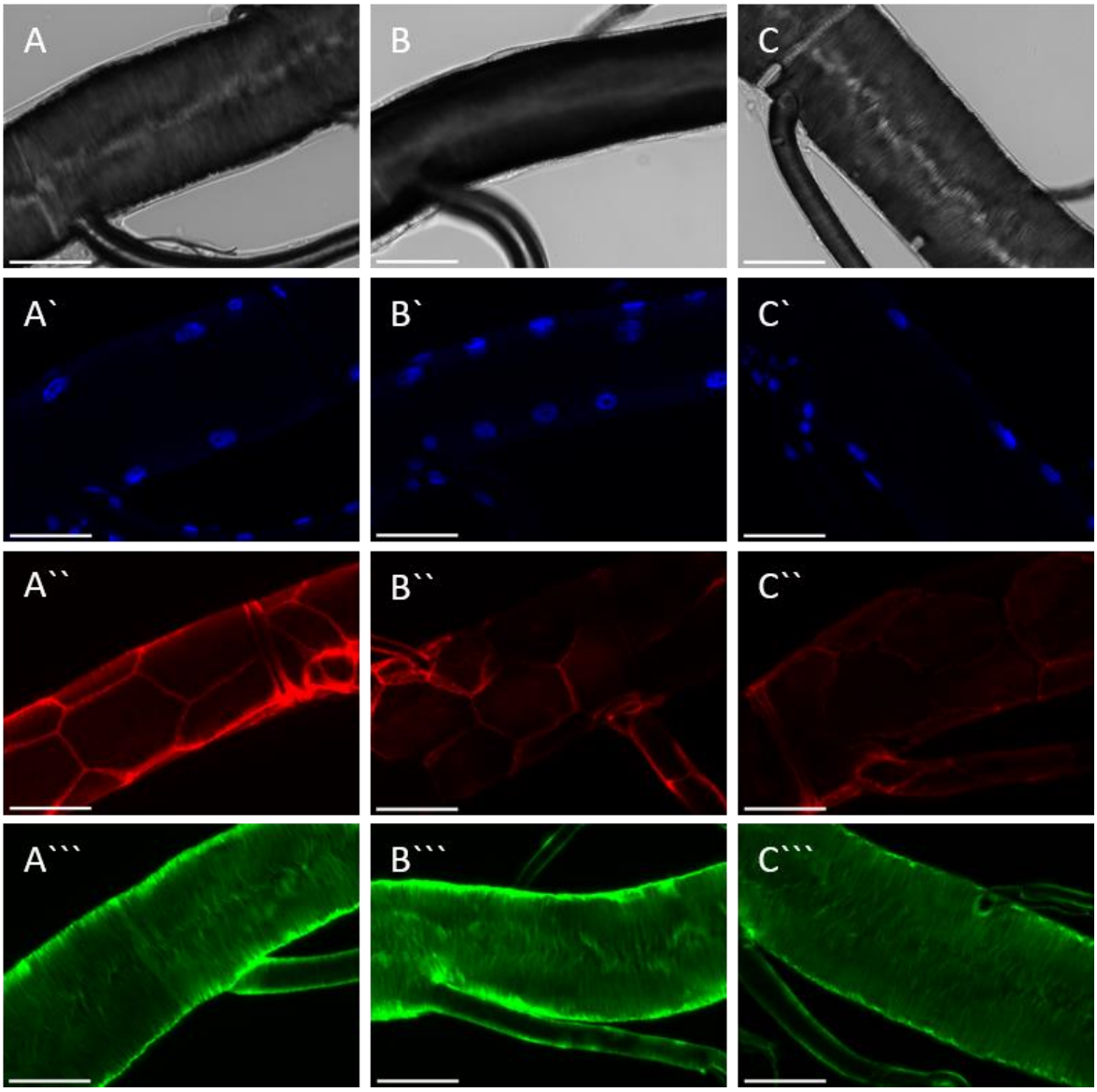

Figure 34: Afatinib and Gefitinib treatment has no impact on epithelial structure of the control trachea. The embryos of *ppk4-Gal4 > w*^{1118} were placed on low-melt CM prepared with either DMSO [0.1 %] (**A**), Afatinib [100 µM] (**B**) or Gefitinib [100 µM] (**C**). The tracheae were dissected on day four after egg laying and stained with DAPI (**A`**-**C`**), an antibody against coracle (**A``**-**C``**) and with a conjugated chitin binding protein (**A```**-**C```**). Scale = 50 µM.

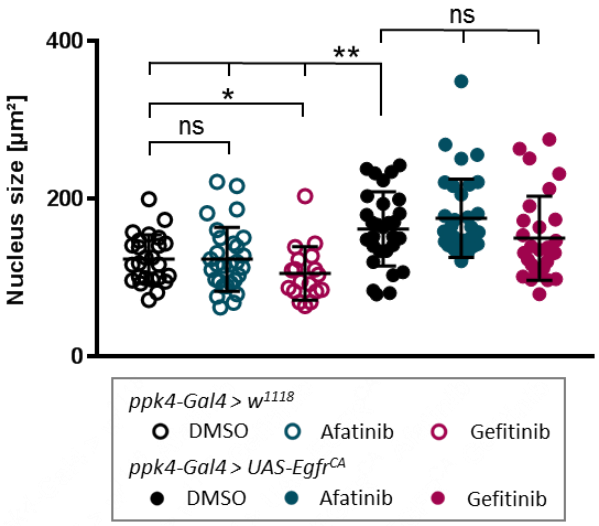

Figure 35: Nucleus size after Afatinib and Gefitinib treatment. The embryos of *ppk4-Gal4 > w*^{1118} (open circles) and *ppk4-Gal4 > UAS-Egfr*^{CA} (filled circles) were treated with either DMSO [0.1 %] (control n = 25, *Egfr*^{CA} n = 29), Afatinib [100 µM] (control n = 29, *Egfr*^{CA} n = 34) or Gefitinib [100 µM] (control n = 18, *Egfr*^{CA} n = 28) and dissected on day four after egg laying. The tracheae were stained with DAPI and analyzed under the microscope in DAPI channel. Quantification of the nucleus size occurred in AxioVision. For the measurement only the 8th segment of the dorsal trunks was used. Represented are means ± SD. Statistical significance was tested with unpaired t-test. * = $p < 0.05$, ** = $p < 0.01$.

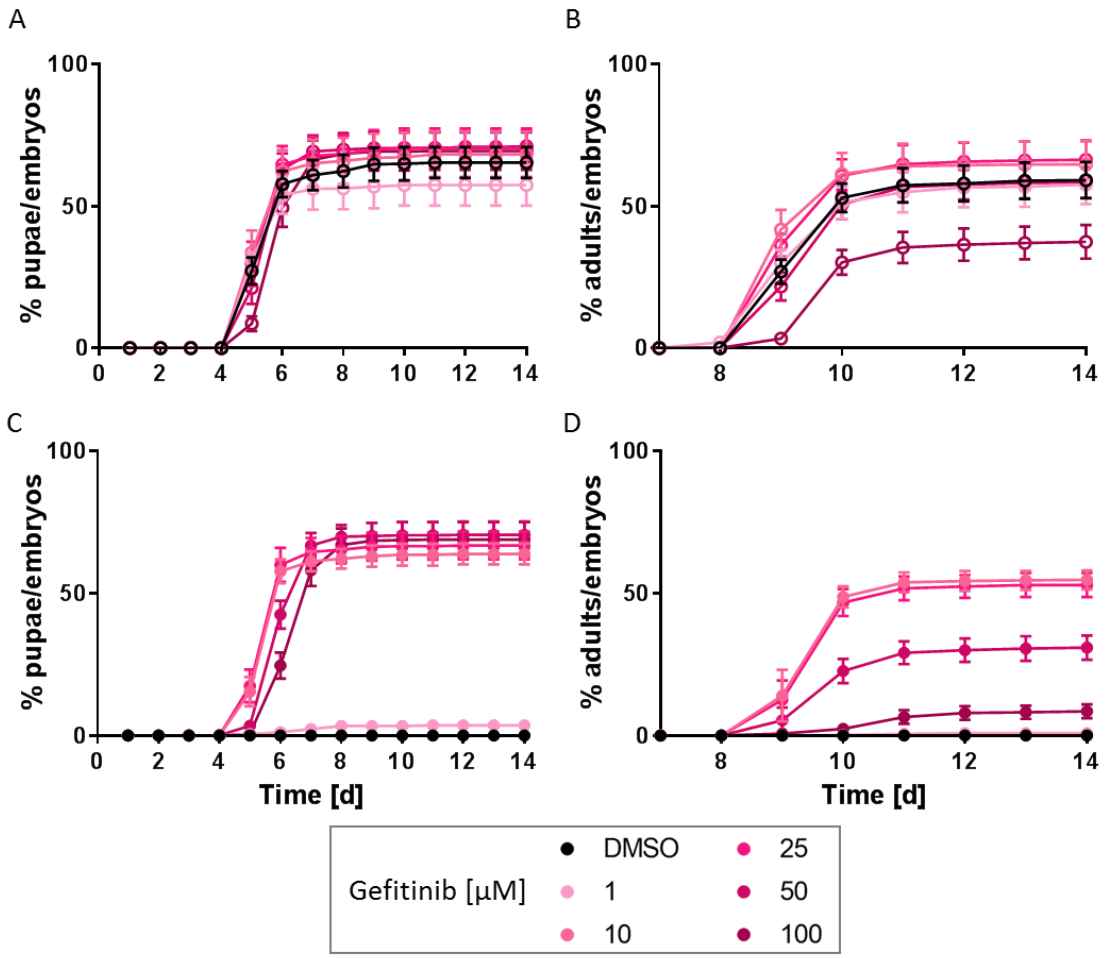

Figure 36: Differences in the development of adult flies in Gefitinib treated *Egfr^{CA}* animals. The embryos of *ppk4-Gal4 > w^{1118}* (**A**, **B**, open circles) and *ppk4-Gal4 > UAS-Egfr^{CA}* (**C**, **D**, filled circles) were placed on low-melt CM prepared with either DMSO [0.1 %] or five different Gefitinib concentrations from 1 µM to 100 µM. The formation of pupae (**A**, **C**) and adults (**B**, **D**) was monitored daily over two weeks in six replicates. Represented are means ± SEM.

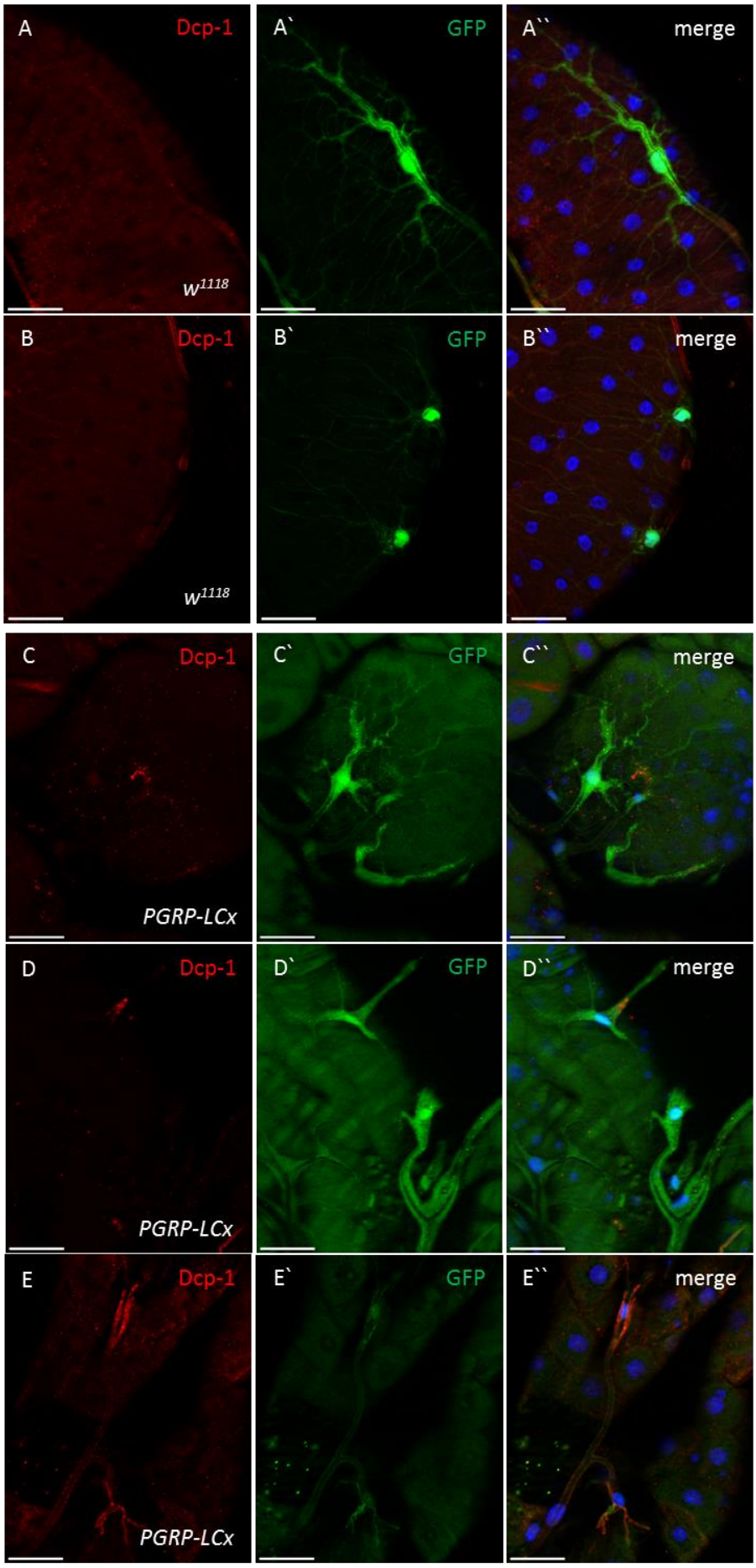

Figure 37: Dcp-1 staining of the terminal cells with ectopic *PGRP-LCx* expression. Dissected intestines of *DSRF-Gal4 > w^{1118}* (**A**, **B**) and *DSRF-Gal4 > UAS-PGRP-LCx* (**C**-**E**) with the connected terminal cells were stained with cleaved *Drosophila* Dcp-1 antibody (**A**-**E**). The terminal cells were counterstained with a GFP antibody (**A`**-**E`**). The merge of both is shown with DAPI staining of the cell nuclei (**A``**-**E``**). Scale = 50 µM.

Table 6: Number of formed pupae after treatment from *Egfr*^{CA} embryos with compounds from a FDA approved drug library.

CatalogNumber	Item Name	#pupae	#2nd	#pupae (Afatinib)
S1005	Axitinib	0		0
S1011	**Afatinib (BIBW2992)**	**9**	**7**	**12**
S1013	Bortezomib (Velcade)	0		0
S1014	Bosutinib (SKI0606)	1		0
S1021	Dasatinib (BMS0354825)	0		0
S1023	**Erlotinib HCl**	**6**	**0**	**10**
S1025	**Gefitinib (Iressa)**	**22**	**26**	**14**
S1026	Imatinib Mesylate	1		1
S1028	Lapatinib Ditosylate (Tykerb)	1		0
S1029	Lenalidomide	0		0
S1033	Nilotinib (AMN0107)	0		0
S1035	Pazopanib HCl	0		0
S1039	Rapamycin (Sirolimus)	0		2
S1040	**Sorafenib (Nexavar)**	**1**		**4**
S1042	Sunitinib Malate (Sutent)	0		1
S1044	Temsirolimus (Torisel)	0		0
S1046	Vandetanib (Zactima)	1		0
S1047	Vorinostat (SAHA)	0		0
S1064	Masitinib (AB1010)	0		0
S1068	Crizotinib (PF002341066)	0		0
S1082	Vismodegib (GDC00449)	0		2
S1119	XL0184 (Cabozantinib)	0		1
S1120	Everolimus (RAD001)	0		0
S1137	Malotilate	0		0
S1144	Ivacaftor (VX0770)	0		0
S1148	Docetaxel (Taxotere)	0		0
S1150	Paclitaxel (Taxol)	0		0
S1156	Capecitabine (Xeloda)	0		0
S1166	Cisplatin	0		0
S1168	Valproic acid sodium salt (Sodium valproate)	0		0
S1178	Regorafenib (BAY 7304506)	0		0
S1185	Ritonavir	0		0
S1188	Anastrozole	1		1
S1189	Aprepitant (MK00869)	0		0
S1190	Bicalutamide (Casodex)	0		0
S1191	Fulvestrant (Faslodex)	0		1
S1193	Thalidomide	0		0
S1196	Exemestane	0		0
S1197	Finasteride	0		0
S1198	Irinotecan	0		0
S1199	Cladribine	0		0

S1200	Decitabine	1		0
S1202	Dutasteride	0		0
S1204	Melatonin	0		0
S1206	Bisoprolol fumarate	0		0
S1208	Doxorubicin (Adriamycin)	0		1
S1209	Adrucil (Fluorouracil)	0		0
S1210	Abitrexate (Methotrexate)	0		0
S1212	Bendamustine HCL	0		0
S1213	Nelarabine (Arranon)	0		0
S1214	Bleomycin sulfate	0		0
S1218	Clofarabine	0		0
S1221	Dacarbazine (DTIC0Dome)	0		0
S1222	Dexrazoxane Hydrochloride	0		1
S1223	Epirubicin HCl	0		1
S1224	Oxaliplatin (Eloxatin)	0		0
S1225	Etoposide (VP016)	0		1
S1227	Evista (Raloxifene Hydrochloride)	0		0
S1228	Idarubicin HCl	0		0
S1229	Fludarabine Phosphate (Fludara)	0		0
S1231	Topotecan HCl	0		0
S1233	20Methoxyestradiol	0		0
S1235	Letrozole	0		0
S1237	Methazolastone	0		0
S1241	Vincristine sulfate	0		0
S1243	Agomelatine	0		0
S1247	Leflunomide	0		1
S1250	MDV3100 (Enzalutamide)	2		0
S1251	Dienogest	1		0
S1252	Entecavir hydrate	0		0
S1255	Nepafenac	1		0
S1256	Rufinamide (Banzel)	0		0
S1257	Posaconazole	0		0
S1258	Prasugrel (Effient)	0		0
S1259	Ramelteon (TAK0375)	0		0
S1260	AMG0073 HCl (Cinacalcet hydrochloride)	0		1
S1261	Celecoxib	0		0
S1267	Vemurafenib (PLX4032)	0		0
S1271	Acarbose	0		0
S1276	Adapalene	0		0
S1278	Altretamine (Hexalen)	0		0
S1280	Amisulpride	0		0
S1281	Aniracetam	0		0
S1282	Artemisinin	0		0
S1283	Asenapine	0		1
S1284	Benazepril hydrochloride	0		0

S1286	Budesonide	0		2
S1287	Bumetanide	0		1
S1288	Camptothecin	0		0
S1289	Carmofur	0		0
S1291	Cetirizine Dihydrochloride	0		0
S1293	Cilnidipine	2		0
S1294	Cilostazol	0		0
S1299	Floxuridine	0		0
S1300	Ftorafur	0		0
S1302	Ifosfamide	0		0
S1304	Megestrol Acetate	0		0
S1305	Mercaptopurine	0		0
S1312	Streptozotocin (Zanosar)	0		0
S1322	Dexamethasone	0		0
S1324	Doxazosin mesylate	0		1
S1326	Edaravone (MCI0186)	0		0
S1328	Etodolac (Lodine)	0		0
S1329	Etomidate	0		0
S1330	Felbamate	0		1
S1331	Fluconazole	0		0
S1332	Flumazenil	0		2
S1333	Fluoxetine HCl	0		0
S1336	Fluvoxamine maleate	0		0
S1340	*Gatifloxacin*	0		1
S1342	Genistein	0		0
S1344	Glimepiride	0		0
S1351	Ivermectin	0		0
S1353	Ketoconazole	0		1
S1354	Lansoprazole	0		0
S1356	Levetiracetam	1		1
S1357	Lidocaine (Alphacaine)	0		1
S1358	Loratadine	0		0
S1359	Losartan potassium	0		1
S1368	Acitretin	0		0
S1374	Doripenem Hydrate	0		0
S1376	Gestodene	0		0
S1377	Drospirenone	0		0
S1378	Ruxolitinib (INCB018424)	1		1
S1379	Isotretinoin	0		0
S1380	Lopinavir (ABT0378)	0		1
S1381	Meropenem	0		0
S1382	Mianserin hydrochloride	0		0
S1385	Mosapride citrate	0		1
S1386	Nafamostat mesylate	1		2
S1389	Omeprazole (Prilosec)	0		1

S1390	Ondansetron hydrochloride (Zofran)	0		0
S1391	Oxcarbazepine	1		0
S1394	Pizotifen malate	0		0
S1396	Resveratrol	0		0
S1397	Rocuronium bromide	1		0
S1398	Stavudine	0		0
S1400	Tenofovir Disoproxil Fumarate	0		0
S1401	*Tenofovir*	0		0
S1403	Tigecycline	0		0
S1404	Trilostane	0		1
S1405	Vecuronium Bromide	1		0
S1407	Bimatoprost	0		1
S1408	Linezolid (Zyvox)	0		0
S1409	Alfuzosin hydrochloride (Uroxatral)	0		0
S1415	Clopidogrel (Plavix)	0		2
S1425	Ranolazine dihydrochloride	0		0
S1426	Repaglinide	1		0
S1430	Rolipram	0		2
S1431	Sildenafil citrate	0		2
S1432	Sumatriptan succinate	0		0
S1436	Tianeptine sodium	0		0
S1437	Tizanidine HCl	1		0
S1438	Topiramate	0		0
S1439	Tranilast (SB 252218)	0		1
S1441	Venlafaxine	0		0
S1442	Voriconazole	0		0
S1443	Zileuton	0		0
S1444	Ziprasidone hydrochloride	0		0
S1445	Zonisamide	0		0
S1457	Atazanavir sulfate	0		0
S1464	*Marbofloxacin*	0		0
S1465	Moxifloxacin hydrochloride	0		0
S1466	Calcitriol (Rocaltrol)	0		0
S1467	Doxercalciferol (Hectorol)	0		0
S1468	Alfacalcidol	0		1
S1483	Iloperidone (Fanapt)	1		0
S1488	Naratriptan HCl	0		0
S1490	Ponatinib (AP24534)	0		0
S1491	Fludarabine (Fludara)	0		0
S1497	Pralatrexate (Folotyn)	0		0
S1500	Betamethasone (Celestone)	0		0
S1501	Mycophenolate mofetil (CellCept)	0		0
S1502	Cephalexin (Cefalexin)	0		0
S1504	Dyphylline (Dilor)	0		0
S1505	Aztreonam (Azactam, Cayston)	0		0

S1508	Alprostadil (Caverject)	0		0
S1512	Tadalafil (Cialis)	0		0
S1514	Cyclosporine (Neoral)	0		0
S1517	Natamycin (Pimaricin)	1		0
S1538	Telaprevir (VX0950)	1		0
S1540	Saxagliptin (BMS0477118,Onglyza)	0		2
S1547	Febuxostat (Uloric)	0		0
S1549	Nebivolol (Bystolic)	1		0
S1550	Pimobendan (Vetmedin)	1		0
S1567	Pomalidomide	0		0
S1569	Tazarotene (Avage)	1		2
S1576	Sulfasalazine (Azulfidine)	0		2
S1578	Candesartan (Atacand)	0		1
S1593	Apixaban	0		2
S1601	Reserpine	1		1
S1603	Furosemide (Lasix)	1		0
S1604	Olmesartan medoxomil (Benicar)	2		0
S1605	Cefdinir (Omnicef)	0		1
S1606	Clotrimazole (Canesten)	0		1
S1607	Rizatriptan Benzoate	0		0
S1608	Pyridostigmine Bromide (Mestinon)	0		0
S1609	Methimazole (Tapazole, Northyx)	0		0
S1610	Metolazone (Zaroxolyn)	3		2
S1611	Cefoperazone (Cefobid)	0		0
S1613	Silodosin (Rapaflo)	1		0
S1614	Riluzole (Rilutek)	2		1
S1615	Risperidone (Risperdal)	1		1
S1618	Sulfameter (Bayrena)	0		0
S1619	Prilocaine	0		0
S1620	Darunavir Ethanolate (Prezista)	1		2
S1622	Prednisone (Adasone)	1		0
S1623	Acetylcysteine	1		1
S1625	Ethinyl Estradiol	0		0
S1626	Naproxen (Aleve)	0		0
S1627	Nitazoxanide (Alinia, Annita)	0		1
S1628	Triamcinolone Acetonide	0		0
S1629	Orlistat (Alli, Xenical)	0		2
S1630	Allopurinol (Zyloprim)	0		0
S1633	Zafirlukast (Accolate)	1		1
S1635	Erythromycin (E0Mycin)	0		0
S1636	Amphotericin B	2		0
S1638	Ibuprofen (Advil)	0		0
S1639	Amprenavir (Agenerase)	1		0
S1640	Albendazole (Albenza)	0		1
S1641	Chlorothiazide	0		0

S1643	Ursodiol (Actigal Urso)	1		0
S1644	Nitrofurazone (Nitrofural)	0		1
S1645	Ketoprofen (Actron)	0		0
S1646	Ketorolac (Toradol)	0		0
S1647	Adenosine (Adenocard)	0		1
S1649	Zolmitriptan (Zomig)	0		0
S1651	Telbivudine (Sebivo, Tyzeka)	0		0
S1652	Monobenzone (Benoquin)	1		0
S1653	Tretinoin (Aberela)	1		0
S1654	Phenylbutazone (Butazolidin, Butatron)	0		0
S1655	Ezetimibe (Zetia)	0		0
S1657	Enalaprilat dihydrate	1		0
S1658	Dofetilide (Tikosyn)	0		0
S1662	Isradipine (Dynacirc)	1		0
S1665	Estrone	0		2
S1666	Flucytosine (Ancobon)	0		0
S1667	Trichlormethiazide (Achletin)	1		0
S1669	Loteprednol etabonate	0		0
S1671	Aminocaproic acid (Amicar)	0		0
S1672	Aminoglutethimide (Cytadren)	0		2
S1673	Aminophylline (Truphylline)	0		0
S1676	Amorolfine Hydrochloride	0		0
S1677	Chloramphenicol (Chloromycetin)	0		0
S1679	Flurbiprofen (Ansaid)	0		1
S1680	Disulfiram (Antabuse)	0		0
S1681	Mesalamine (Lialda)	0		1
S1683	Ipratropium bromide	1		0
S1685	Sulfanilamide	0		0
S1688	*Betamethasone Dipropionate*	1		1
S1689	Betapar (Meprednisone)	0		0
S1690	Betamethasone valerate (Betnovate)	1		0
S1691	Praziquantel (Biltricide)	0		1
S1692	Busulfan (Myleran, Busulfex)	0		0
S1693	Carbamazepine (Carbatrol)	0		0
S1696	Hydrocortisone (Cortisol)	1		1
S1701	Desonide	0		0
S1702	Didanosine (Videx)	0		0
S1703	Divalproex sodium	0		0
S1704	Emtricitabine (Emtriva)	0		1
S1705	Progesterone (Prometrium)	1		0
S1706	Lamivudine (Epivir)	0		0
S1708	Hydrochlorothiazide	0		0
S1709	Estradiol	0		0
S1712	Deferasirox (Exjade)	0		0
S1713	Piroxicam (Feldene)	0		1

S1714	Gemcitabine (Gemzar)	0		0
S1715	Glipizide (Glucotrol)	0		0
S1716	Glyburide (Diabeta)	0		0
S1718	Adefovir Dipivoxil (Preveon, Hepsera)	0		1
S1719	Zalcitabine	0		0
S1721	Azathioprine (Azasan, Imuran)	0		0
S1723	Indomethacin (Indocid, Indocin)	0		0
S1725	Terbinafine (Lamisil, Terbinex)	0		0
S1727	Levonorgestrel (Levonelle)	1		0
S1729	Gemfibrozil (Lopid)	0		0
S1730	Indapamide (Lozol)	0		1
S1732	Mitotane (Lysodren)	1		2
S1733	Methylprednisolone	0		1
S1734	Meloxicam (Mobic)	0		0
S1735	Mesna (Uromitexan, Mesnex)	2		0
S1736	Methocarbamol (Robaxin)	0		1
S1737	Prednisolone (Hydroretrocortine)	0		1
S1738	Telmisartan (Micardis)	0		1
S1739	Thiabendazole	0		2
S1740	Guaifenesin (Guaiphenesin)	1		3
S1741	Rifabutin (Mycobutin)	0		0
S1742	Nevirapine (Viramune)	0		0
S1743	Esomeprazole magnesium (Nexium)	0		0
S1744	Niacin (Nicotinic acid)	0		2
S1747	Nimodipine (Nimotop)	1		1
S1748	Nisoldipine (Sular)	2		1
S1754	Oxybutynin (Ditropan)	0		1
S1756	**Enoxacin (Penetrex)**	**0**		**4**
S1759	**Pitavastatin calcium (Livalo)**	**1**		**6**
S1760	Rifapentine (Priftin)	0		0
S1761	Suprofen (Profenal)	0		0
S1762	Pyrazinamide (Pyrazinoic acid amide)	0		1
S1763	Quetiapine fumarate (Seroquel)	0		3
S1764	Rifampin (Rifadin, Rimactane)	0		0
S1767	Beta Carotene	0		0
S1768	Cefditoren pivoxil	0		0
S1770	Sulfadiazine	0		1
S1771	Chlorprothixene	0		0
S1773	Oxytetracycline (Terramycin)	0		0
S1776	Toremifene Citrate (Fareston, Acapodene)	1		0
S1777	Ethionamide	0		0
S1778	Trifluridine (Viroptic)	1		0
S1782	Azacitidine (Vidaza)	0		0
S1784	Vidarabine (Vira0A)	0		0
S1786	Verteporfin (Visudyne)	0		0

S1787	Teniposide (Vumon)	0		0
S1790	Rifaximin (Xifaxan)	0		0
S1792	Simvastatin (Zocor)	0		0
S1793	Ramipril (Altace)	0		0
S1794	Fenofibrate (Tricor, Trilipix)	0		0
S1799	Ranolazine (Ranexa)	0		1
S1801	Ranitidine (Zantac)	0		0
S1802	Acadesine	0		0
S1805	Acetylcholine chloride	0		0
S1806	Acipimox	0		0
S1807	Acyclovir (Aciclovir)	0		2
S1808	Nifedipine (Adalat)	0		0
S1811	Amiloride hydrochloride (Midamor)	0		0
S1813	Amlodipine besylate (Norvasc)	0		0
S1816	Chlorpheniramine Maleate	0		0
S1823	Fenoprofen calcium	1		0
S1825	Erdosteine	1		1
S1827	Betaxolol hydrochloride (Betoptic)	0		0
S1828	Proparacaine HCl	0		0
S1829	Pranlukast	0		0
S1830	Oxfendazole	0		0
S1831	Carvedilol	2		1
S1832	Atracurium besylate	0		1
S1833	Butoconazole nitrate	0		0
S1835	Azithromycin (Zithromax)	0		0
S1836	Albendazole Oxide (Ricobendazole)	0		1
S1839	Chloroxine	1		0
S1840	Lomustine (CeeNU)	0		0
S1843	Chenodeoxycholic acid	0		0
S1845	Cimetidine (Tagamet)	1		0
S1847	Clemastine Fumarate	1		0
S1848	Curcumin	0		0
S1849	Daidzein	0		0
S1854	Bifonazole	0		0
S1855	Pefloxacin mesylate	0		1
S1856	Metoprolol tartrate	0		0
S1859	Diethylstilbestrol (Stilbestrol)	0		3
S1865	Diltiazem HCl (Tiazac)	0		1
S1866	Diphenhydramine HCl (Benadryl)	0		1
S1869	Dapoxetine hydrochloride (Priligy)	0		0
S1876	Valaciclovir HCl	0		0
S1878	Ganciclovir	0		0
S1880	Roxatidine acetate HCl	0		0
S1881	Protionamide (Prothionamide)	1		1
S1883	Idoxuridine	0		0

S1884	Sparfloxacin	0		0
S1885	Felodipine (Plendil)	0		0
S1888	Deflazacort (Calcort)	0		1
S1890	Nizatidine	0		0
S1891	Carbidopa	1		0
S1894	Valsartan (Diovan)	0		0
S1895	Dipyridamole (Persantine)	1		0
S1896	Hydroxyurea (Cytodrox)	1		0
S1897	Potassium iodide	0		0
S1898	Tropisetron	0		0
S1899	Nicotinamide (Niacinamide)	0		0
S1902	Vitamin B12	0		0
S1903	Diclofenac	0		0
S1904	Avobenzone (Parsol 1789)	0		0
S1905	Amlodipine (Norvasc)	0		1
S1907	Metronidazole (Flagyl)	0		0
S1908	Flutamide (Eulexin)	0		2
S1909	Fluvastatin sodium (Lescol)	0		2
S1910	Tioconazole	0		2
S1913	Tropicamide	0		1
S1914	Pregnenolone	0		0
S1915	Sulfamethoxazole	0		0
S1916	Sulfisoxazole	1		0
S1917	Crystal violet	0		0
S1920	Haloperidol (Haldol)	1		0
S1921	Phenindione (Rectadione)	0		0
S1928	Alibendol	0		0
S1929	Irsogladine	1		1
S1933	Triamcinolone (Aristocort)	0		1
S1934	Nystatin (Mycostatin)	1		1
S1937	Isoniazid (Tubizid)	1		0
S1940	Levofloxacin (Levaquin)	0		0
S1941	Enalapril maleate (Vasotec)	0		0
S1949	Menadione	0		0
S1952	Methoxsalen (Oxsoralen)	0		0
S1956	Miconazole nitrate	0		1
S1957	Sulfamethizole (Proklar)	0		0
S1958	Sulbactam	1		0
S1959	Tolfenamic acid	0		0
S1960	Pranoprofen	0		0
S1962	Sulphadimethoxine	0		0
S1964	Rimantadine (Flumadine)	0		2
S1965	Primidone (Mysoline)	0		0
S1969	Nefiracetam (Translon)	0		0
S1971	Nicorandil (Ikorel)	0		0

S1972	Tamoxifen Citrate (Nolvadex)	0		0
S1974	Meglumine	1		0
S1975	Aripiprazole (Abilify)	0		0
S1978	Methscopolamine (Pamine)	0		0
S1979	Amiodarone HCl	0		0
S1983	Adenine hydrochloride	1		0
S1987	Mometasone furoate	1		0
S1988	Propylthiouracil	0		1
S1992	Fluticasone propionate (Flonase, Veramyst)	0		2
S1994	Lacidipine (Lacipil, Motens)	0		0
S2001	Elvitegravir (GS09137)	0		0
S2003	Maraviroc	0		0
S2005	Raltegravir (MK00518)	0		0
S2006	Pyrimethamine	0		0
S2007	Sulindac (Clinoril)	0		0
S2011	Pramipexole dihydrochloride monohydrate	0		1
S2015	Suplatast tosylate	0		0
S2016	Mirtazapine (Remeron, Avanza)	0		0
S2017	Benidipine hydrochloride	0		0
S2020	Formoterol hemifumarate	0		0
S2021	Chlormezanone (Trancopal)	0		0
S2024	Ketotifen fumarate (Zaditor)	0		1
S2025	Urapidil HCl	0		0
S2026	Ginkgolide A	0		1
S2028	Diclazuril	0		1
S2029	Uridine	0		0
S2030	Flunarizine 2HCl	0		0
S2031	Fenticonazole nitrate	0		0
S2032	Rebamipide	0		0
S2035	Epalrestat	0		0
S2036	Aspartame	0		0
S2037	Candesartan cilexetil (Atacand)	0		1
S2038	Phentolamine mesilate	0		0
S2040	Nimesulide	0		0
S2041	Dyclonine HCl	0		0
S2043	Memantine HCl (Namenda)	0		0
S2044	Cyproheptadine HCl (Periactin)	0		0
S2045	Doxifluridine	0		0
S2046	Pioglitazone hydrochloride (Actos)	0		0
S2047	Lornoxicam (Xefo)	0		0
S2051	Captopril (Capoten)	1		0
S2052	Oxytetracycline dihydrate	0		0
S2053	Cytidine	0		0
S2054	Orphenadrine citrate (Norflex)	0		0
S2055	Gimeracil	0		0

S2057	Cyclophosphamide monohydrate	0		0
S2058	Tolnaftate	0		0
S2059	Terazosin HCl (Hytrin)	0		0
S2060	Bromhexine HCl	0		0
S2061	Lovastatin (Mevacor)	0		1
S2062	Tiopronin (Thiola)	0		0
S2064	Balofloxacin	0		0
S2065	Lafutidine	1		2
S2066	Moxonidine	1		0
S2067	Ozagrel HCl	0		0
S2069	Argatroban	0		0
S2074	Mecarbinate	0		1
S2075	Rosiglitazone HCl	0		0
S2077	Atorvastatin calcium (Lipitor)	1		0
S2078	Famotidine (Pepcid)	0		0
S2079	Moexipril HCl	3		1
S2080	Cleviprex (Clevidipine)	0		0
S2082	Adiphenine HCl	0		0
S2084	Duloxetine HCl (Cymbalta)	0		0
S2085	Trimebutine	0		2
S2086	Ivabradine HCl (Procoralan)	1		1
S2087	Rivastigmine tartrate (Exelon)	0		1
S2090	Dexmedetomidine HCl (Precedex)	0		0
S2091	Betaxolol (Betoptic)	2		0
S2092	Detomidine HCl	0		0
S2096	Almotriptan malate (Axert)	0		3
S2097	Ambrisentan	0		0
S2098	Bexarotene	0		**4**
S2099	Temocapril HCl	0		0
S2101	Gabexate mesylate	0		0
S2102	Rasagiline mesylate	0		0
S2103	Naltrexone HCl	0		0
S2104	Levosulpiride (Levogastrol)	2		0
S2108	Flunixin meglumin	1		0
S2109	Imidapril (Tanatril) HCl	0		0
S2111	Lapatinib	0		0
S2113	Cisatracurium besylate (Nimbex)	1		0
S2114	Dronedarone HCl (Multaq)	1		0
S2116	Conivaptan HCl (Vaprisol)	0		1
S2118	Ibutilide fumarate	0		0
S2119	Probucol	0		0
S2120	Arbidol HCl	0		0
S2121	Licofelone	0		0
S2123	Dextrose (D0glucose)	3		1
S2124	Xylose	0		0

S2125	Mestranol	0		0
S2126	Naftopidil (Flivas)	1		0
S2127	S0(+)0Rolipram	0		0
S2128	**Bazedoxifene HCl**	**0**		**6**
S2130	Atropine sulfate monohydrate	0		0
S2131	Roflumilast (Daxas)	1		1
S2152	*Sitafloxacin Hydrate*	0		1
S2154	BIBR01048 (Dabigatran)	0		0
S2159	**Tebipenem pivoxil (L0084)**	**0**		**7**
S2169	Rosuvastatin calcium (Crestor)	0		0
S2199	Aliskiren hemifumarate	1		1
S2205	OSI0420 (Desmethyl Erlotinib)	0		0
S2215	DAPT (GSI0IX)	0		0
S2217	Irinotecan HCl Trihydrate (Campto)	0		2
S2221	Apatinib (YN968D1)	0		1
S2225	TAME	0		1
S2229	Eltrombopag (SB04971150GR)	0		0
S2233	Esomeprazole sodium (Nexium)	0		1
S2240	Fesoterodine fumarate (Toviaz)	0		1
S2264	Artemether (SM0224)	1		0
S2293	DL0Carnitine hydrochloride	0		0
S2328	Nalidixic acid (NegGram)	0		1
S2376	Ammonium Glycyrrhizinate	0		0
S2381	D0Mannitol (Osmitrol)	0		0
S2393	Sorbitol (Glucitol)	0		0
S2408	Cephalomannine	0		0
S2409	100Deacetylbaccatin0III	0		0
S2410	Paeoniflorin	0		0
S2411	Geniposide	0		0
S2412	Genipin	0		0
S2413	Geniposidic acid	0		0
S2443	Tolbutamide	0		0
S2446	Levosimendan	0		0
S2451	Amantadine hydrochloride (Symmetrel)	0		0
S2452	Amfebutamone (Bupropion)	0		0
S2453	Benserazide	0		0
S2454	Bupivacaine hydrochloride (Marcain)	0		0
S2455	Bethanechol chloride	0		0
S2456	Chlorpromazine (Sonazine)	0		0
S2457	Clindamycin hydrochloride (Dalacin)	0		0
S2458	Clonidine hydrochloride (Catapres)	0		0
S2459	Clozapine (Clozaril)	0		0
S2460	Pramipexole (Mirapex)	0		1
S2461	Domperidone (Motilium)	0		0
S2466	Estriol	0		0

S2467	Famciclovir (Famvir)	0		0
S2468	Fenbendazole	0		0
S2470	Fluocinolone acetonide (Flucort0N)	0		0
S2471	Gallamine triethiodide (Flaxedil)	0		0
S2475	Imatinib (Gleevec)	0		0
S2476	Itraconazole (Sporanox)	0		0
S2479	Lincomycin hydrochloride (Lincocin)	0		1
S2480	Loperamide hydrochloride	2		0
S2481	Manidipine (Manyper)	2		0
S2484	Milrinone (Primacor)	0		0
S2485	Mitoxantrone Hydrochloride	0		0
S2486	Moroxydine	0		0
S2487	Mycophenolic (Mycophenolate)	0		1
S2489	Nateglinide (Starlix)	0		0
S2491	Nitrendipine	0		0
S2492	Novobiocin sodium (Albamycin)	0		0
S2493	Olanzapine (Zyprexa)	1		0
S2494	Olopatadine hydrochloride (Opatanol)	0		1
S2495	Oxymetazoline hydrochloride	0		0
S2496	Ozagrel	0		0
S2497	Pancuronium (Pavulon)	0		2
S2499	Phenoxybenzamine HCl	1		0
S2500	Propafenone (Rytmonorm)	0		0
S2502	Quinine hydrochloride dihydrate	1		0
S2503	Racecadotril (Acetorphan)	3		0
S2504	Ribavirin (Copegus)	2		1
S2505	Rosiglitazone maleate	0		0
S2506	Roxithromycin (Roxl0150)	0		2
S2508	Scopolamine hydrobromide	0		0
S2509	Sotalol (Betapace)	0		2
S2510	Spectinomycin hydrochloride	0		0
S2512	Tenoxicam (Mobiflex)	2		0
S2515	Vardenafil hydrochloride trihydrate	0		0
S2516	Xylazine HCl	2		0
S2517	Maprotiline hydrochloride	1		0
S2519	Naphazoline hydrochloride (Naphcon)	0		0
S2521	Epinephrine bitartrate (Adrenalinium)	0		0
S2522	L0Adrenaline (Epinephrine)	0		0
S2524	Phenytoin sodium (Dilantin)	1		0
S2525	Phenytoin (Lepitoin)	0		0
S2527	Methacycline hydrochloride (Physiomycine)	0		0
S2528	Ciclopirox (Penlac)	0		0
S2529	Dopamine hydrochloride (Inotropin)	0		0
S2533	Ritodrine hydrochloride (Yutopar)	0		0
S2534	Isoconazole nitrate (Travogen)	0		0

S2535	Econazole nitrate (Spectazole)	0		0
S2536	Miconazole (Monistat)	0		0
S2537	Secnidazole (Flagentyl)	0		0
S2538	Acetanilide (Antifebrin)	0		0
S2541	Clomipramine HCl	0		0
S2542	Phenformin hydrochloride	0		0
S2543	Ceftiofur HCl	0		0
S2545	Scopine	0		0
S2547	Tiotropium Bromide hydrate	0		0
S2549	Trospium chloride (Sanctura)	0		0
S2550	Tolterodine tartrate (Detrol LA)	1		0
S2551	Sulbactam sodium (Unasyn)	0		0
S2552	Azelastine hydrochloride (Astelin)	1		0
S2553	50Aminolevulinic acid hydrochloride	0		0
S2555	Clarithromycin (Biaxin, Klacid)	0		0
S2556	Rosiglitazone (Avandia)	0		0
S2557	Terbinafine hydrochloride (Lamisil)	0		0
S2559	Cortisone acetate (Cortone)	0		0
S2560	Amiloride hydrochloride dihydrate	0		0
S2561	Clomifene citrate (Serophene)	1		1
S2564	Cloxacillin sodium (Cloxacap)	0		0
S2565	Amoxicillin sodium (Amox)	0		0
S2566	Isoprenaline hydrochloride	1		0
S2567	Medroxyprogesterone acetate	2		0
S2569	Phenylephrine HCl	0		1
S2570	Prednisolone acetate (Omnipred)	1		1
S2573	Tetracaine hydrochloride (Pontocaine)	0		0
S2574	Tetracycline HCl	0		0
S2576	Xylometazoline HCl	0		2
S2577	Phenacetin	0		0
S2579	Zidovudine (Retrovir)	1		1
S2581	Quinapril HCl (Accupril)	1		0
S2583	Thiamphenicol (Thiophenicol)	0		0
S2584	Clobetasol propionate	1		1
S2585	Brompheniramine	2		1
S2586	**Dimethyl Fumarate**	**4**	0	**1**
S2589	**Miglitol (Glyset)**	**4**	0	**1**
S2590	Pioglitazone (Actos)	1		0
S2593	Tolvaptan (OPC041061)	1		0
S2594	Pramiracetam	0		0
S2596	Clindamycin palmitate HCl	0		0
S2599	L0Thyroxine	0		1
S2601	Gliclazide (Diamicron)	0		1
S2602	Acemetacin (Emflex)	1		0
S2603	Tioxolone	1		0

S2604	Dehydroepiandrosterone (DHEA)	0		0
S2605	Idebenone	0		0
S2606	Mifepristone (Mifeprex)	1		0
S2607	Buflomedil HCl	0		0
S2608	Fluocinonide (Vanos)	0		2
S2610	Lonidamine	0		0
S2613	Clorsulon	0		0
S2614	Arecoline	0		1
S2615	Noradrenaline bitartrate monohydrate (Levophed)	0		1
S2680	**PCI032765 (Ibrutinib)**	**5**	**7**	**10**
S2721	Nilvadipine (ARC029)	0		1
S2807	Dabrafenib (GSK2118436)	0		0
S2830	Clindamycin	0		1
S2853	Carfilzomib (PR0171)	0		0
S2900	Cobicistat (GS09350)	0		0
S3000	Carbazochrome sodium sulfonate	0		0
S3002	Rivaroxaban (Xarelto)	0		1
S3005	Paroxetine HCl	0		0
S3007	Zanamivir	0		1
S3008	Zaltoprofen	0		0
S3012	Pazopanib	0		0
S3015	Amoxicillin (Amoxycillin)	0		0
S3017	Aspirin (Acetylsalicylic acid)	0		0
S3018	Niflumic acid	0		0
S3019	Ciclopirox ethanolamine	0		0
S3021	Rimonabant (SR141716)	0		0
S3022	Cabazitaxel (Jevtana)	0		0
S3023	Bufexamac	1		0
S3024	Lamotrigine	0		0
S3025	PMSF (Phenylmethylsulfonyl Fluoride)	0		1
S3027	Fenoprofen calcium hydrate	0		3
S3031	Linagliptin (BI01356)	0		1
S3032	Bindarit	0		0
S3033	Vildagliptin (LAF0237)	0		1
S3035	Daunorubicin HCl (Daunomycin HCl)	0		0
S3036	Pravastatin sodium	0		1
S3037	Bepotastine Besilate	0		0
S3038	Fosaprepitant dimeglumine	0		0
S3043	Rofecoxib (Vioxx)	0		0
S3045	Cinepazide maleate	0		0
S3046	Azilsartan (TAK0536)	0		0
S3047	Otilonium Bromide	0		0
S3048	Solifenacin succinate	1		1
S3053	Azelnidipine	0		0
S3054	Alverine Citrate	0		0

S3057	Azilsartan Medoxomil (TAK0491)	0		2
S3060	Medetomidine HCl	0		0
S3062	Diclofenac Potassium	0		0
S3063	Diclofenac Diethylamine	0		0
S3066	Naloxone HCl	0		0
S3073	Caspofungin acetate	1		0
S3075	Dexmedetomidine	0		0
S3078	Beclomethasone dipropionate	0		0
S3079	Atovaquone (Atavaquone)	0		0
S3080	Etravirine (TMC125)	0		1
S3081	Ulipristal	0		0
S3083	Indacaterol Maleate	0		0
S3100	20Thiouracil	0		0
S3104	Moguisteine	0		0
S3105	Nadifloxacin	0		0
S3106	Pidotimod	0		0
S3113	Pyridoxine hydrochloride	0		0
S3114	Vitamin C (Ascorbic acid)	0		0
S3116	Sulfathiazole	0		0
S3117	Oxybutynin chloride	0		1
S3121	Ornidazole	0		0
S3124	Dexamethasone acetate	0		0
S3129	Trimethoprim	0		0
S3130	Biotin (Vitamin B7)	0		1
S3132	Sulfamerazine	0		0
S3133	Sulfamethazine	0		0
S3137	Sodium salicylate	0		0
S3138	Methylthiouracil	0		0
S3139	Methenamine (Mandelamine)	0		0
S3140	Milnacipran HCl	0		0
S3144	Darifenacin HBr	0		0
S3146	Tripelennamine HCl	0		1
S3147	Entacapone	0		0
S3149	Estradiol valerate	0		0
S3150	Articaine HCl	0		0
S3151	Gliquidone	0		0
S3154	Butenafine HCl	0		0
S3155	Mepivacaine HCl	0		0
S3160	Ethynodiol diacetate	0		0
S3161	Sertaconazole nitrate	0		2
S3162	Tylosin tartrate	0		0
S3163	Benztropine mesylate	0		0
S3167	Altrenogest	0		1
S3170	Ampicillin sodium	0		0
S3172	Anagrelide HCl	0		0

S3173	Antipyrine	0		0
S3175	Atomoxetine HCl	0		0
S3176	Betahistine 2HCl	0		1
S3178	Brinzolamide	0		2
S3179	Carbenicillin disodium	2		0
S3181	Flumequine	0		0
S3183	Amitriptyline HCl	0		0
S3185	Adrenalone HCl	0		1
S3186	Azatadine dimaleate	0		1
S3188	(+,0)0Octopamine HCl	0		1
S3189	Ropinirole HCl	0		0
S3195	Azlocillin sodium salt	0		0
S3196	Azacyclonol	0		1
S3199	Reboxetine mesylate	0		1
S3200	Triflusal	0		0
S3201	Trifluoperazine 2HCl	0		0
S3202	Catharanthine	2		1
S3204	Meptazinol HCl	0		0
S3208	Fexofenadine HCl	0		0
S3209	Amidopyrine	1		0
S3212	Moclobemide	0		1
S4000	Pergolide mesylate	0		0
S4003	Lithocholic acid	0		0
S4004	Ethambutol dihydrochloride	0		2
S4007	Pentamidine isethionate	0		0
S4009	Mirabegron (YM178)	0		0
S4010	Acebutolol HCl	0		0
S4011	Ampiroxicam	0		1
S4012	Desloratadine	1		0
S4014	Hyoscyamine (Daturine)	2		0
S4015	Cyclamic acid	1		0
S4016	Ouabain	0		0
S4017	Allylthiourea	0		0
S4019	Avanafil	1		0
S4020	Sodium Picosulfate	0		0
S4021	Tolcapone	0		0
S4022	Probenecid (Benemid)	0		0
S4023	Procaine (Novocaine) HCl	0		0
S4024	Homatropine Methylbromide	0		2
S4025	Homatropine Bromide	0		0
S4026	Hydroxyzine 2HCl	0		0
S4027	Flavoxate HCl	0		0
S4031	Aclidinium Bromide	0		0
S4034	Diphemanil methylsulfate	0		0
S4035	Vitamin D2	0		0

S4037	Doxapram HCl	0		0
S4038	Dibucaine HCL	0		0
S4039	Methazolamide	0		1
S4040	norethindrone	1		0
S4041	olsalazine sodium	0		0
S4042	nafcillin sodium monohydrate	1		0
S4043	tetrahydrozoline hydrochloride	0		0
S4044	toltrazuril	0		0
S4045	Pheniramine Maleate	0		0
S4046	Estradiol Cypionate	0		0
S4047	Bisacodyl	0		0
S4048	Carbimazole	0		0
S4049	Bextra (valdecoxib)	0		0
S4050	valganciclovir hydrochloride	0		1
S4051	Nabumetone	0		0
S4053	Sertraline HCl	0		0
S4054	Spironolactone	0		0
S4056	Retapamulin	0		0
S4057	Methyclothiazide	0		0
S4058	Ropivacaine HCl	0		0
S4059	Sodium Nitroprusside	0		0
S4060	Erythromycin Ethylsuccinate	0		1
S4062	Ronidazole	0		0
S4063	Vitamin D3 (Cholecalciferol)	0		1
S4064	Escitalopram oxalate	0		0
S4065	Guanabenz acetate	0		0
S4068	tinidazole	0		1
S4070	Guanidine HCl	0		0
S4072	Decamethonium bromide	0		0
S4073	Aminosalicylate sodium	0		0
S4074	Sodium nitrite	0		1
S4075	Pyrithione zinc	0		0
S4076	Propranolol HCl	0		1
S4077	Mequinol	0		0
S4078	Mefenamic acid	0		0
S4079	Ticagrelor	0		1
S4080	triamterene	0		0
S4081	sulfacetamide sodium	0		0
S4082	Spiramycin	0		0
S4084	Lomerizine HCl	0		2
S4085	Levobetaxolol HCl	0		0
S4086	Loxapine Succinate	0		2
S4088	Flumethasone	0		1
S4089	Halobetasol Propionate	0		2
S4090	Fenspiride HCl	0		0

S4092	Pramoxine HCl	0		0
S4095	Difluprednate	0		0
S4096	Droperidol	0		0
S4097	Dydrogesterone	0		0
S4099	Dexlansoprazole	0		0
S4100	Esmolol HCl	0		0
S4101	Voglibose	0		0
S4102	Eprosartan Mesylate	0		0
S4104	Diminazene Aceturate	0		0
S4105	Closantel Sodium	0		0
S4106	Closantel	0		0
S4107	Clofazimine	0		0
S4111	Dicloxacillin Sodium	0		0
S4114	Triclabendazole	0		0
S4116	Isovaleramide	0		0
S4120	Sulconazole Nitrate	0		0
S4122	Tilmicosin	0		0
S4128	Troxipide	0		0
S4132	Deoxyarbutin	0		0
S4135	Clorprenaline HCL	0		0
S4136	Carprofen	0		0
S4138	Dropropizine	0		0
S4144	Amprolium HCl	0		0
S4146	Bacitracin	0		0
S4147	Azithromycin Dihydrate	0		0
S4148	Ampicillin Trihydrate	0		0
S4149	Amfenac Sodium (monohydrate)	0		0
S4151	Penfluridol	0		0
S4152	Ethamsylate	0		0
S4155	Chlorzoxazone	0		1
S4159	Bezafibrate	0		0
S4160	Penicillin G Sodium	0		0
S4161	Benzoic acid	1		0
S4162	Benzethonium chloride	0		0
S4164	Doxofylline	0		0
S4165	Benzydamine Hydrochloride	0		0
S4166	Chlorpropamide	0		0
S4167	Cyromazine	0		0
S4169	Teriflunomide	2		1
S4170	Coumarin	0		0
S4171	Choline Chloride	0		0
S4172	**Cetylpyridinium Chloride**	**4**	**0**	**0**
S4173	10Hexadecanol	0		0
S4175	Sulfaguanidine	2		0
S4176	Trometamol	0		0

S4177	Uracil	0		0
S4178	Climbazole	3		0
S4179	Mezlocillin Sodium	0		0
S4181	Nicardipine HCl	0		0
S4182	Nifuroxazide	1		1
S4184	Penciclovir	0		0
S4185	Tiratricol	0		0
S4186	Domiphen Bromide	0		0
S4187	Salicylanilide	1		0
S4188	Sasapyrine	0		0
S4189	Cyclandelate	0		0
S4190	Cinchophen	0		0
S4191	Betamipron	0		0
S4192	Chlorquinaldol	0		0
S4194	Azaguanine08	0		0
S4195	Broxyquinoline	0		1
S4196	Ethacridine lactate monohydrate	3		0
S4197	Bemegride	0		0
S4198	Aminothiazole	0		0
S4199	Antazoline HCl	0		0
S4200	Tolperisone HCl	1		0
S4201	Florfenicol	0		0
S4203	Furaltadone HCl	0		0
S4204	Isosorbide	0		0
S4205	Dibenzothiophene	0		0
S4206	Cysteamine HCl	0		0
S4207	Clofibric acid	0		1
S4208	Chromocarb	0		0
S4209	Chlorocresol	0		0
S4210	Benzocaine	0		0
S4211	Montelukast Sodium	0		0
S4213	Dirithromycin	0		0
S4214	Sucralose	0		0
S4216	Valnemulin HCl	0		0
S4217	Liothyronine Sodium	0		0
S4219	Azaperone	0		0
S4220	Bosentan	0		1
S4221	Benzbromarone	0		0
S4222	Piperacillin Sodium	0		0
S4223	Mevastatin	0		0
S4225	Mexiletine HCl	0		0
S4227	Fidaxomicin	0		1
S4228	Fluorometholone Acetate	0		0
S4229	Oxybuprocaine HCl	0		0
S4230	Oxaprozin	0		1

S4231	Pilocarpine HCl	0		0
S4232	Nithiamide	0		1
S4233	Zoxazolamine	0		0
S4235	Phenazopyridine HCl	0		0
S4237	Primaquine Diphosphate	0		0
S4238	Cepharanthine	0		0
S4239	Bergapten	0		0
S4240	Doxylamine Succinate	0		0
S4242	Cetrimonium Bromide	0		0
S4243	Deoxycorticosterone acetate	0		0
S4244	Serotonin HCl	0		0
S4245	Sodium ascorbate	0		0
S4269	Vinorelbine Tartrate	0		0
S4274	Rotigotine	0		0
S4282	Nelfinavir Mesylate	0		0
S4285	Ospemifene	0		0
S4295	Meclofenamate Sodium	0		0
S4297	Mupirocin	0		0
S4303	90Aminoacridine	0		0
S4305	Anisotropine Methylbromide	0		0
S4308	Benzthiazide	0		1
S4311	Calcium Gluceptate	0		0
S4312	Carbadox	0		0
S4314	Ceftazidime Pentahydrate	0		0
S4321	Diphenylpyraline HCl	0		0
S4322	Disopyramide Phosphate	0		0
S4326	Ethoxzolamide	0		0
S4327	Famprofazone	0		0
S4330	Isoetharine Mesylate	0		0
S4333	Mepiroxol	0		0
S4334	Mesoridazine Besylate	0		0
S4335	Metaproterenol Sulfate	0		1
S4336	Metaraminol Bitartrate	0		0
S4339	Meticrane	0		0
S4340	Moxalactam Disodium	0		0
S4341	Nalmefene HCl	1		0
S4342	Nialamide	0		0
S4343	Oxethazaine	2		0
S4345	Pentoxifylline	0		0
S4348	Piromidic Acid	0		0
S4349	Procyclidine HCl	1		0
S4351	Ractopamine HCl	0		0
S4353	Terfenadine	0		0
S4357	Tacrine HCl	0		1
S4358	Pimozide	1		0

S4359	Carbachol	0		0
S4360	Tolmetin Sodium	1		0
S4362	Glafenine HCl	1		0
S4363	Noscapine HCl	0		1
S4364	Phenothrin	0		0
S4365	Phthalylsulfacetamide	0		0
S4368	Carbenoxolone disodium salt	0		0
S4370	Nicotine Ditartrate	0		0
S4371	Pridinol Methanesulfonate	0		0
S4372	Triflupromazine HCl	0		2
S4373	Dicyclomine HCl	0		0
S4374	Thioridazine HCl	0		1
S4375	Mepenzolate Bromide	0		0
S4376	Aceclidine HCl	0		1
S4377	Imipramine HCl	0		0
S4381	Proadifen HCl	0		0
S4382	Pyrilamine Maleate	0		1
S4384	Difloxacin HCl	0		0
S4385	Fosfomycin Tromethamine	0		0
S4386	Acetarsone	0		0
S4389	Bephenium Hydroxynaphthoate	1		0
S4390	Brucine	0		0
S4391	Camylofin Chlorhydrate	0		0
S4394	Clofoctol	0		1
S4397	Diperodon HCl	0		0
S4398	Isoxicam	0		0
S4401	Nifenazone	0		0
S4402	Oxeladin Citrate	0		0
S4404	Pasiniazid	0		0
S4407	Prochlorperazine Dimaleate	0		0
S4408	Procodazole	0		0
S4414	Sodium 40aminohippurate Hydrate	0		1
S4416	Trimipramine Maleate	0		0
S4505	Vinblastine sulfate	0		0
S5001	Tofacitinib citrate (CP0690550 citrate)	0		0
S5003	FK0506 (Tacrolimus)	0		0
S5004	Pimecrolimus	0		1

Positive hits are highlighted. #pupae = number of counted pupae, #2nd = number of pupae after verification in a second testing, #pupae (Afatinib) = number of pupe after testing in combination with Afatinib [2 µM].

Sequence map of pBPGUw-*ppk11*:

Features:

AttB1 : [107 : 83 - CCW]
ppk11-Prom : [165 : 1588 - CW]
Gal4 DNA-binding domain : [1890 : 2330 - CW]
Gal4 activation domain : [4190 : 4532 - CW]
GAL4 terminator : [4537 : 4779 - CW]

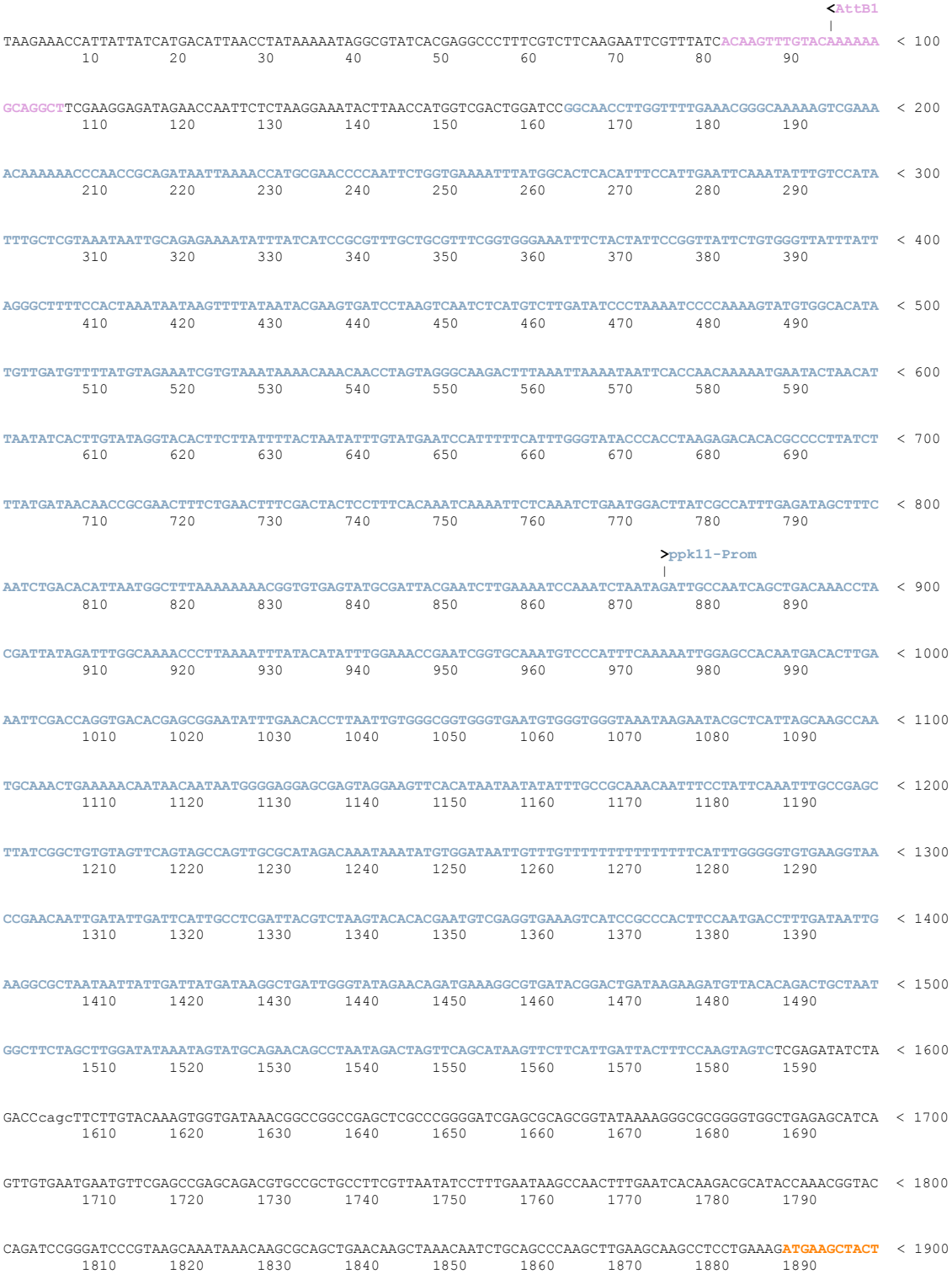

```
GTCTTCTATCGAACAAGCATGCGATATTTGCCGACTTAAAAAGCTCAAGTGCTCCAAAGAAAAACCGAAGTGCGCCAAGTGTCTGAAGAACAACTGGGAG  < 2000
        1910      1920      1930      1940      1950      1960      1970      1980      1990

TGTCGCTACTCTCCCAAAACCAAAAGGTCTCCGCTGACTAGGGCACATCTGACAGAAGTGGAATCAAGGCTAGAAAGACTGGAACAGCTATTTCTACTGA  < 2100
        2010      2020      2030      2040      2050      2060      2070      2080      2090

        >Gal4 DNA-binding domain
        |
TTTTTCCTCGAGAAGACCTTGACATGATTTTGAAAATGGATTCTTTACAGGATATAAAAGCATTGTTAACAGGATTATTTGTACAAGATAATGTGAATAA  < 2200
        2110      2120      2130      2140      2150      2160      2170      2180      2190

AGATGCCGTCACAGATAGATTGGCTTCAGTGGAGACTGATATGCCTCTAACATTGAGACAGCATAGAATAAGTGCGACATCATCATCGGAAGAGAGTAGT  < 2300
        2210      2220      2230      2240      2250      2260      2270      2280      2290

AACAAAGGTCAAAGACAGTTGACTGTATCGATTGACTCGGCAGCTCATCATGATAACTCCACAATTCCGTTGGATTTTATGCCCAGGGATGCTCTTCATG  < 2400
        2310      2320      2330      2340      2350      2360      2370      2380      2390

GATTTGATTGGTCTGAAGAGGATGACATGTCGGATGGCTTGCCCTTCCTGAAAACGGACCCCAACAATAATGGGTTCTTTGGCGACGGTTCTCTCTTATG  < 2500
        2410      2420      2430      2440      2450      2460      2470      2480      2490

TATTCTTCGATCTATTGGCTTTAAACCGGAAAATTACACGAACTCTAACGTTAACAGGCTCCCGACCATGATTACGGATAGATACACGTTGGCTTCTAGA  < 2600
        2510      2520      2530      2540      2550      2560      2570      2580      2590

TCCACAACATCCCGTTTACTTCAAAGTTATCTCAATAATTTTCACCCCTACTGCCCTATCGTGCACTCACCGACGCTAATGATGTTGTATAATAACCAGA  < 2700
        2610      2620      2630      2640      2650      2660      2670      2680      2690

TTGAAATCGCGTCGAAGGATCAATGGCAAATCCTTTTTAACTGCATATTAGCCATTGGAGCCTGGTGTATAGAGGGGGAATCTACTGATATAGATGTTTT  < 2800
        2710      2720      2730      2740      2750      2760      2770      2780      2790

TTACTATCAAAATGCTAAATCTCATTTGACGAGCAAGGTCTTCGAGTCAGGTTCCATAATTTTGGTGACAGCCCTACATCTTCTGTCGCGATATACACAG  < 2900
        2810      2820      2830      2840      2850      2860      2870      2880      2890

TGGAGGCAGAAAACAAATACTAGCTATAATTTTCACAGCTTTTCCATAAGAATGGCCATATCATTGGGCTTGAATAGGGACCTCCCCTCGTCCTTCAGTG  < 3000
        2910      2920      2930      2940      2950      2960      2970      2980      2990

ATAGCAGCATTCTGGAACAAAGACGCCGAATTTGGTGGTCTGTCTACTCTTGGGAGATCCAATTGTCCCTGCTTTATGGTCGATCCATCCAGCTTTCTCA  < 3100
        3010      3020      3030      3040      3050      3060      3070      3080      3090

GAATACAATCTCCTTCCCTTCTTCTGTCGACGATGTGCAGCGTACCACAACAGGTCCCACCATATATCATGGCATCATTGAAACAGCAAGGCTCTTACAA  < 3200
        3110      3120      3130      3140      3150      3160      3170      3180      3190

GTTTTCACAAAAATCTATGAACTAGACAAAACAGTAACTGCAGAAAAAAGTCCTATATGTGCAAAAAAATGCTTGATGATTTGTAATGAGATTGAGGAGG  < 3300
        3210      3220      3230      3240      3250      3260      3270      3280      3290

TTTCGAGACAGGCACCAAAGTTTTTACAAATGGATATTTCCACCACCGCTCTAACCAATTTGTTGAAGGAACACCCTTGGCTATCCTTTACAAGATTCGA  < 3400
        3310      3320      3330      3340      3350      3360      3370      3380      3390

ACTGAAGTGGAAACAGTTGTCTCTTATCATTTATGTATTAAGAGATTTTTTCACTAATTTTACCCAGAAAAAGTCACAACTAGAACAGGATCAAAATGAT  < 3500
        3410      3420      3430      3440      3450      3460      3470      3480      3490

CATCAAAGTTATGAAGTTAAACGATGCTCCATCATGTTAAGCGATGCAGCACAAAGAACTGTTATGTCTGTAAGTAGCTATATGGACAATCATAATGTCA  < 3600
        3510      3520      3530      3540      3550      3560      3570      3580      3590

CCCCATATTTTGCCTGGAATTGTTCTTATTACTTGTTCAATGCAGTCCTAGTACCCATAAAGACTCTACTCTCAAACTCAAAATCGAATGCTGAGAATAA  < 3700
        3610      3620      3630      3640      3650      3660      3670      3680      3690

CGAGACCGCACAATTATTACAACAAATTAACACTGTTCTGATGCTATTAAAAAAACTGGCCACTTTTAAAATCCAGACTTGTGAAAAATACATTCAAGTA  < 3800
        3710      3720      3730      3740      3750      3760      3770      3780      3790

CTGGAAGAGGTATGTGCGCCGTTTCTGTTATCACAGTGTGCAATCCCATTACCGCATATCAGTTATAACAATAGTAATGGTAGCGCCATTAAAAATATTG  < 3900
        3810      3820      3830      3840      3850      3860      3870      3880      3890

TCGGTTCTGCAACTATCGCCCAATACCCTACTCTTCCGGAGGAAAATGTCAACAATATCAGTGTTAAATATGTTTCTCCTGGCTCAGTAGGGCCTTCACC  < 4000
        3910      3920      3930      3940      3950      3960      3970      3980      3990

TGTGCCATTGAAATCAGGAGCAAGTTTCAGTGATCTAGTCAAGCTGTTATCTAACCGTCCACCCTCTCGTAACTCTCCAGTGACAATACCAAGAAGCACA  < 4100
        4010      4020      4030      4040      4050      4060      4070      4080      4090

CCTTCGCATCGCTCAGTCACGCCTTTTCTAGGGCAACAGCAACAGCTGCAATCATTAGTGCCACTGACCCCGTCTGCTTTGTTTGGTGGCGCCAATTTTA  < 4200
        4110      4120      4130      4140      4150      4160      4170      4180      4190

ATCAAAGTGGGAATATTGCTGATAGCTCATTGTCCTTCACTTTCACTAACAGTAGCAACGGTCCGAACCTCATAACAACTCAAACAAATTCTCAAGCGCT  < 4300
        4210      4220      4230      4240      4250      4260      4270      4280      4290
```


>Gal4 activation domain
TTCACAACCAATTGCCTCCTCTAACGTTCATGATAACTTCATGAATAATGAAATCACGGCTAGTAAAATTGATGATGGTAATAATTCAAAACCACTGTCA < 4400
4310 4320 4330 4340 4350 4360 4370 4380 4390
CCTGGTTGGACGGACCAAACTGCGTATAACGCGTTTGGAATCACTACAGGGATGTTTAATACCACTACAATGGATGATGTATATAACTATCTATTCGATG < 4500
4410 4420 4430 4440 4450 4460 4470 4480 4490
ATGAAGATACCCCACCAAACCCAAAAAAAGAGTAAAATGAATCGTAGATACTGAAAAACCCCGCAAGTTCACTTCAACTGTGCATCGTGCACCATCTCAA < 4600
4510 4520 4530 4540 4550 4560 4570 4580 4590
>GAL4 terminator
TTTCTTTCATTTATACATCGTTTTGCCTTCTTTTATGTAACTATACTCCTCTAAGTTTCAATCTTGGCCATGTAACCTCTGATCTATAGAATTTTTTAAA < 4700
4610 4620 4630 4640 4650 4660 4670 4680 4690
TGACTAGAATTAATGCCCATCTTTTTTTTGGACCTAAATTCTTCATGAAAATATATTACGAGGGCTTATTCAGAAGCTTATCGATACCGTCGACTAAAGC < 4800
4710 4720 4730 4740 4750 4760 4770 4780 4790